2017-12-13

On the Interaction between Superabsorbent Hydrogels and Cementitious Materials

Khashayar Farzanian
University of Miami, kh.farzanian88@gmail.com

UNIVERSITY OF MIAMI

ON THE INTERACTION BETWEEN SUPERABSORBENT HYDROGELS AND CEMENTITIOUS MATERIALS

By

Khashayar Farzanian

A DISSERTATION

Submitted to the Faculty
of the University of Miami
in partial fulfillment of the requirements for
the degree of Doctor of Philosophy

Coral Gables, Florida

December 2017

UNIVERSITY OF MIAMI

A dissertation submitted in partial fulfillment of
the requirements for the degree of
Doctor of Philosophy

ON THE INTERACTION BETWEEN SUPERABSORBENT HYDROGELS AND CEMENTITIOUS MATERIALS

Khashayar Farzanian

Approved:

_____ Ali Ghahremaninezhad, Ph.D. Assistant Professor of Civil Engineering	_____ Antonio Nanni, Ph.D. Professor of Civil Engineering
_____ Landolf Rhode-Barbarigos, Ph.D. Assistant Professor of Civil Engineering	_____ Prannoy Suraneni, Ph.D. Assistant Professor of Civil Engineering
_____ Qingda Yang, Ph.D. Associate Professor of Mechanical Engineering	_____ Ryan L. Karkkainen, Ph.D. Assistant Professor of Mechanical Engineering
_____ Edward A. Dauer, Ph.D. Research Associate Professor of Biomedical Engineering	_____ Guillermo Prado, Ph.D. Dean of the Graduate School

FARZANIAN, KHASHAYAR (Ph.D., Civil Engineering)
On the Interaction between Superabsorbent Hydrogels and Cementitious Materials (December 2017)

Abstract of a dissertation at the University of Miami.

Dissertation supervised by Dr. Ali Ghahremaninezhad.
No. of pages in text. (140)

Autogenous shrinkage induced cracking is a major concern in high performance concretes (HPC), which are produced with low water to cement ratios. Internal curing to maintain high relative humidity in HPC with the use of an internal water reservoir has proven effective in mitigating autogenous shrinkage in HPC. Superabsorbent polymers (SAP) or hydrogels have received increasing attention as an internal curing agent in recent years. A key advantage of SAP is its versatility in size distribution and absorption/desorption characteristics, which allow it to be adapted to specific mix designs. Understanding the behavior of superabsorbent hydrogels in cementitious materials is critical for accurate design of internal curing. The primary goal of this study is to fundamentally understand the interaction between superabsorbent hydrogels and cementitious materials.

In the first step, the effect of chemical and mechanical conditions on the absorption of hydrogels is investigated. In the second step, the desorption of hydrogels in contact with porous cementitious materials is examined to aid in understanding the mechanisms of water release from superabsorbent hydrogels (SAP) into cementitious materials. The dependence of hydrogel desorption on the microstructure of cementitious materials and relative humidity is studied. It is shown that the capillary forces developed at the interface between the hydrogel and cementitious materials increased the desorption of the hydrogels. The size

of hydrogels is shown to influence desorption, beyond the known size dependence of bulk diffusion, through debonding from the cementitious matrix, thereby decreasing the effect of the Laplace pressure on desorption. In the third step, the desorption of hydrogels synthesized with varied chemical compositions in cementitious materials are investigated. The absorption, chemical structure and mechanical response of hydrogels swollen in a cement mixture are studied. The effect of the capillary forces on the desorption of hydrogels is investigated in relation to the chemical composition of the hydrogels. In the second set of experiments of this part, the behavior of the hydrogels in a hydrating cement paste is monitored by tracking the size and morphology evolution of hydrogels interacting with the cement paste matrix. It is shown that the changes on the surface characteristics of hydrogels as a result of interactions with the pore solution and cement particles can affect the desorption rate of hydrogels in contact with a porous cementitious material. Scanning electron microscopic (SEM) examination demonstrates two different desorption modes with distinct morphologies of hydrogels depending on the chemical composition of hydrogels. The effect of the interfacial bonding between the hydrogels and the cementitious matrix and its relation to the desorption is illustrated. The desorption of hydrogels with different chemical compositions in blended cement mixture containing different supplementary cementitious materials (SCMs) such as slag, fly ash, silica fume and two types of glass powders, are examined. The absorption/desorption kinetics of hydrogels in different hydrating blended cement mixtures are monitored by freeze drying the samples at different times. The surface characteristics of different hydrogels after interaction with pore solution, cement particles and SCMs particles are examined and their relation to

interfacial bonding is illustrated. It is shown that different SCMs can cause distinct changes on interfacial bonding.

The understanding of hydrogel behavior in cementitious materials helps with accurate mixture design for internal curing. The kinetics of desorption is crucial for the purpose of internal curing. The understanding of release mechanisms and the change in the hydrogel morphology is important for the self-healing and self-sealing applications.

Two major contributions of this research are (1) to show the effect of **capillary forces** developed at the interface between cementitious matrix and hydrogel which can increase the rate of desorption dramatically and (2) to illustrate the chemo-physical interaction between cement pore solution and hydrating particles with hydrogels which can affect the interfacial bonding between hydrogel and cement. These two main contributions will be useful to understand the absorption and desorption behavior of hydrogel in cementitious materials.

Two main strengths of experimental procedures of this research are (1) use of in-house synthesis of hydrogels that permits establishing a link between the chemical composition of hydrogels and their behavior in cementitious materials and (2) use of freeze drying for the **first time** to monitor the behavior of hydrogels interacting with a hydrating cementitious matrix.

Table of Contents

List of Figures

List of Abbreviations

a = *contact radius*

AA = *acrylic acid*

Alg = *alginate*

AM = *acrylamide*

APS = *ammonium persulfate*

$Ca(OH)_2$ = *calcium hydroxide*

$–COO^-$ = *carboxylate groups*

$D_{macrovoid}$ = *macrovoid thickness*

$D_{initial}$ = *thickness of dried hydrogel*

E = *Young's modulus*

G = *shear modulus*

G_d =*energy release rate*

h = *hydrogel layer thickness*

KCl = *potassium chloride*

L = *thickness of deformed specimen*

L_0 = *thickness of undeformed specimen*

MBA = *N, N'- methylenebisacrylamide*

NaOH = sodium hydroxide

NaCL = sodium chloride

P = *applied normel force*

P_{Lap} = *Laplace pressure*

Q = *absorption (water content)*

R = *sphere radius*

R_a = *surface roughness*

V_0 = *volume of hydrogel disk at the start of the desorption*

V_t = *volume of hydrogel disk at different times*

W_s = *weight of swollen hydrogel*

W_d = *weight of dry hydrogel*

μ_0 = *reference chemical potential corresponding to chemical potential of the fluid under atmospheric pressure*

μ_h = *chemical potential of fluid in hydrogel*

σ = *nominal stress*

σ_{xx} = *biaxial stress in the layer*

λ = *deformation ratio*

γ = *fluid surface tension*

γ_i = *interfacial energy*

δ = *depth of indentation*

π = *Pi*

ν = *Poisson's ratio*

Π = *osmotic pressure*

Ω = *molar volume of the fluid*

Γ = *interfacial toughness at the interface between hydrogel and porous matrix*

Chapter 1: Introduction

Concrete is the second most consumed material in the world after water. Concrete is an important component of our infrastructure and society. Concrete is comprised of cement, water, and aggregates. Portland cement was invented in 1824 by Joseph Aspdin and since then it began to become the most widely used construction material worldwide.

It has become evident that conventional concrete designed solely on the basis of compressive strength shows deficiencies in regard to durability performance including frost resistance, impermeability, and thermal cracking.

Demand for high performance concrete (HPC) has seen an increase over the past several decades to address the deficiencies related to conventional concrete. HPC, by definition, is expected to possess adequate workability, high strength, low permeability, superior dimensional stability and long-term durability [1]. HPC has constantly growing number of applications: marine construction, high-rise buildings, bridge decks and piers, thin-wall shells, airport pavements and many others. However, HPC advancement is hindered by its early-age cracking sensitivity [2]. In addition, there are other supplementary cementitious materials, such as fly ash, silica fume, glass powders and slag, commonly used in HPC to enhance the mechanical properties, durability, cosmetic aspects and microstructure of concrete [3]. HPC is prepared with low water to cement ratios (below 0.4) which is prone to self-desiccation that results in autogenous shrinkage. Autogenous shrinkage is restrained by aggregates and other external components which lead to early age cracking. Early age cracking in HPC constitutes a major concern limiting its intended service life [4–7].

1.1 Autogenous shrinkage

It is critical to understand the source and reasons for these cracking. One of the major reasons for cracking is autogenous shrinkage which can cause stress development in concrete and lead to crack formation. The autogenous shrinkage is different from chemical shrinkage which is a term used for a phenomenon in which the absolute volume of cement and water decrease with progressive hydration of cement [8,9]. Autogenous shrinkage of cement paste is defined as the macroscopic volume reduction of cement paste during hydration which occurs with no moisture transferred to the exterior surrounding environment. It is a result of chemical shrinkage affiliated with the hydration of cement particles [10,11]. As long as the cement paste is in the plastic phase, the chemical shrinkage is totally converted into an overall volume change. After first solid skeletons are formed in the hardening cement paste, the stiffness increases and makes a relatively hard and fixed boundary for pore fluid [12,13]. As a result, gas bubbles start to nucleate and grow in the bigger pores due to a drop in relative humidity as water is consumed during hydration [13,14]. A schematic of gas bubbles nucleation and growth in a hydrating cement paste is shown in Figure 1-1. Due to bubbles and therefore menisci creation in the pores, tensile stresses increase in the pore solution which pull the skeletons close to each other and cause a bulk shrinkage.

Since the tensile strength of the cement paste is very low at early age, this bulk shrinkage can create micro-cracking at early age. Basically, the drop of relative humidity (RH) due to hydration causes the autogenous shrinkage. One of the most effective ways to mitigate the drop in RH and consequently preventing the early age autogenous shrinkage cracking is internal curing.

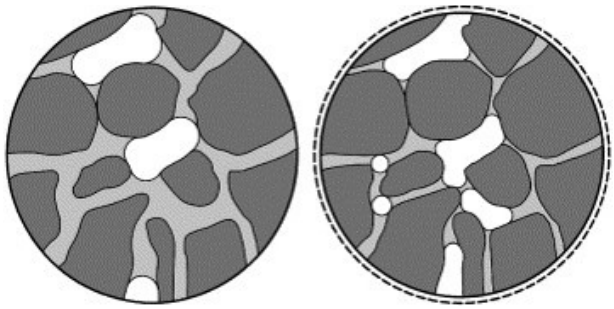

Figure 1-1 Schematic representation of a cross-section of a hydrating cement paste. Left: low degree of hydration. Right: high degree of hydration. Solid matter (hydrates and unhydrated cement) is shown as dark gray, pore water as light gray and empty pore volume as white (adapted from [13]).

1.2 Internal curing

Traditionally curing is referred to maintenance of a satisfactory moisture content and temperature in concrete for a period of time immediately following placing and finishing [15–19]. As mentioned previously, reduced RH is the main cause of early age micro-cracking in HPC. After placing the concrete different approaches based on the operational conditions are usually used to either prevent evaporation of water from concrete surface or providing extra water on the external surface to mitigate the drop in RH. This procedure is considered as external curing and can be implemented in different ways such as ponding and immersion, fogging and sprinkling, wet coverings, use of impervious paper, plastic sheets etc. [20].

For a porous ceramic like cement paste external curing cannot provide moisture in an effective time range. Since, the pore structure of cement paste (concrete) is very fine and the material is dense (especially for HPC) and also usually the concrete elements are thick, mass transport in this material takes a very long time which is not desirable for curing (see Figure 1-2). To have better durability extra water needs to be provided internally to reduce

the transport length to allow efficient distribution of the extra water within the microstructure of concrete. This technique that is utilized to provide extra water internally, without affecting the initial water to cement ratio of concrete mixtures, is called *Internal Curing*. Internal curing has proven effective in alleviating autogenous shrinkage cracking in high performance concrete [4,5,12,21–31]. In addition, water released from hydrogels contributes to the hydration of unhydrated cement particles, further densifying the microstructure. This improves the durability and mechanical performance of the cementitious materials [31]. Internal curing can be achieved by using pre-wetted lightweight aggregate [11,32,33] as a reservoir of water (see Figure 1-2).

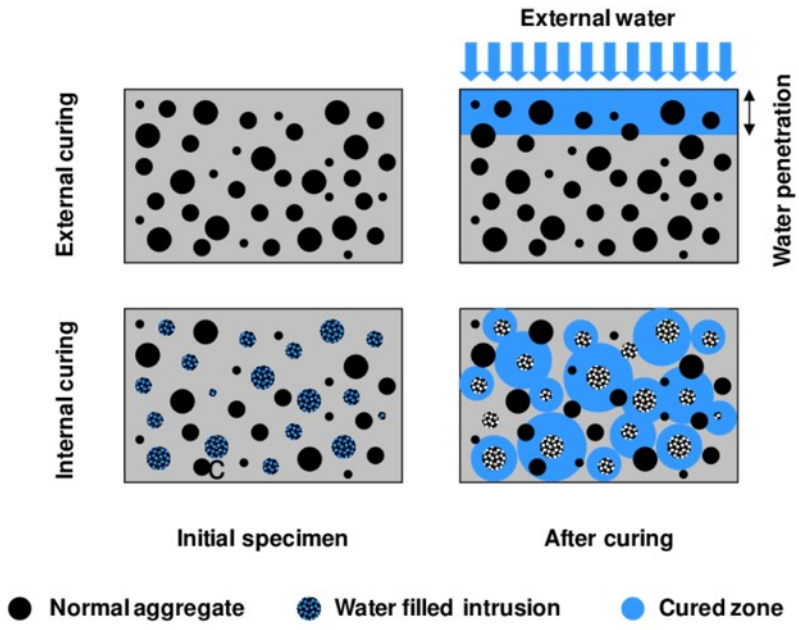

Figure 1-2 Conceptual illustration of the differences between external and internal curing (Adapted from [32])

At the beginning of the 21st century, a new concept of internal curing by means of using fine superabsorbent polymer (SAP hydrogel) particles in concrete mixture was introduced by Jensen and Hansen [5,30]. This concept permits formation of a controlled reservoir of

water (swollen hydrogel), which can release water in cement paste in response to a reduction in RH. There are other envisioned benefits related to use of SAP including self-sealing and delivery of bio-inspired self-healing materials [31,34–37]. Of course, the primarily purpose of using SAP in cementitious material is for internal curing, but in Figure 1-3 and Figure 1-4 the schematic of other concepts are illustrated too.

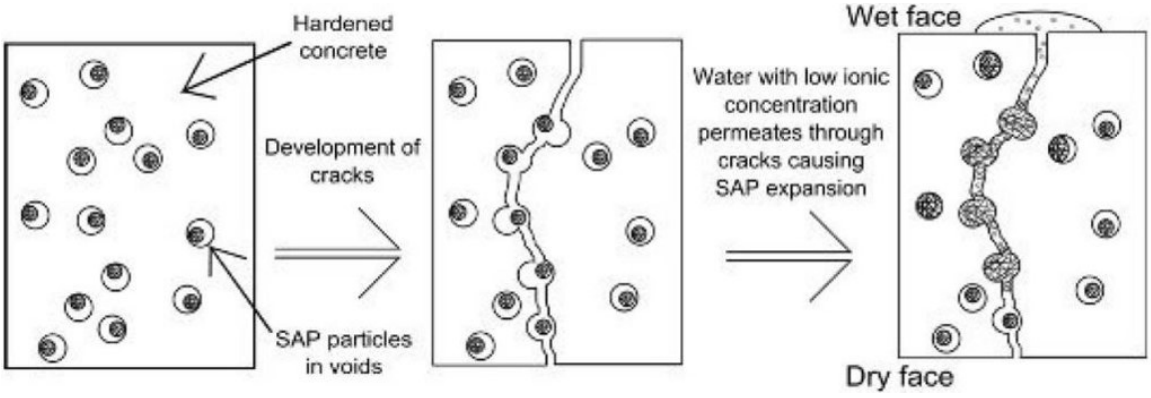

Figure 1-3 Schematic for the self-sealing concept (Adapted from [35])

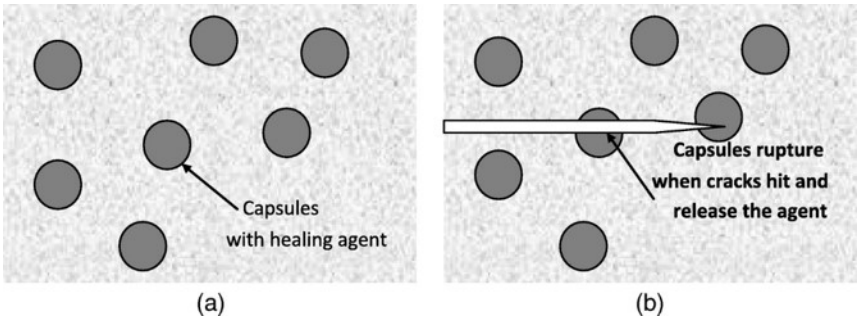

Figure 1-4 Schematic for the delivery of self-healing materials concept (Adapted from [37])

A large number of benefits can be envisioned from using hydrogels as a vehicle for incorporating additives, including chemical and mineral admixtures, nanoparticles, etc., in cementitious materials. The presence of certain additives at the beginning could adversely affect other processes in cementitious materials; for example, delayed hydration and strength gain due to addition of shrinkage reducing admixtures (SRA) [1,38–41].

Engineering hydrogel encapsulated SRA to release at a desired time permits optimum performance of additives in cementitious materials. The fundamental understanding of the behavior of hydrogels in cementitious materials is necessary in order to achieve successful designs for internal curing, self-sealing and delivery of self-healing materials. Unfortunately, the behavior of hydrogels in cementitious materials is poorly understood. During the last two decades several investigations have been performed in order to understand the absorption/desorption behavior of hydrogels in cementitious materials. Majority of these investigations were performed to understand the absorption/desorption behavior of hydrogel in synthetic pore solutions or extracted pore solutions [42–44] and the effect of commercial hydrogels on the micro-macro-scale behavior of cementitious materials [45–47].

Improvements in the hydration of cementitious materials when SAP was used due to internal curing has been documented in the past [27,48,49]. Prior studies have examined the effect of SAP on the microstructure densification of cementitious materials [29,49–52]. The influence of SAP on the transport properties was also studied by researchers [26,27,53]. However, addition of SAP has been found to result in formation of macrovoids, which impact the compressive strength of cementitious materials [7,29,44,54,55]. It is important to mention that factors including cement mix proportion and the physical and chemical characteristics of SAP strongly affect their influence on cementitious materials [7,26,28,44,56].

Supplementary cementitious materials (SCMs) are widely used in concrete to enhance the durability and extend the service life of infrastructure. The use of SCMs is in part motivated by the need to reduce Portland cement production which generates greenhouse

emissions and impacts the environment [57–59]. The cement clinker and SCMs hydrate simultaneously and influence on each other. The blended cement paste composition and pore fluid affect the overall hydration and pozzolanic reactions (by fly ash) are known to occur later as pozzolans need to react with the calcium hydroxide formed in cement hydration [60]. As the degree of hydration of fly ash increases, the autogenous shrinkage also increased in time [61]. The investigation by Jensen and Hansen [62] show that silica fume addition markedly increases autogenous shrinkage as well as the autogenous relative humidity change. Slag-cement mixtures showed greater autogenous shrinkage than ordinary concrete in the research of Lee et al [63]. Due to the slower rate of SCMs reaction, the initial total amount of autogenous shrinkage is lower compared to an ordinary Portland cement mixtures. However, internal curing by means of SAPs seems to be successful, independent of this long term higher rate of shrinkage in mixtures with SCMs [60]. Prior research has shown the benefits of SCMs such as fly ash [64–67], slag [68–70], glass powder [71–79], silica fume [80,81] and metakaolin [82,83] to cementitious material behaviors.

1.3 Superabsorbent polymer (SAP hydrogel)

In general, hydrogels are crosslinked polymer networks that have the ability to absorb noticeable amount of water. Hydrogels can be classified in different bases [84]:

- Source: natural or synthetic origins
- Polymeric composition: homopolymeric, copolymeric and multipolymer
- Configuration: amorphous, semi-crystalline and crystalline
- Type of crosslinking: chemical and physical cross-link junctions

- Physical appearances: matrix, film, or microsphere
- Network electrical charge: nonionic (neutral), ionic, amphoteric electrolyte (ampholytic) containing both acidic and basic groups and zwitterionic (polybetaines) containing both anionic and cationic groups

Hydrogels are responsive to different types of stimuli such as chemical effects (pH, ionic strength, solvent composition and molecular species) and physical effects (temperature, electric or magnetic field, light, pressure, mechanical loading or sound)[85,86]. This stimuli responsive behavior of hydrogels is a benefit since it can be used to design smart material systems. As long as the behavior of hydrogels under different conditions is known, stimuli can be used as a motivation or trigger to activate the desirable properties [87,88].

There are various types of hydrogels which can be utilized in different conditions for different purposes. Hydrogels can be used in different technologies such as agricultural[89,90], tissue engineering [88,91–93], drug delivery system [94,95], sealing [96,97], water desalination [98,99], food additive [100], biomedical application [101–103] or recently infrastructure materials [5,30]. In order to use hydrogels in the design of smart material systems, the main step is to fully understand the behavior of this material in the specific application's environment and condition.

Recently, studies have been performed to understand the chemical behavior of hydrogels in cementitious materials. The hydrogels used in cementitious materials are typically polyelectrolytes, so they are sensitive to the pH and ionic strength of the environment. As illustrated in Figure 1-5 and Figure 1-6, hydrogels are naturally porous, meaning the mass transport through this material is possible. Of course, there is a difference

in this type of porosity compared to other porous material such as ceramics (cement paste). Schematic of polymer network expansion of hydrogels after exposure to solvent is also illustrated in Figure 1-5. In Figure 1-6, a microstructure of a freeze dried hydrogel demonstrating the micro-macro porosity of the hydrogel is shown.

By definition, hydrogels are polymer networks having hydrophilic properties [84]. Hydrogels are generally prepared from hydrophilic monomers; however, in order to regulate hydrogel's behavior such as mechanical properties or absorption capacity, hydrophobic monomers can be incorporated in the polymer networks [104,105]. Hydrophobic polymers are generally synthetic and mechanically strong which are very beneficial for tissue engineering applications [106].

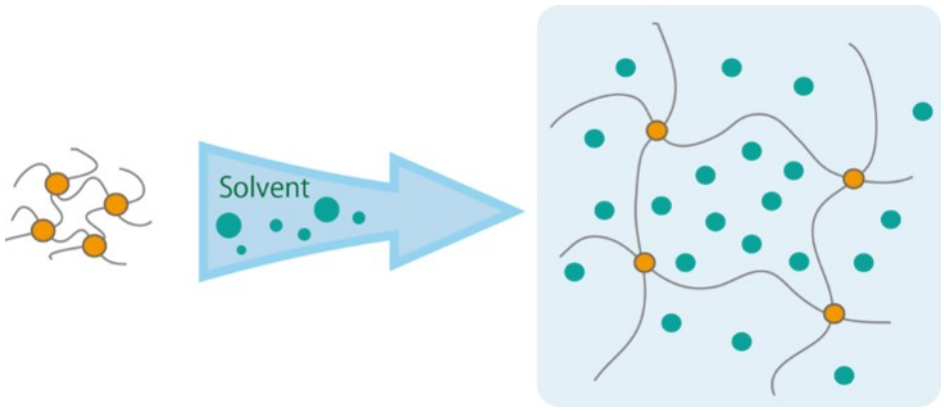

Figure 1-5 Schematic of absorption of a solvent by polymeric networks with crosslinked junctions (yellow circles)

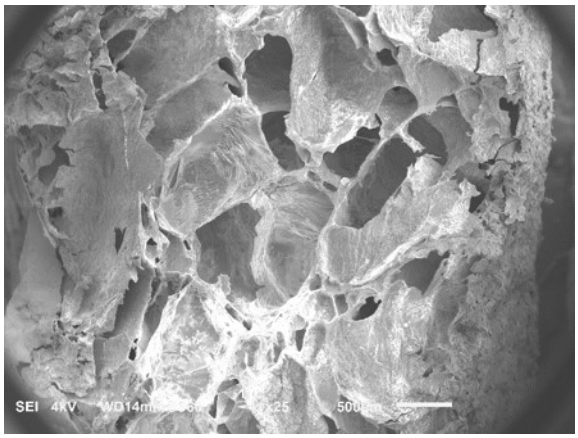

Figure 1-6 SEM imaging of microstructure of freeze dried poly(sodium acrylate-acrylamide) hydrogel with covalent crosslinking

There are different types of polymerization for hydrogel synthesis. Any of these techniques can be used to form gelation: bulk, solution and suspension polymerization. Generally, there are three integral parts of hydrogels: monomer, cross-linker and initiator. The polymerization techniques used for hydrogel synthesis are briefly described as follows [84]:

- *Bulk polymerization:* Bulk polymerization is the simplest technique which involves only monomers and monomer-soluble initiators. The bulk polymerization of monomers to make a homogeneous hydrogel produces a glassy, transparent polymer matrix which can be produced in a wide variety of forms including films and membranes, rods, particles, and emulsions [107].
- *Solution polymerization/cross-linking:* In this technique the ionic or neutral monomers are mixed with the multifunctional cross-linking agent and polymerization is initiated thermally by UV-irradiation or by redox initiator system [108].

- *Suspension polymerization or inverse-suspension polymerization:* This technique is very useful if the preparation of beads or microsphere is needed. If the polymerization process is water-in-oil (W/O) it is called "inverse-suspension polymerization", but more common technique is oil-in-water (O/W) which is called suspension polymerization. There is no need for grinding of hydrogel to prepare micro particles and the particles will be spherical compared with irregular shaped ground hydrogels [109–111].
- *Grafting to a support:* usually hydrogels prepared by bulk polymerization have a weak structure with low mechanical properties. To improve that hydrogel can be grafted on surface coated onto a stronger support. In this technique, hydrogel polymerization process is involved with extra steps to graft the hydrogel to a substrate such as starch in order to increase the hydrogel's properties [112–114]
- *Polymerization by irradiation:* ionizing with high energy radiation, like gamma rays and electron beams, has been used as an initiator to prepare the hydrogels of unsaturated compounds. The major advantage of the irradiation initiation over the chemical initiation is the production of relatively pure and initiator-free hydrogels [115,116].

Different methods are used to characterize the physical, chemical and mechanical properties of hydrogels. The physicochemical analysis contains morphological and microstructural imaging, evaluation of color, transparency, and degree of polymerization, chemical bonds characterization, and thermal and X-ray analyses [117]. The rubber elasticity and poroelasticity theories are usually utilized for constitutive modeling of

hydrogels as mechanical property characterization [118]. However, these theories are applicable to swollen state of hydrogels with median capacity of water. In the cases of high swelling capacity hydrogels and in their fully swollen state these theories might not be able to provide a realistic deformation of hydrogels.

A schematic of interaction between hydrogels and cementitious material is depicted in Figure 1-7. When hydrogel is placed in a fresh cement slurry, the absorption starts subjected to ionic effect present in the cement slurry as a result of cement dissolution. In addition, hydrogel absorption is influenced by the mechanical pressure of the cement slurry mass and the constraint of the stiffening matrix with hydration. At a later point, when the relative humidity of the matrix is dropped due to water consumption during hydration, the difference in the chemical potential of the water in the hydrogel and in the surrounding matrix provide a driving for the desorption of hydrogel into the matrix. This provides a general picture of absorption and desorption of hydrogels in cementitious materials.

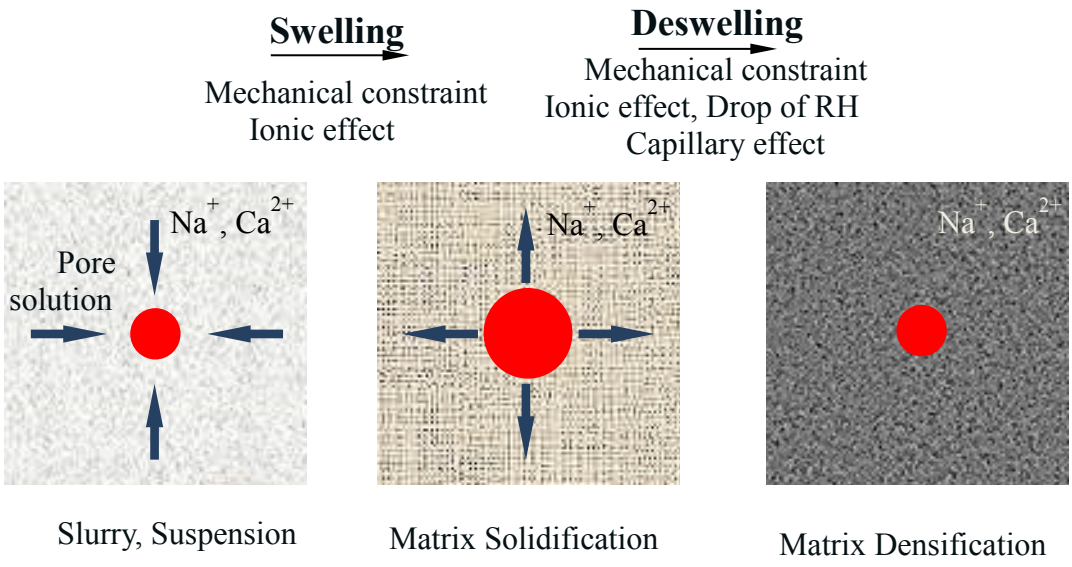

Figure 1-7 Schematic of interaction between hydrogels and cementitious material

1.4 Objectives and Problem Statements

HPCs are more prone to early age cracking than normal concrete which adversely impacts the durability of this material [119]. Superabsorbent polymers (SAP) have received increasing attention as an internal curing agent in recent years [5,25–30]. A key advantage of SAP is its versatility in size distribution and absorption/desorption characteristics, which allow it to be adapted to specific mix designs.

The **Objective 1** of this study is to understand the absorption behavior of hydrogels in cementitious material. The exact absorption of hydrogels in cementitious materials is needed for accurate design of internally cured cementitious materials. Inaccurate determination of hydrogel absorption will alter the effective water to cement ratio, which can impact the desired outcome.

The **Objective 2** of this investigation is to understand the desorption behavior of hydrogels in cementitious materials. The importance of hydrogel desorption can be emphasized by examining two scenarios. In the first scenario, if water release from hydrogels starts too early while the cementitious matrix is still plastic and able to accommodate the volume change due to hydration, the effect of hydrogel will be limited to simply an increase in initial water/cement ratio of the mixture. In the second scenario, if the water release occurs too late and water does not reach regions with decreased relative humidity, autogenous shrinkage can take place. In both cases, hydrogels are not expected to prevent autogenous shrinkage induced crack formation in the cementitious matrix.

The **Objective 3** of this investigation is to understand the effect of different types of supplementary cementitious materials (SCM) such as fly ash, slag, silica fume, glass powder on the hydrogel desorption behavior. As previously mentioned, HPCs usually

contain one or more SCMs which can influence the pore solution chemistry, cement matrix microstructure, RH and hydration rate. All these parameters potentially affect hydrogel desorption behavior.

It is worth mentioning that an understanding of the fundamental desorption behavior of hydrogels is also important for applications where hydrogels are used as a delivery vehicle of encapsulated materials. In the case of self-sealing applications, the morphology change of hydrogels during desorption can influence their re-swelling and crack sealing.

1.5 Dissertation outline

In Chapter 1 an introduction about the internal curing and use of SAP as an internal curing material is provided.

In Chapter 2, the experimental techniques, materials and sample preparation procedures are explained in details.

Chapter 3 focuses on hydrogel absorption and the effect of capillary forces on the desorption of hydrogels in contact with porous cementitious materials

In Chapter 4, the effect of chemical composition of hydrogels on hydrogel desorption in cementitious materials is investigated.

Chapter 5 discusses the influence of different SCMs on the hydrogel absorption/desorption behavior and the effect of hydrogel on surrounding matrix microstructure.

Chapter 6 provides conclusions and future work.

Chapter 2: Experiments

This chapter covers all the experimental techniques, devices, materials and sample preparation procedures that are used through the entire study to examine the behavior of hydrogels in cementitious materials. The hydrogel synthesis was performed in our own laboratory in order to have a control on the chemical and physical structure of hydrogels. This can be critical in regard to the interpretation of hydrogel's absorption/desorption behavior. The experimental techniques such as AFM, SEM, Profilometry, Micro mechanical, nano-mechanical, FTIR, MIP, and freeze drying are described in detail.

2.1 Materials

2.1.1 Commercial SAP

A total of four different SAPs designated as SAP1, SAP2, SAP3, and SAP4 were used in this study. SAP1 was obtained from Universe of Science, Inc., and SAP2-SAP4 were provided by Emerging Technologies. SAP1, SAP3, and SAP4 were made of sodium salts of crosslinked polyacrylic acid, and SAP2 was a potassium salt of crosslinked polyacrylic acid-polyacrylamide copolymer. The exact chemical composition of the commercial SAPs as well as polymerization techniques and conditions are not released by the vendors. SEM imaging from SAP1-SAP4 particles are illustrated in Figure 2-1(a-d) and their particle size distributions are plotted in Figure 2-1 (e) which gives noticeable information regarding morphology and particle size of SAPs. The plots are smoothed using the curve fit toolbox in MATLAB. The median particle size of SAP1, SAP2, SAP3, and SAP4 was calculated to be 197 μm, 59 μm, 140 μm, and 60 μm, respectively, analyzing 100 particles of each SAP micrograph using ImageJ software. The size of each particle was calculated as the

diameter of a circle with the same area as the projected particle. The shape of the SAPs are irregular in general, but it is shown that SAP3 is spongy-porous compared with angular SAP1, SAP2 and SAP4.

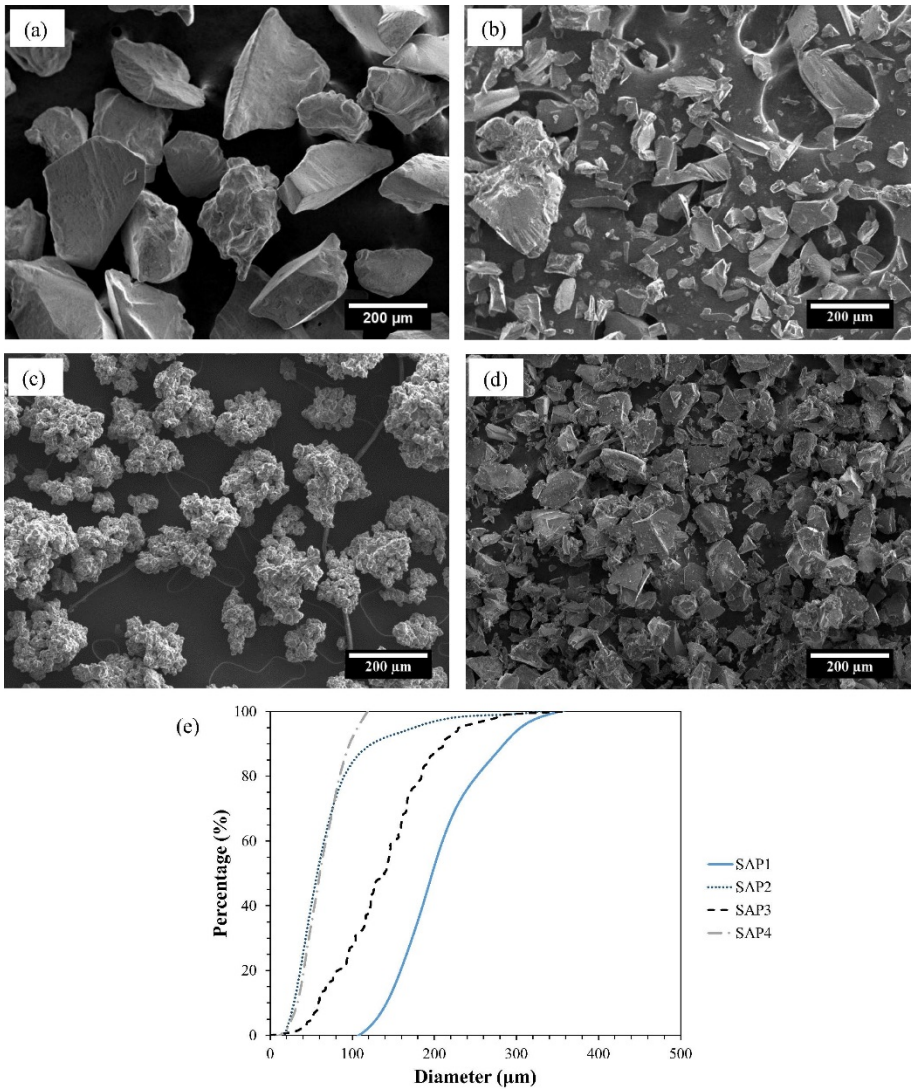

Figure 2-1 Scanning electronic microscopy micrograph of (a) SAP1, (b) SAP2, (c) SAP3, and (d) SAP4. (e) Particle size distributions of SAPs. (Adapted from [44])

The absorption/desorption behavior of SAPs is related to their chemical composition, molecular crosslinking, particle size, particle shape and solution chemistry they come in contact with (such as: ionic strength and pH) [42,43,120–122]. Since exact chemical compositions of these commercial SAPs are not known, in this study they are only used to evaluate the effect of mechanical pressure in distilled water and ionic solutions. Also, they are used for tea-bag test of absorption in extracted cement pore solution and distilled water, and SEM imaging of macro-void and morphology of SAP in cement paste as an observation.

2.1.2 Hydrogel

As previously mentioned, chemical composition of commercial SAPs are not known and even though the behavior of SAPs in the synthetic pore solution and extracted pore solution was extensively investigated in the past [43,54,120], the relation and link between the chemistry of different SAPs and cement slurry is poorly known. In order to have better insight from the chemo-physical behavior of different hydrogels and be able to investigate the relation between molecular structures of hydrogels and cement paste environment, hydrogels in this study were synthesized in our laboratory. All the commercial SAPs are called SAP1-4 and all the synthesized ones are called hydrogel. Controlling the chemical composition of hydrogels allows us to investigate link between the absorption/desorption behavior of hydrogels and their molecular structures.

Poly (sodium acrylate-co-acrylamide) copolymers with different chemical compositions are studied in this investigation and their compositions are listed in Table 1. Hydrogels are synthesized using the free radical polymerization method as described in Horkay [121]. All the materials are purchased from Sigma-Aldrich and used as received.

Main monomers are acrylic acid (AA) and acrylamide (AM). Hydrogels with different AA (g) /AM (g) ratios are prepared. AA is dissolved in 50 ml of distilled water and partially neutralized with 13.5% (wt) of sodium hydroxide before polymerization. AM is added to the solution and 0.025 g of N, N'- methylenebisacrylamide crosslinking agent (MBA) is added to the solution. The solution is stirred for 30 minutes to allow all the materials to fully dissolve. Dissolved oxygen is removed from the solution by bubbling the solution with argon for 3-5 min. The final step consists of adding 0.064 g of ammonium persulfate (APS) to initiate polymerization. After 5 minutes of stirring, the solution is poured in specific molds consisting of two glass plates sandwiching with a rubber gasket with varied thicknesses (0.5-3.5 mm) in order to control the initial thickness of hydrogel samples. In addition, glass molds allow us to have hydrogel layers with smooth surfaces without any wrinkles. The molds are placed in an oven and gelation occurred at 60 ºC for 2 to 3 hours dependent on the AA/AM ratio. The hydrogel layers are demolded, the hydrogel sheet edges which are in contact with rubber gasket are cut and their surfaces cleaned with alcohol for a few minutes to remove residual/unreacted monomers from the surface. The influence of the mold used during the synthesis by free radical polymerization of a hydrogel on the structure of its free surface is significant on surface characterization such as adhesion, in the past investigations it is shown that by increasing the hydrophilicity property of mold surface the final hydrogel has the lowest discrepancy between the bulk and the surface of the hydrogel [123]. Since the major effort in this study is focused on the interfacial bonding between hydrogel and porous cement paste the glass molds are used and the surface close to rubber gasket is not used in order to have the lowest discrepancy between the bulk and the surface of hydrogels. The hydrogels are placed in distilled water

for 1-3 hours (in the cases for bulk use it is kept in distilled water over night), then removed from distilled water and placed on a plastic mesh to allow hydrogel surface and body to become free of wrinkles or creases. The next day after the last cleaning, the hydrogels will be either punched, grind or cut before the drying process. Disks with a diameter of 16 mm are cut from the hydrogels using a punch and allowed to dry overnight in an oven at 60 ºC. All hydrogel disks have the same initial dry dimension of 9 mm in diameter; disks with varied thicknesses are prepared for different experiments as described later. Hydrogel disks with a dry thickness of 0.25-0.28 mm are utilized for absorption measurement and in situ experiments in order to have a similar diffusion length compared to SAP particles commonly used in cementitious materials. Hydrogel disks with a thickness of 1.6 mm in the dry condition are prepared to be used in the elastic shear modulus measurement, FTIR analysis, roughness measurement and AFM adhesion measurement. Thicker disks are used in these experiments to allow sample handling for these experiments. In order to examine the desorption of hydrogels in a hydrating cementitious matrix, thin micro-strip are cut from the thin hydrogel layers using a razor blade and then dried. The dry cross section of the micro-strip is in the range of 0.25-0.28 mm, which is similar to the thickness of the hydrogel disks used in the absorption experiments and is comparable to the size of SAP used in the cementitious materials.

In order to increase the alternatives for hydrogel choices and also bring more functionality into the hydrogel-cement system, the Double-Network (DN) hydrogels are synthesized via two step sequential free-radical polymerization process from acrylamide-alginate monomers [124–127]. The compositions are listed in Table 1, after dissolving all the components (monomers, cross-linker and initiator) in water, in the first step, a hydrogel

composed of covalently cross-linked network structure of AM (acrylamide) is formed via polymerization in oven at 60 ºC. This hydrogel is made of one monomer, but the second monomer which was dissolved in the initial solution is hidden in the hydrogel at the end of first step. The hydrogel sheets subsequently are submerged into a synthetic solution for alginate to form ionic-crosslinking, after taking the hydrogel out of oven and demolding it. The obtained hydrogel so-called DN hydrogel is immersed and washed in distilled water again to reach the equilibrium swelling state and cleaned from unreacted monomers and initiator. The synthesized pore solution compositions are listed in the Table 2. The synthetic pore solution chemistry is close to cement pore solution in order to have better compatibility. The pH level is adjusted to 13.00 by adding hydrochloric acid (HCl).

Table 1 Hydrogel compositions

Hydrogel Type	***AA (g)***	***AM (g)***	***NaOH (g)***	***MBA (g)***	***APS (g)***	***Distilled Water (g)***
H-1	9	1	1.215	0.025	0.064	50
H-2	5	5	0.675	0.025	0.064	50
H-3	1	9	0.135	0.025	0.064	50
H-A	6	4	0.810	0.043	0.064	50
H-B	0	10	0	0.043	0.064	50

Table 2 Synthesized pore solution compositions

	Ca(OH)2 (g)	*KCl (g)*	*NaCl (g)*	*NaOH (g)*	*Distilled water (g)*
Synthetic pore solution	2.24	29.82	11.69	8.00	1000

2.1.3 Cementitious material

In this study, two major types of cement paste were prepared: 1) cement substrate with different water to cement ratios in order to use as substrate, 2) cement paste with embedded hydrogel or mixed with SAPs with different water to cement ratios in order to investigate the interaction behavior between hydrogels and cement paste. To have consistency in all the samples a lignosulfonate-based superplasticizer (WRDA® 60, W. R. Grace & Co.-Conn.) at a concentration of 0.5% of the cement mass is added to the all mixtures.

Cementitious substrates are prepared by mixing type I Portland cement and water with three water to cement ratios of 0.25, 0.45, and 0.65, according to ASTM C 109. Three water to cement ratios are used to vary microstructure in the cementitious materials with an increase in porosity with increasing water to cement ratio. Cement mixture cubes of 50 mm dimensions are cast in two layers with each layer being tamped 32 strokes with a tamper. The cubes are placed in a moist room with a relative humidity more than 95% and at a temperature of 23 ± 2 ºC for 24 hours. Then, the cubes are demolded and stored in a saturated lime solution for seven days. After seven days, the cubes are submerged in acetone for 12 h to stop hydration. Then, the cubes are cut in half using a saw and the cut surfaces are polished with SiC sand papers of 180, 320, 600, and 1200 grit sizes. The samples are cleaned in an ultrasonicator for 20 minutes to remove the polishing compounds stuck on the surface. Bleeding is observed on the surface of the cement paste cubes with a

water to cement ratio of 0.65; only a portion of these cubes away from the top surface is used in sample preparation to avoid bleeding portion of samples. The samples are saturated in distilled water for 48 h and, subsequently, placed in dry boxes with relative humidity levels of 75%, 85%, and 95% for one to two months. To achieve three different relative humidity levels of 75%, 85% and 95%, saturated salt solutions namely, sodium chloride, potassium chloride and potassium nitrate, respectively, are used in respective dry boxes. The goal is to have cementitious materials with varied microstructures and varied relative humidity levels to permit investigating the effect of these characteristics on the capillary forces and desorption of hydrogels. It should be mentioned that the conditioning procedure used here allows to condition the region near the surface as the entire interior of the sample would require a much longer time to be conditioned [128,129]. The cementitious material substrates are designated CM-0.25, CM-0.45, and CM-0.65, corresponding to the different water to cement ratios used in the experiments.

In general, shrinkage reducing admixtures (SRA) reduces the surface tension of pore fluid, and are used in cementitious materials with low water to cement ratios to reduce shrinkage and mitigate crack formation [130,131]. It is described that SRA is mainly composed of amphiphilic (i.e., surfactant) molecules that when added to an aqueous solution, accumulate at the solution–air interface and can significantly reduce the interfacial tension. In this investigation, SRA was used to study on the effect of the pore fluid interfacial tension on the desorption of hydrogels in cementitious materials. There are two main reasons for this investigations: 1) we can manipulate the capillary forces in cement pores and this can be another evidence for the effect of capillary forces on the desorption of hydrogel, if by decreasing capillary tension (using SRA) the rate of hydrogel

desorption in contact with the cement substrate decreased, 2) SRA is commonly used in HPC which can affect on the desorption behavior of hydrogel and needed to be studied. In order to examine the effect of SRA on the desorption of hydrogels, cementitious material substrates were saturated in a solution containing 5% of SRA, composed of hexylene glycol (Eclipse® Floor, W. R. Grace & Co.-Conn.), for three days and then placed in the dry box with the 75% relative humidity for about one month.

2.1.4 Diluted cement slurry

Extracted or synthetic pore solutions are typically used to examine the chemical effects of the pore solution on hydrogels [42,43,122,132–134]. However, the extracted and synthetic pore solutions do not account for potential interactions between the hydrogels and the hydrating cement particles. Thus, in this study hydrogels are studied in a diluted cement mixture to allow the examination of the combined effect of pore solution and hydrating cement particles on hydrogel behavior. The diluted cement mixture is prepared with a water to cement ratio of 5 (or 2, it is mentioned in their section) and poured in polypropylene tubes. Hydrogel thin disks are submerged in the polypropylene tubes and sealed. The tubes are agitated periodically to maintain uniform dispersion in the cement mixture. Then hydrogels are removed from the diluted cement mixture at different times, surface cleaned and their mass measured using a balance with a precision of 0.001 g. Absorption (water content) was determined using the following equation:

$$Q = \frac{(W_s - W_d)}{W_d} \quad (1)$$

Where W_s is the weight of swollen hydrogel and W_d is the weight of dry hydrogel. Two samples are used in the experiments and the average value is reported. The diluted slurry

samples are also used for FTIR, AFM adhesion, elastic shear modulus measurement, surface roughness and desorption test of hydrogel in contact with cement substrate. This technique allows us to model the real case more accurately.

2.1.5 Mix design for cement paste blended with SCMs

Supplementary cementitious materials are used as a partial replacement for Portland cement. Five different type of SCMs are used: slag, silica fume, fly ash, glass powder VCAS and glass powder CS400. The percentage of replacement in all of the mixtures are 40% of cement by weight, except silica fume which is replaced by 20%. The SCMs and cement powder are mixed together properly for 3-5 minutes by using mixer before adding water. This allows the uniform distribution of powders and prevent agglomeration of SCMs. The water to cement ratio is 0.35 and lignosulfonate-based superplasticizer (WRDA® 60, W. R. Grace & Co.-Conn.) at a concentration of 0.5% of the cement mass is added to the all mixtures.

2.2 Experimental techniques

2.2.1 Elastic shear modulus measurement

Hydrogels resemble natural rubbers in their property to elastically respond to applied stresses. Rubbers are materials that respond to external stresses with almost instantaneous and fully reversible deformation. A hydrogel subjected to a moderate deformation, up to 20%, will fully and instantaneously reverse the deformation to original state. This elastic behavior of hydrogels can be explained by rubber elasticity theory originally developed by Treloar and Flory [135–139].

The mechanical behavior of hydrogel can have an important role in different mechanisms of desorption which is explained in details in the corresponding section. The mechanical property such as shear modulus (G) is highly sensitive to the water content of the hydrogel and chemical interaction between hydrogel and pore solution and hydrating cement particles. In order to examine the effect of the diluted cement mixture on the mechanical behavior of hydrogels, hydrogel disks at swollen state were subjected to compressive tests. Hydrogel disks were removed from diluted cement mixture after 6 hours, surface cleaned and placed on the bottom plate of the fixture in a material testing machine. The hydrogel disks were uniaxially compressed by the top plate in the displacement controlled mode at a rate of 0.0195 mm/s. Both plates were made of a transparent glass and covered by silicone oil to prevent lateral friction during the compressive loading. The transparent glass allows us to control plausible rupture or imperfection in samples during the test in order to increase the accuracy of the results. The load-displacement curves were used to calculate the shear modulus of the hydrogel disks assuming a rubber elasticity constitutive model for the hydrogels [135,140]. The shear modulus, G, was calculated from the following equation [121]:

$$\sigma = G(\lambda - \lambda^{-2}) \tag{2}$$

where λ is the deformation ratio ($\lambda = L/L_0$, L and L_0 are the thickness of the deformed and undeformed specimen, respectively) and σ is nominal stress. The average value of two samples is calculated as the shear modulus of each hydrogel. The mechanical test setup is illustrated in Figure 2-2. The displacement provided by California bearing ratio device, force data acquisition is done by FUTEK load cell.

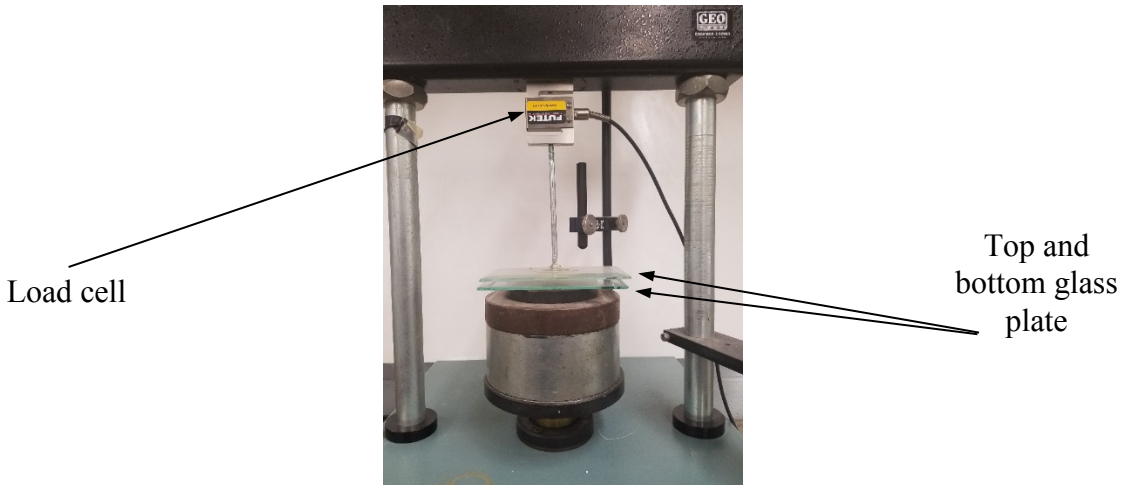

Figure 2-2 Mechanical test setup

2.2.2 FTIR analysis

Infrared spectroscopy probes the chemical bond vibrations. Functional groups can be associated with characteristic infrared absorption bands, which correspond to the fundamental vibrations of the functional groups [141–143]. The infrared spectra are quick and easy to achieve and refer to the spectrum region between the visible and microwave regions. In theory, infrared radiation is absorbed by molecules and converted into energy of molecular vibration; when the radiant energy matches the energy of a specific molecular vibration, absorption occurs. The frequencies at which a molecule absorbs radiation give information on the groups present in the molecule[141,144].

In this study, FTIR is used to examine the change in the chemical structure of the hydrogels as a result of interaction with the diluted cement mixture. As shown in the corresponding section, a thin skin with a different color and stiffness from the bulk of hydrogels is observed to form on the surface of the hydrogels used in the experiment. Thus, in order to identify the chemical nature of the skin and its contrast with the bulk hydrogel,

the FTIR analysis was performed on both the surface and the interior bulk of the hydrogels. The hydrogel surface was directly placed on a PerkinElmer Paragon 1000 FTIR with the ATR accessory which allows us to identify the samples chemical structure from fresh samples. In order to scan the interior bulk of the hydrogels, a starter notch was introduced at the edge using a blade and the top layer was peeled off to have a smooth surface in the interior bulk of the hydrogels. This method ensures that the interior bulk remains intact during sample preparation. The FTIR device is shown in Figure 2-3. The hydrogel samples are taken out of diluted cement slurry, surface cleaned with alcohol and placed on the device after couple of minutes in order to evaporate the extra alcohol.

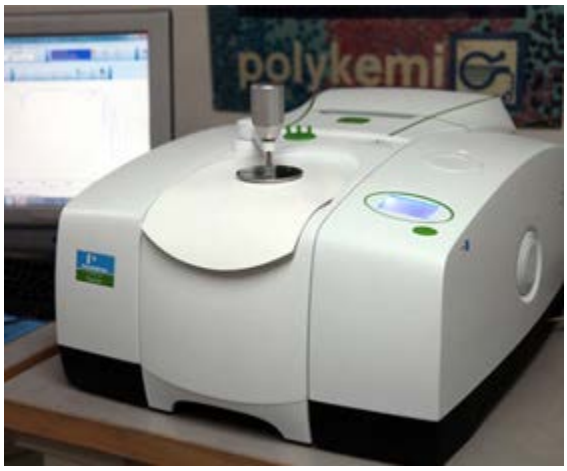

Figure 2-3 PerkinElmer Paragon 1000 FTIR with the ATR accessory

2.2.3 AFM adhesion measurement

Mechanical properties and other surface interaction forces of soft materials have a significant role in the mechanistic behavior of soft materials such as hydrogel. The ability to measure adhesion force, Young's modulus and other surface characterizations of soft materials allows us to determine and interpret major number of complex phenomena which involve elastic contacts. The use of the Atomic Force Microscopy (AFM) as a micro-

indenter to measure elastic properties and other surface interaction forces was introduced by Burnham and Colton [145] and followed by Tao et al. and Radmacher et al. [146,147]. In these methodologies by using AFM, the force-displacement curves are collected and suitable contact mechanics models are utilized to determine the Young's modulus, adhesion force and other material properties. In order to investigate soft materials like hydrogel, a micro-indentation AFM based approach is commonly used. In this approach, the cantilever tip is modified by attaching a micro-sphere glass on the tip [145,148–150]. The schematic of approach, contact, retract and separation of AFM cantilever on a soft sample (cell, hydrogel, etc.) is illustrated in Figure 2-4. By collecting the force-displacement curve the materials properties will be obtained.

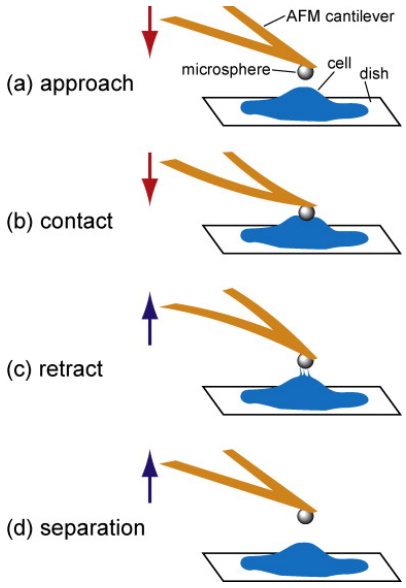

Figure 2-4 Schematic of AFM micro-indentation with micro-sphere glass bead attached to cantilever (Adapted from [151])

In this section, the experimental technique which is used to investigate the effect of diluted cement mixture on the hydrogel surface adhesion is explained. Since the hydrogel surface plays an important role on the interaction between the hydrogels and a cementitious

matrix and can potentially affect the desorption of hydrogels, it is important to characterize the dependence of hydrogel skin adhesion on the chemical composition of hydrogels. To this end, the AFM-based adhesion contact measurement assuming the Johnson-Kandall-Roberts (JKR) [152] contact mechanics theory is used. This method describes the elastic contact behavior of an elastic sphere in contact with an elastic half-space accounting for adhesion between the two surfaces. The JKR model is a good approximation for the load-indentation relationship of soft materials with a large value of sphere radius R [153]. This model is described as shown below:

$$P = \frac{4Ea^3}{3R(1-\nu^2)} - 2\sqrt{2\pi\frac{E\gamma_i a^3}{(1-\nu^2)}} \qquad \delta = \frac{a^2}{R} - \sqrt{\frac{2\pi a\gamma_i}{\frac{E}{(1-\nu^2)}}} \tag{3, 4}$$

where P is the applied normal force, E is the Young's modulus of the sample, a is contact radius, R is the sphere radius, ν is the Poisson's ratio of the sample, γ_i is the interfacial energy and δ is the depth of indentation.

The adhesion contact measurement was carried out using an AFM (AFM Workshop) which is illustrated in Figure 2-5. A glass microsphere with a diameter of about 50 μm attached to the end of the AFM probe was brought into contact with the hydrogel surface. The microsphere is then retracted from the hydrogel until the attractive forces are no longer able to resist. The maximum attractive force is calculated from the maximum deflection of the cantilever using the elastic beam theory. The probe was purchased from APPNANO with a width of about 40 μm and initial stiffness (K) of 36-90 N/m. The glass sphere was purchased from Polyscience Inc. and an epoxy paste was used to attach the glass microsphere to the probe's end which is shown in Figure 2-6. The Sader method was

applied to determine the spring constant of the AFM cantilever using its resonant frequency and plan view dimensions [154]. The AtomicJ software was utilized to obtain the adhesion force and Young's modulus of the skin. About 20 indentations at random locations on the surface of hydrogels were performed in about one hour. Hydrogel samples taken fresh from the diluted cement mixture were cleaned with alcohol, excess alcohol wiped with Kimwipes and then used in the AFM measurement in air.

Figure 2-5 AFM (AFM Workshop)

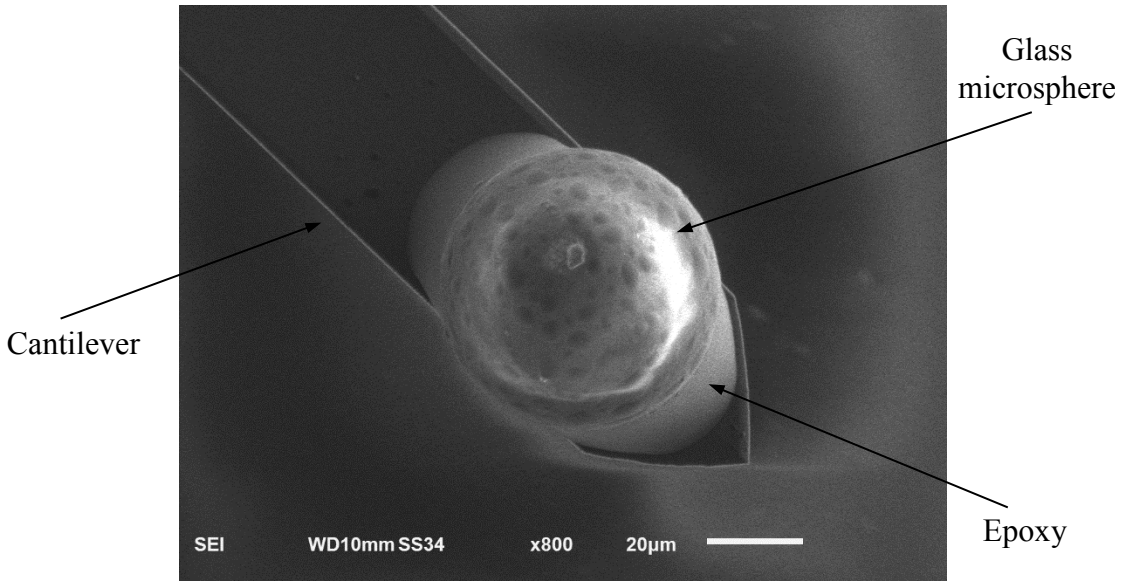

Figure 2-6 Glass microsphere attached on the cantilever.

2.2.4 Surface roughness measurement

In order to obtain insights into the potential changes in the surface morphology of hydrogels after interactions with the pore solution and cement particles, the hydrogel surface was examined using profilometry. The surface of swollen hydrogels was imaged with the Nanovea profilometer PS50 using a 3.5 mm optical pen which provides a resolution of 20-25 nm which is shown in Figure 2-7. The surface was scanned at a step size of 3 µm over an area of 2×2 mm^2. Each scan took about 30 minutes in room condition with RH of about 65-75%. Duplicate samples were used in the experiments and the average roughness is reported. The difference in the duplicate samples was less than 4%.

(a)

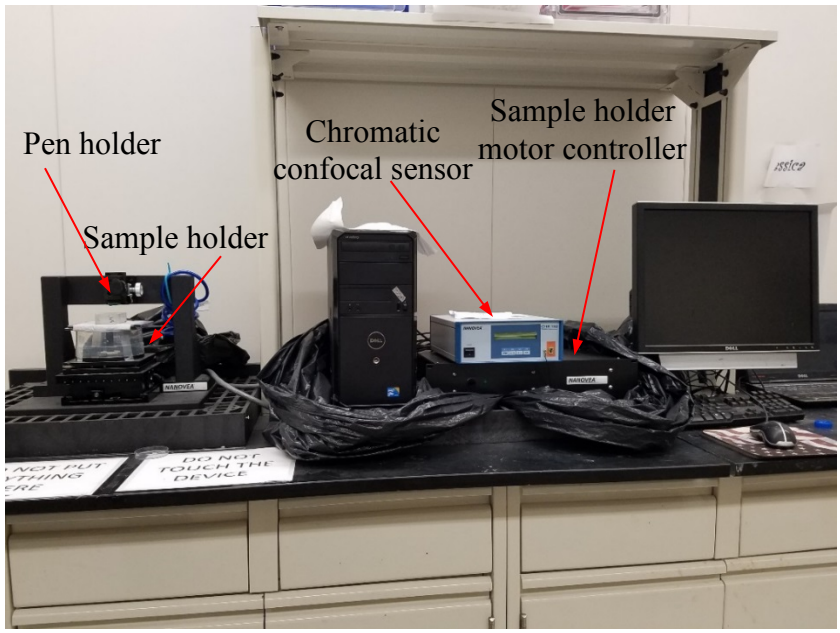

(b)

Figure 2-7 (a) Nanovea profilometer PS50 (b) 3.5 and 12 mm optical pen

2.2.5 Desorption of hydrogel in contact with cement substrate

The desorption behavior of hydrogel in contact with cement paste substrate is investigated in two sections, chapter 2 and chapter 3. The main concept of this experiment is the same, but due to different objectives the experimental details are different. As mentioned below, in the chapter 2 where the main focus is to elucidate the effect of capillary forces on the hydrogel desorption behavior in contact with cement substrate, one type of hydrogel (H-A) is swollen in NaCl solution ($[Na^+]$ =1 mol) and different type of cement paste substrates are used. But in chapter 3, different types of hydrogels with different chemical compositions are swollen in diluted cement slurry. One cement substrate

is used to study on the effect of cement pore solution chemistry and hydrogel chemical compositions on the desorption behavior of hydrogels.

In chapter 2: desorption of hydrogel layers (H-A) was carried out by placing 0.7 mm thick hydrogel layers (in swollen state in the NaCl solution) onto the polished surface of the cementitious material substrates. The entire hydrogels/cementitious material substrates were kept in the dry boxes with varied relative humidity levels. Hydrogel layers were also placed onto a Teflon substrate, which is hydrophobic and did not apply the capillary forces to the hydrogel layers, and therefore, permitted a comparison with the hydrogel layers with contact with the cementitious material substrates. The hydrogel layers with contact with cementitious material substrates (CM-0.25, CM-0.45, and CM-0.65) were designated H-0.25, H-0.45, and H-0.65, respectively. The hydrogel layers without contact with a cementitious material substrate were designated H-O. It should be noted that desorption of H-0.25, H-0.45, and H-0.65 was allowed from the top surface through evaporation and the bottom surface due to the capillary suction. Desorption of H-O was allowed only from the top surface. This difference in the boundary conditions will be considered in the discussion of the results presented later. The desorption of hydrogel layers was obtained by measuring the change in volume using optical profilometry. A Nanovea profilometer PS50 was used to measure the change in three dimensions of the hydrogel layers which is illustrated in Figure 2-7. Hydrogel layers were scanned at a step size of 60 μm. To measure desorption at various times, the hydrogel layers/substrates were removed from the dry box and scanned with the profilometer in the room condition with about 65% relative humidity. Each scan took about 7-10 min, which was not expected to affect the desorption of hydrogel layers. Duplicate hydrogel layers/substrates were used in the experiments and their average

was reported. The results from duplicates were in a good agreement with each other and the maximum difference from the average was less than 4%.

In chapter 3: desorption behavior of different hydrogel layers (H-2 and H-3) swollen in diluted cement slurry in contact with one cement substrate (CM-0.45) in one relative humidity (RH=95%) is investigated. The imaging was conducted with a step size of 18 µm and 60 µm in the x and y directions, respectively. The water loss of hydrogel disks was measured using 1-(V_t/V_0) where V_t and V_0 are the volume of hydrogel disk at different times and at the start of the desorption test, respectively (in both chapters). In order to compare the desorption of the hydrogels with and without contact with a cementitious substrate, hydrogels were also placed on top of a plastic mesh with an opening size of 7 mm in the drybox with RH of 95%. The desorption of these hydrogels was measured in the same manner as those in contact with a cementitious substrate. Duplicate samples were used for each test and the standard error was less than 6%. The scanning setup and drybox are shown in Figure 2-8.

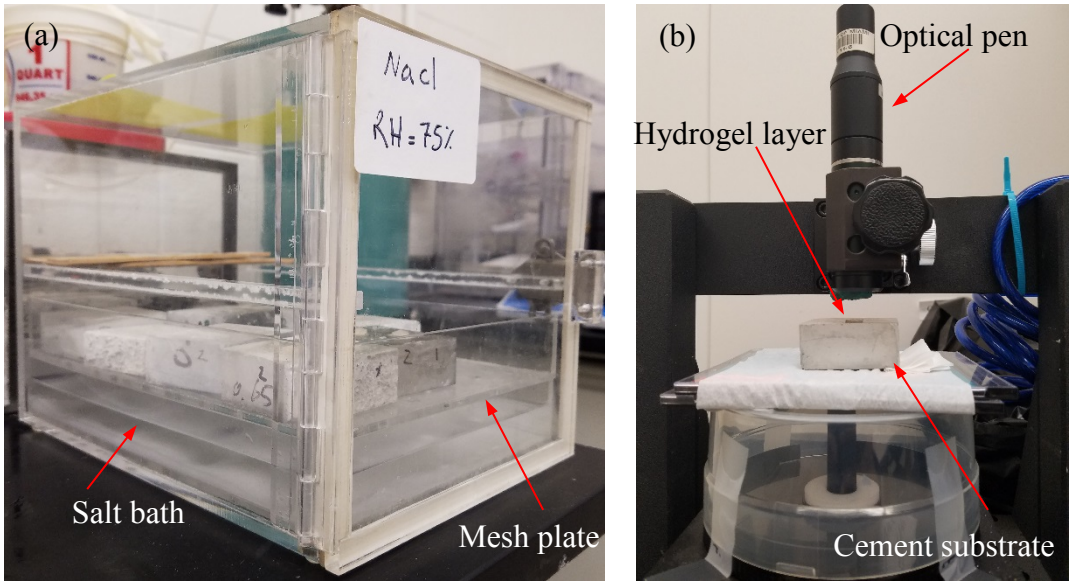

Figure 2-8 (a) Drybox with salt bath (b) scanning setup

2.2.6 Pore structure analysis (Mercury Intrusion Porosimetry)

Mercury intrusion porosimetry (MIP) is a widely used technique for characterizing the distribution of pore sizes in cement-based materials. It is a simple and quick indirect technique, but it has limitations when applied to materials that have irregular pore geometry. MIP is based on the premise that a non-wetting liquid (one having a contact angle greater than 90°) will only intrude capillaries under pressure. Mercury must be forced using pressure into the pores of a material [155–157]. Although there are evidences which indicate that the conditions that must be met for MIP measurements are not fully satisfied in cement-based systems, but the MIP method is still valid for comparative studies [158].

In order to gain insight into the effect of microstructure on the desorption behavior of the hydrogel layers, the pore structure of the substrates with varied water to cement ratios is measured using mercury intrusion porosimetry (MIP). To this end, cube samples with a dimension of 25 mm were cut from the substrates. The samples were dried in a vacuum oven at 40 ºC until no change in mass was observed. Porosimetry was performed using a Quantachrome Poremaster - Automatic Pore Size Analyzer with pressures up to 410 MPa. In Figure 2-9 the schematic of pore types and MIP test concept is indicated.

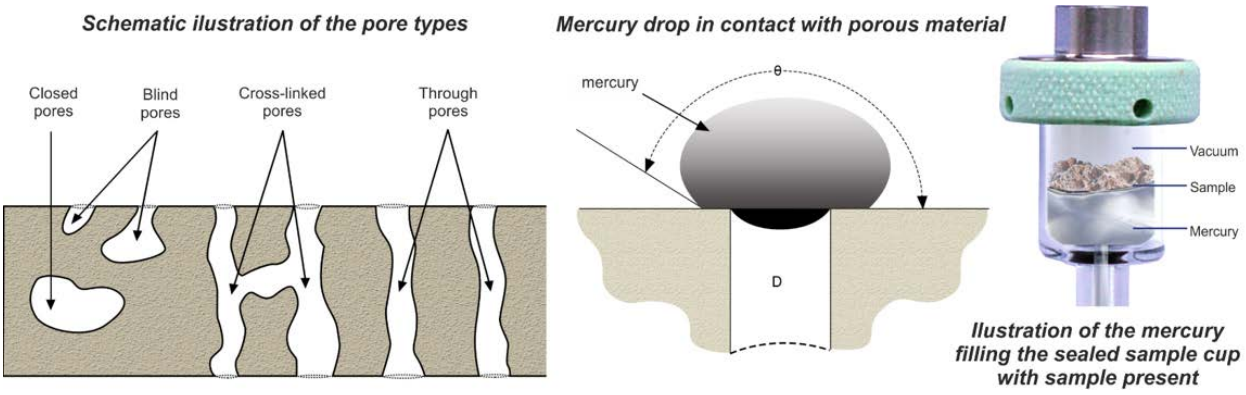

Figure 2-9 Schematic of pore types and MIP test concept (Adapted from [159])

2.2.7 SEM imaging

A scanning electron microscope (SEM) is a mature technique to investigate the surface morphology of different types of samples. This technique allows us to observe the samples at very high magnification. A normal scanning electron microscope operates at a high vacuum. The basic principle is that a beam of electrons is generated by a suitable source, typically a tungsten filament or a field emission gun. The electron beam is accelerated through a high voltage (for example 20 kV) and pass through a system of apertures and electromagnetic lenses to produce a thin beam of electrons, then the beam scans the surface of the specimen by means of scan coils. Electrons are emitted from the specimen by the action of the scanning beam and collected by a suitably-positioned detector [160,161]. The schematic diagram of SEM and the JEOL SEM device which is used in this study is shown in Figure 2-11 (a) and (b). Since the electrical conductivity is critical for imaging quality, most of the samples are set in epoxy and gold coated from 10 to 30 nm with Cressington sputter coater which is shown in Figure 2-10.

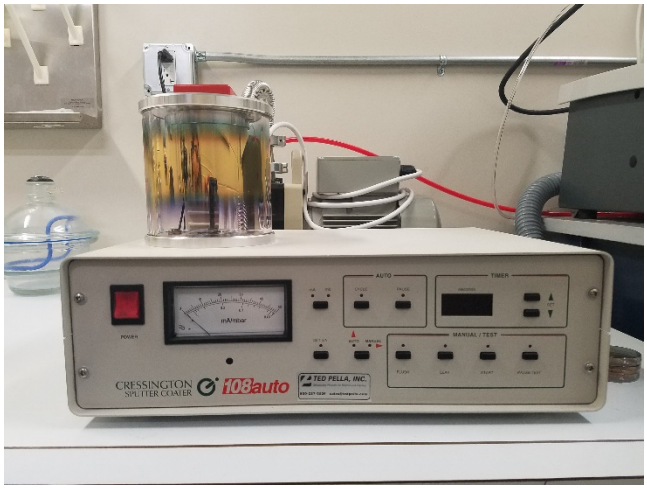

Figure 2-10 Cressington sputter coater

(a)

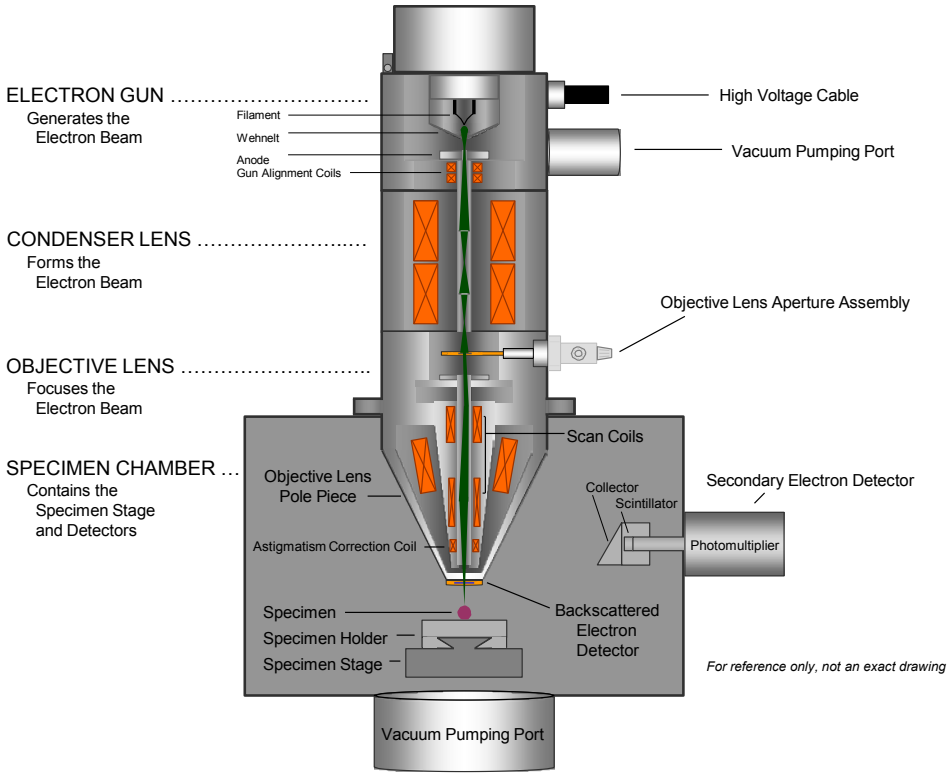

(b)

Figure 2-11 (a) Schematic diagram of SEM, (b) JEOL SEM device

2.2.8 Freeze drying technique to measure the evolution of hydrogel in situ

The majority of studies related to hydrogels as an internal curing agent have been performance oriented and show the effects of hydrogel as an internal curing agent on cement paste properties from an engineering point of view (such as autogenous shrinkage

measurement, compressive strength, etc.). The main focus in these studies is modified macroscale properties of the cement paste with hydrogel admixtures [5,30,47]. Only a few investigations have been published on the detailed mechanisms and kinetics of water migration within the cement-based material, release mechanism and chemo-mechanical behavior of hydrogel in situ, including, for example, water migration from hydrogel into the surrounding matrix, desorption mechanisms, repeatability of swelling as self-sealing agent, effect of hydrogel on surrounding cement matrix pore microstructure or the onset and duration of water release [162–166]. These investigations have been performed by utilizing neutron tomography, nuclear magnetic resonance (NMR) relaxometry and isothermal calorimetry in order to visualize and quantify the water release, monitor hydrating cement pastes containing an individually designed SAP sample and characterize the impact of SAP on the hydration kinetics of cement pastes [25,163,165–167]. The majority of these experimental techniques are very expensive and the results do not provide information at micro-scale interfacial bonding between hydrogel and cement paste. Therefore the chemo-mechanical behavior of hydrogels in cementitious based material is poorly known. In this study, an experimental technique is used for the very first time in order to monitor the volumetric evolution of hydrogels in cementitious based material as an absorption/desorption index. In this technique, by utilizing liquid nitrogen, cement paste samples with embedded a single hydrogel micro-strip are frozen instantly at specific interval time, subsequently dried under high vacuum in order to remove the water (ice) whereas the hydrogel microstructure is kept intact. In the next step, SEM imaging is performed to examine the evolution of hydrogel size, morphology, and the bond between the hydrogel and the cementitious matrix. Since this technique is used for the first time for

this purpose, the freeze drying's principles, procedure and modifications are explained in details as follows.

Freeze drying technique, also known as lyophilization, is referred to as a removal of ice or other frozen solvents from a material through the sublimation procedure. As opposed to the destructive effects of drying from the liquid state, freeze-drying, under proper conditions, permits the preservation of three major specimen characteristics: morphology, solubility, and chemical integrity [168]. This technique has a wide range of application from pharmaceutical and biotechnology industries, food and agricultural industries, nanotechnology, chemical synthesis, etc. [169–177]. The main principle involved in freeze drying is a phenomenon called sublimation, where water passes directly from solid state (ice) to the vapor state without passing through the liquid state. Sublimation of water can take place at pressures and temperature below triple point i.e. 4.58 mm of Hg and 0.01 ºC as it is indicated at phase diagram of water in Figure 2-12 (a). The samples to be dried are first frozen in liquid nitrogen and then subjected to a high vacuum so that frozen liquid sublimes leaving only solid skeleton of the original samples [172,178]. Freeze-drying has been used extensively for the fabrication of porous hydrogels for tissue engineering [179–181]. Since water don't evaporate, there is no gross change in volume other than the slight expansion resulting from the crystallization of ice. This means the skeleton volume of hydrogel just before freezing is the same as after drying [179,182].

In principle, the freeze drying technique which is utilized in both chapter 4 and chapter 5 is the same, just slight modifications are applied in order to avoid wrinkling of hydrogel micro-strip in cement paste in chapter 5. Here both procedures are explained in detail.

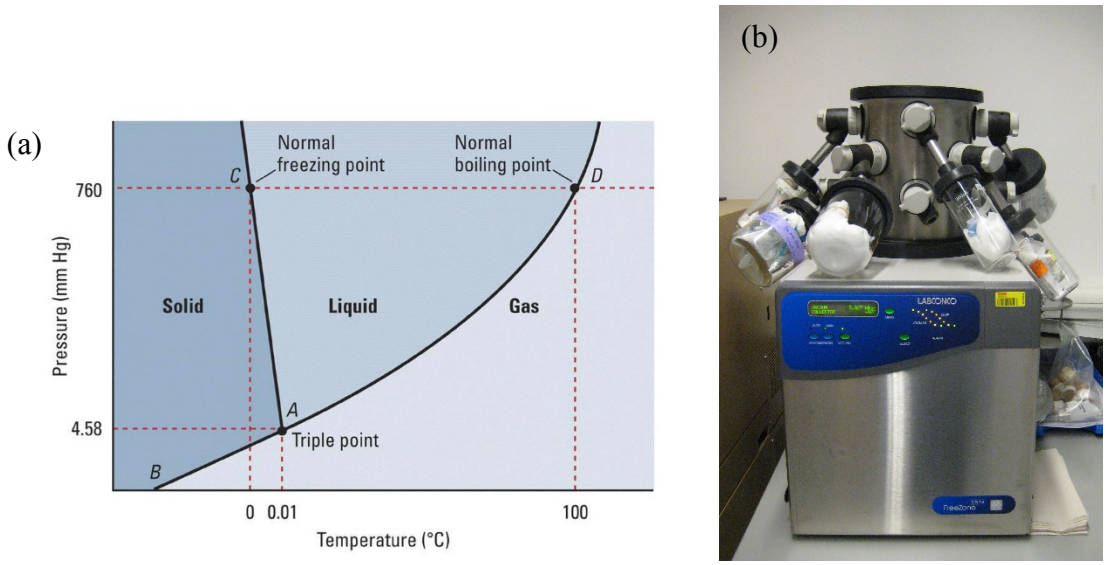

Figure 2-12 (a) Phase diagram of water (Adapted from [183])(b) freeze-drying device

In chapter 4, cement paste with a water to cement ratio of 0.3 and the superplasticizer at a concentration of 0.5%, by cement mass, is prepared and poured into a polypropylene tube with a diameter of 14 mm. In the first step, the polypropylene tubes are half way filled with cement slurry. Then, the hydrogel micro-strip are inserted at the center along the axial direction of the tube and the tubes are filled up fully at the end. The tubes are shaken to improve consolidation and immediately sealed. In order to track the time variation of absorption and desorption, the tubes filled with cement paste and hydrogel micro-strip are dipped in liquid nitrogen at different times in order to stop hydration and any mass transport.

Since it is very important to ensure that freeze-drying does not affect the size and morphology of hydrogels and the change in size and morphology is only due to their interaction with the cementitious matrix, the samples are broken by creating a notch on the sample surface and using a bending moment to avoid touching the cross section surface of the hydrogel micro-strip or cementitious matrix. This allows the cross section of the

hydrogel micro-strip to be directly exposed to the negative pressure during sublimation and prevents melting of the hydrogels, which can be the source of shrinkage or volume change and should be avoided. The samples are placed in a freezer at -25 ºC overnight. The next day, they are transferred to a freezer at -80 ºC for 1-3 days. The samples are then placed in a Labconco lyophilizer to dry for 2-3 days which is illustrated in Figure 2-12 (b). The reason for using two different freezers is space limitation due to the large number of samples to account for statistical variability as well as the different times at which samples had to be subjected to freezing. As shown later in the SEM imaging results, the success of this procedure to preserve the hydrogel morphology can be verified from the SEM images of the hydrogel micro-strip corresponding to the early hours showing swollen hydrogels which does not indicate any shrinkage (hydrogel is fully swollen and fills the void completely). The SEM imaging is conducted in a JEOL (JSM-6010PLUS/LA) SEM with an accelerating voltage and spot size of 5-10 kV and 40-50, respectively. All the images are taken at the high vacuum pressure mode. SEM imaging is performed on 5-10 replicates for each hydrogel composition to account for statistical variability. The desorption of hydrogels is calculated as the ratio of the change in the cross sectional area of each hydrogel micro-strip at different times to the cross sectional area of the void surrounding the hydrogel micro-strip. This definition of desorption is consistent with the desorption of swollen hydrogel disks in contact with a cementitious substrate. The area of the void surrounding the hydrogel micro-strip is considered to be the maximum swelling of each hydrogel micro-strip at which time the fresh cementitious matrix is relatively stiff and does not fill back the void as the hydrogel shrinks in size.

In chapter 5 a simple modification is applied to increase the imaging resolution of this technique. Instead of using 14 mm diameter tube, a 30 mm Polypropylene tube is used. The tube is cut along the longitudinal axis by almost one fourth of the diameter as shown in Figure 2-13 (a). In the next step, half of the tube is filled with cement paste as shown in Figure 2-13 (b). Then, a hydrogel micro-strip is placed on top of cement slurry and remained there for 3 to 5 minutes (Figure 2-13) (c). As shown in Figure 2-13 (d), the micro-strip starts to swell and wrinkle since it is constrained to the cement slurry. In the next step, micro-strip is removed from the cement paste with two tweezers, stretched to de-wrinkle and put back on top of the cement paste as it is shown in Figure 2-13 (e). At the end the rest of the tube is filled with cement paste and sealed Figure 2-13 (f). All the procedure is done in a bucket with high and constant relative humidity and no air flow. This procedure helps to avoid any wrinkling during the experiment.

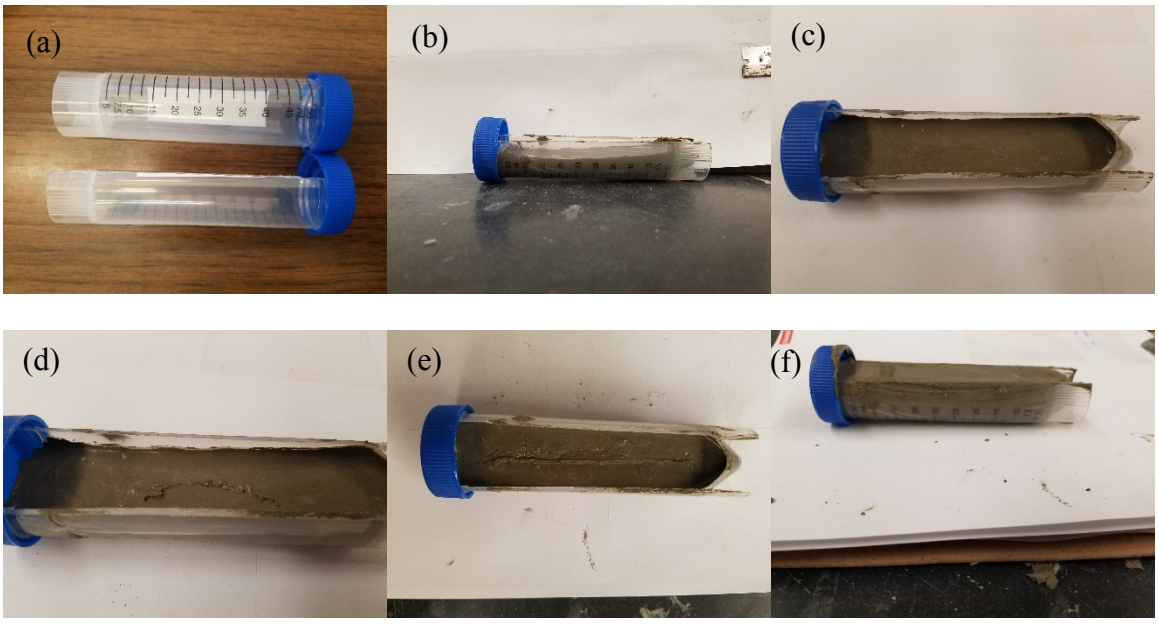

Figure 2-13 (a) Tubes before and after cutting (b) half-filled tube with cement paste (c) microsrtip hydrogel is placed on the cement paste (d) hydrogel wrinkling after 2-5 minutes (e) de-wrinkle microstrip with tweezers (f) Fill the tube fully.

2.2.9 SAP absorption

It is known that the water absorption capacity of ionic SAPs, which include the SAPs used here, is dependent on the chemical composition, including ionic strength and pH, of the solution they come in contact with [42,121,122]. Pore solution in a cementitious mixture possesses various ions, including Na^+ , K^+ , Ca^{2+}, OH^-, etc., as a result of cement dissolution and hydration. Thus, it is expected that the presence and concentration of these ions strongly affect the absorption capacity and kinetics of SAPs. The absorption of SAPs in synthetic pore solutions and extracted pore solutions was investigated in the past [43,54,120]. In this paper, the absorption behavior of SAPs in a pore solution obtained from a cementitious mixture is examined. This provides more realistic information regarding the amount of water SAPs absorb in a cementitious mixture; this amount of water determines the available water that can be released from SAPs at a later time for internal curing. The pore solution is extracted from fresh cement pastes with a water to cement ratio of 0.4 mixed according to ASTM C305. Water and cement were mixed for 30 s at a slow speed and then the mixer is stopped and the paste is allowed to rest for 15 s. The final mixing is done at a medium speed for 60 s. A type II Portland cement is used in the mixtures. The fresh cement pastes are filtered through a glass microfiber filter in a filtration setup under a negative pressure. The filtration process starts 45 min after the initial contact of water and cement. The pore solution is transferred to polypropylene bottles and sealed after extraction to avoid carbonation at room temperature.

In order to have better understating on the effect of cement pore solution on absorption capacity and the kinetics of absorption, the absorption of SAP1 particles in the pore solution and distilled water is measured using the teabag method [120]. Teabags were pre-

wetted in the pore solution or distilled water and their mass is measured using an analytical balance with a 0.001 g resolution. Then, 0.1 g of each SAP1 in dry condition is poured into a teabag and immersed in the solution. The mass of the teabag is monitored every 1 min for 10 min, then every 5 min until 20 min, and then every 10 min until 100 min. For each mass measurement, the teabag containing SAPs is taken out of the solution, surface dried with Kimwipes to remove the excess fluid, and then its mass is measured. Teabags are immersed in the solution right after each mass measurement. The pore solution is sealed with Parafilm to prevent carbonation except for the mass measurement of teabags. Absorption is calculated as the ratio of measured wet mass to the dry mass of SAP. Two teabag tests are performed with each SAP and the average values are reported. There is very likely some liquid adsorbed onto the surface or trapped between particles; however, no pressure is applied to the teabag to avoid damage to the SAPs. The absorption of SAPs is also examined with microscopy and was consistent with the absorption obtained with the teabag method. This indicates that the amount of residual water in between SAP particles does not seem to be considerable to affect the results pertaining to the properties of the cement paste.

Mechanical pressure resulting from the weight of cementitious materials can significantly affect the absorption behavior of SAPs due to boundary constraint, particularly before the setting occurs. To elucidate the relation between mechanical pressure and the absorption behavior of SAPs, a custom made setup was devised as shown in Figure 2-14. The setup consists of an acrylic cylinder of diameter 19 mm attached at the bottom to a porous ceramic. The cylinder is filled with dry SAP1 up to an overall thickness of 3 mm. To simulate pressure on SAP1, varied weights are placed on top of the SAP

particles. A disk with a diameter slightly smaller than the cylinder diameter and with a thickness of 10 mm is cut from the porous ceramic and placed between the SAP1 particles and weights to allow flow of distilled water to the SAPs. In this configuration, SAP1 particles are assumed to be constrained in the lateral direction and subjected to a pressure in the vertical direction. Therefore, the swelling is permitted only in the vertical direction. In order to allow a uniform absorption from both the top and bottom of the SAP1, the cylinder is filled with distilled water and the porous ceramic base is placed in a container filled with distilled water. The absorption behavior of SAPs is measured by monitoring the change in the height of the porous disk with time. A camera is used to take images of the disk at various times and the height measurement is carried out by analyzing the images in MATLAB. The height measurement is used to estimate the change in the bulk volume of the SAPs.

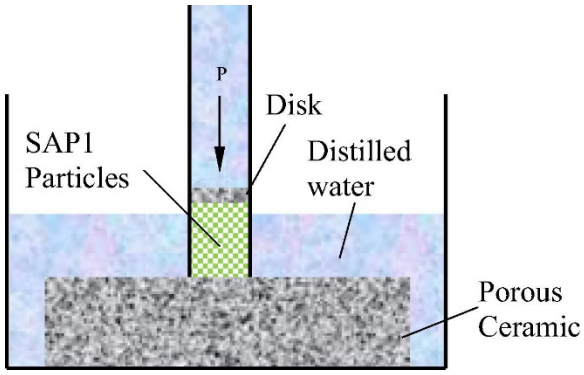

Figure 2-14 Schematic of hydrostatic pressure due to constrain and weight. (Adapted from [44]

Chapter 3: Mechanical effect on hydrogel absorption/desorption behavior

In this chapter, in the first two sections 3.1 and 3.2, the effect of pressure on swelling the SAP1 in distilled water and ionic solution is investigated. At the end, the so-called teabag test is utilized to compare the absorption kinetics and capacity of SAP1-4 in distilled water and extracted pore solution. In these two sections the commercial SAPs are used in order to make these set of observations and comparisons.

In Section 3.3, a synthesized hydrogel H-A is used in order to provide a mechanistic investigation of the desorption of hydrogels in contact with a porous cementitious materials. H-A swollen in sodium chloride solution is placed on top of the cement paste substrate to measure the kinetics and final state of desorption. Also, a fracture mechanics approach is utilized to investigate the thickness effect on desorption mechanisms (debonding). It is important to mention that the cement paste substrate is used as a porous ceramic and the chemistry of cement paste is not considered here, the effect of cement paste chemistry will be explained in detail in chapter 4.

3.1 The effect of mechanical pressure on absorption of hydrogels

The absorption behavior of SAP1 in distilled water under pressures of 0 kPa, 1.5 kPa, 2.2 kPa, and 3.4 kPa is shown in Figure 3-2 (a). The absorption is plotted in vol/vol dry. Only the initial absorption of SAP1 corresponding to 0 kPa pressure is shown in the figure; the equilibrium absorption under 0 kPa is expected to be close to that shown in Figure 3-2 (a) which is obtained using the teabag method. It is seen that the equilibrium absorption, as well as the absorption rate, of SAP1 decreased significantly with increasing external pressure. The dependence of absorption of SAP1 on the mechanical pressure due to constraint can be explained on the basis of the total free energy of a SAP viewed as

polymeric networks in a solvent. It can be shown that in a SAP's polymeric networks, the total stress is balanced with stress arising from the network stretching and osmotic pressure due to the mixing of the polymeric networks and solvent, ionic interactions, and chemical potential change in the solvent [184]. When SAPs are subjected to an external mechanical pressure, they reach their thermodynamic equilibrium at a lower absorption level corresponding to a lower volumetric swelling. The results presented here signify the importance of mechanical pressure on SAPs' response. SAPs can experience mechanical pressure in a cementitious material due to the weight of the mixture and hardening of the cement paste which exerts a constraint for the absorption of soft SAPs; it is expected that the pressure from the weight of cementitious materials would be higher than those studied here. In addition, SAPs can be constrained by the cementitious matrix with a varying stiffness, which increases rather quickly in the early hydration of the cement particles. In order to couple the mechanical pressure and ionic effect, the absorption behavior of SAP1 in distilled water under pressures of 0 kPa, 1.5 kPa, 2.2 kPa, and 3.4 kPa for different ionic solution is measured and shown in Figure 3-2 (b-d). Therefore, it is critical to account for the complex chemical and mechanical interactions occurring in a cementitious-SAP system in order to obtain a better understanding of SAPs behavior for internal curing applications.

In Figure 3-2 (e), it is illustrated that the final absorption capacity of SAP1 is almost the same for different ionic solution under high pressure. This can show that the effect of pressure can be more dominant for SAP1. Since the pressure in cement paste is expected to be higher, the chemo-mechanical coupling has an important role in absorption capacity. Also, in Figure 3-2 (b-d) the difference between 1.5, 2.2 and 3.4 kPa is negligible,

especially by increasing the pressure this difference becomes less dominant. This is evidence for low sensitivity of SAP1 to higher pressure in high concentration of ions.

(a)

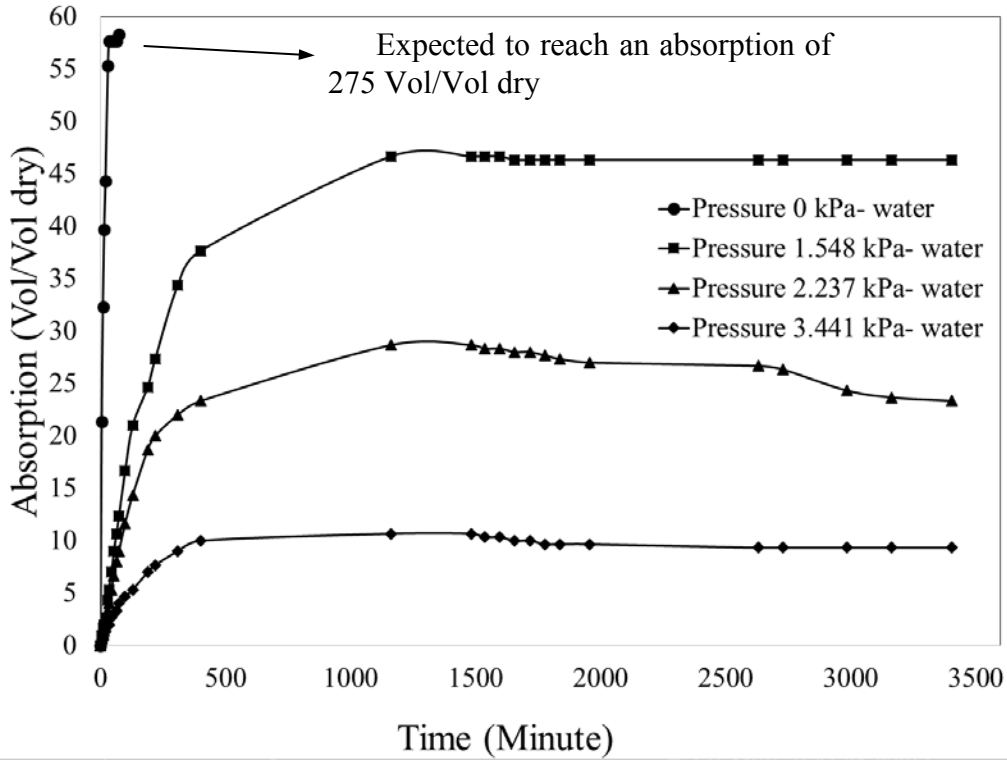

(b)

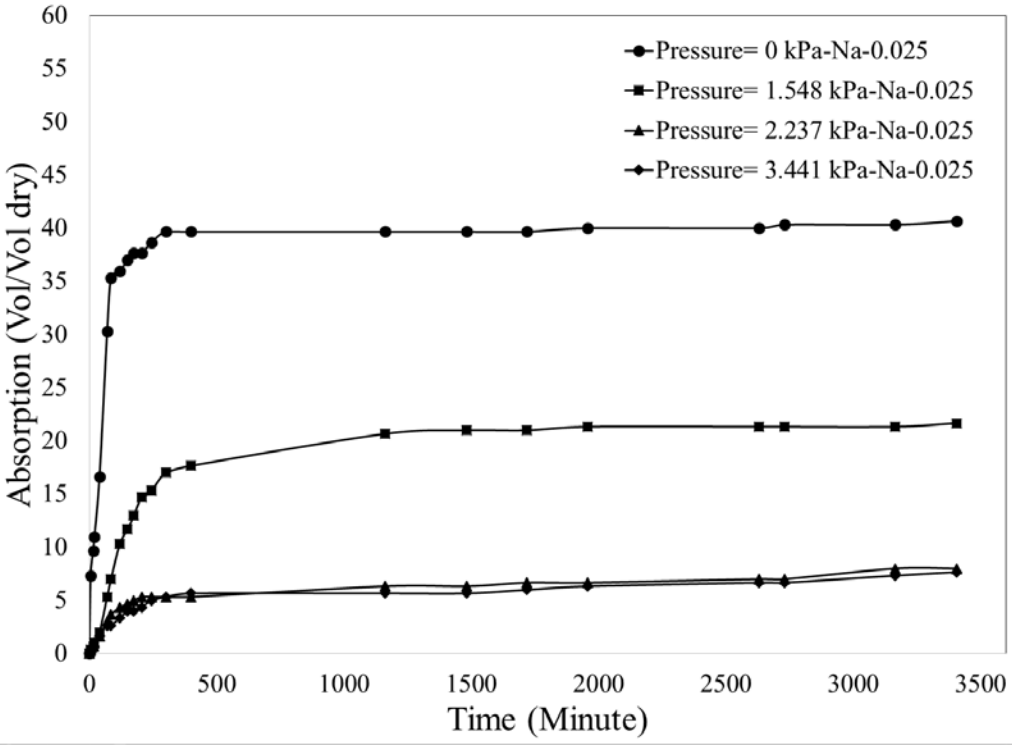

(c)

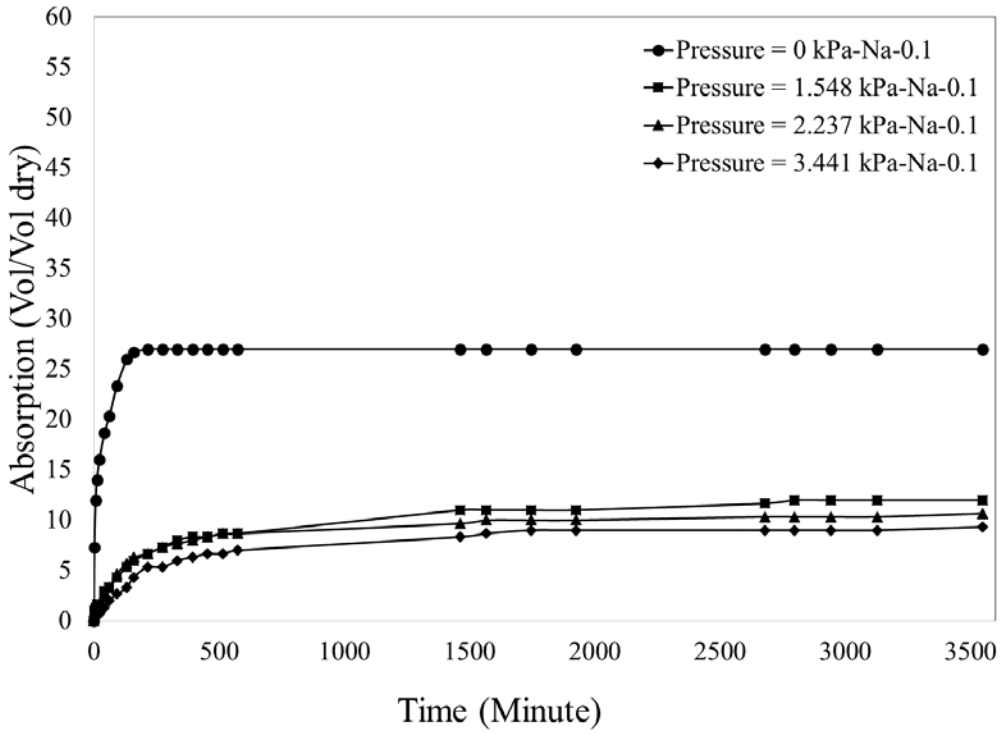
Pressure = 0 kPa-Na-0.1
Pressure = 1.548 kPa-Na-0.1
Pressure = 2.237 kPa-Na-0.1
Pressure = 3.441 kPa-Na-0.1
Absorption (Vol/Vol dry)
Time (Minute)
0
5
10
15
20
25
30
35
40
45
50
55
60
0
500
1000
1500
2000
2500
3000
3500

(d)

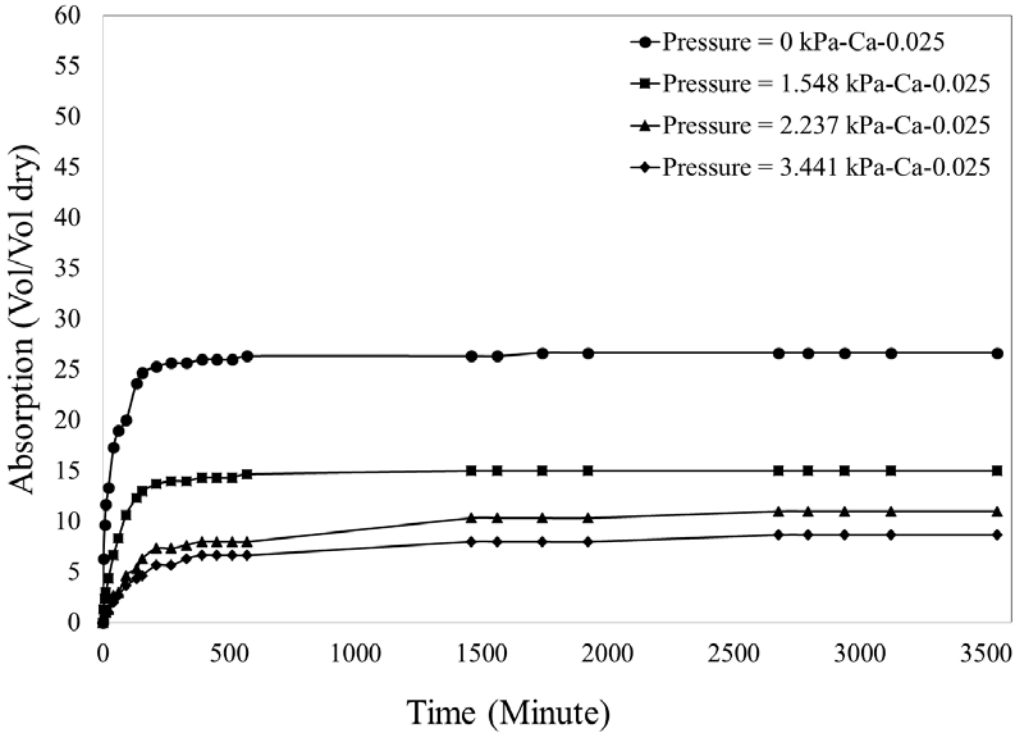
Pressure = 0 kPa-Ca-0.025
Pressure = 1.548 kPa-Ca-0.025
Pressure = 2.237 kPa-Ca-0.025
Pressure = 3.441 kPa-Ca-0.025
Absorption (Vol/Vol dry)
Time (Minute)
0
5
10
15
20
25
30
35
40
45
50
55
60
0
500
1000
1500
2000
2500
3000
3500

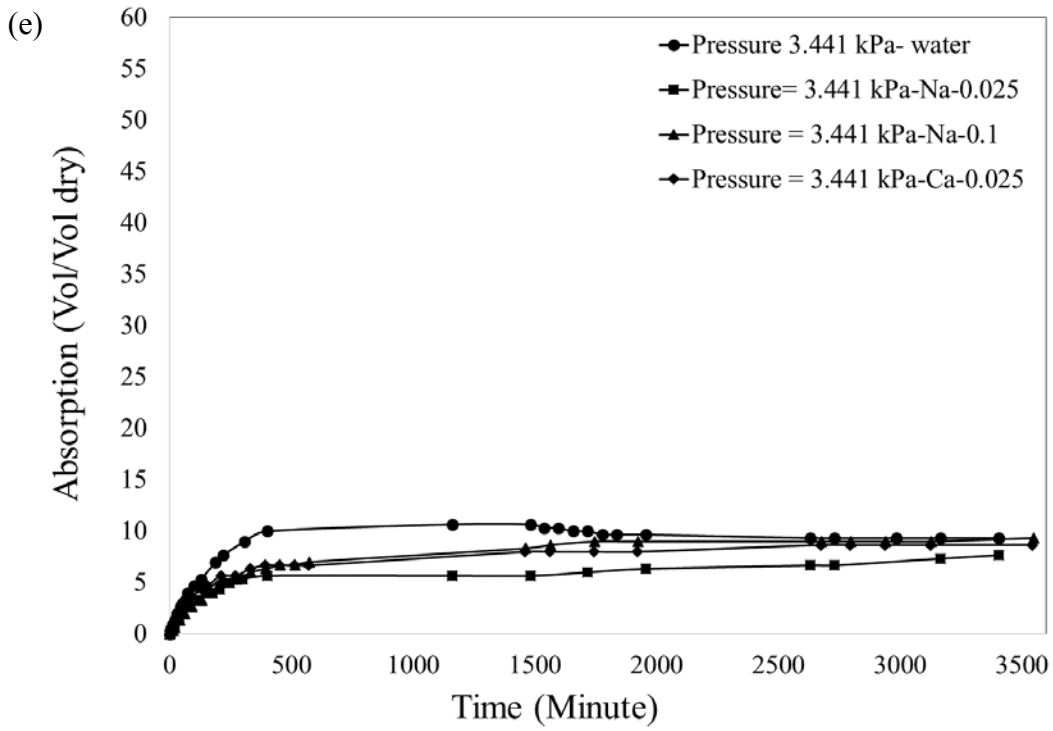

Figure 3-1 Absorption behavior of SAP1 under pressures of 0 kPa, 1.5 kPa, 2.2 kPa, and 3.4 kPa in (a) distilled water (Adapted from [44]), (b) $[Na^+] = 0.025$ (c) $[Na^+] = 0.1$ (d) $[Ca^+] = 0.025$ (e) absorption of SAP1 in distilled water, $[Na^+] = 0.025$, $[Na^+] = 0.1$, $[Ca^+] = 0.025$ under pressure of 3.4 kPa.

3.2 Comparison of absorption in distilled water and in extracted pore solution

The absorption behavior of SAP1-SAP4 in distilled water and the cement pore solution is shown in Figure 3-2 (a) and (b), respectively. There are evident differences observed in the behavior of SAPs in the two different environments, as seen in the figures. It is seen from Figure 3-2(a) that all SAPs show a large absorption in the range of 275–475 (g/ g dry) in distilled water. All SAPs reach their equilibrium absorption in distilled water during the measurement time. SAP3 exhibits the highest absorption and the highest absorption rate among all the SAPs. The high absorption of SAP3 can be attributed to its molecular

structure, as well as morphology, providing a large surface area in this SAP. SAP1 and SAP4 show a similar equilibrium absorption in spite of a different absorption behavior in the beginning. The behavior of SAPs in the pore solution reveal contrasting features from that in distilled water. All SAPs show desorption with time after a steep initial absorption. It is seen that the SAPs reach their absorption in the pore solution to be about 19 (g/g dry) and 27 (g/g dry) for SAP1 and SAP2, respectively, and about 6–9 (g/g dry) for SAP3 and SAP4. Interestingly, SAP2 exhibits the highest absorption and SAP3 reaches a modest absorption in the pore solution which can be due to ionic strength of the extracted pore solution. In fact, in next chapter by examining the varied chemical compositions of hydrogels, it reveals that Acrylic acid based hydrogels are more sensitive to ionic strength. The desorption of SAPs in the pore solution is related to the migration of ions from the pore solution into the SAPs, resulting in a screening effect, which reduces the electrostatic repulsion in the polymeric networks of the SAPs [121]. The initial steep increases in the absorption of SAPs in the pore solution could be due to a faster diffusion of water molecules than ions into the SAPs. This is supported by the observation from Figure 3-2 (a) and (b), where SAP3 show the highest absorption in the distilled water and the highest initial absorption in the pore solution. The large desorption of SAP3 and SAP4 in the pore solution can be attributed to a high composition of anionic acrylic acid monomers in these SAPs compared to SAP1 and SAP2. This behavior is in agreement with the observation by Schröfl et al. 2012 [120], where the relation between SAPs molecular structure and their absorption was studied. The results obtained from the absorption measurement indicate the strong dependence of SAPs behavior on the SAPs type, size distribution, and the

environment. These factors must be closely examined in the design of cementitious materials containing SAPs.

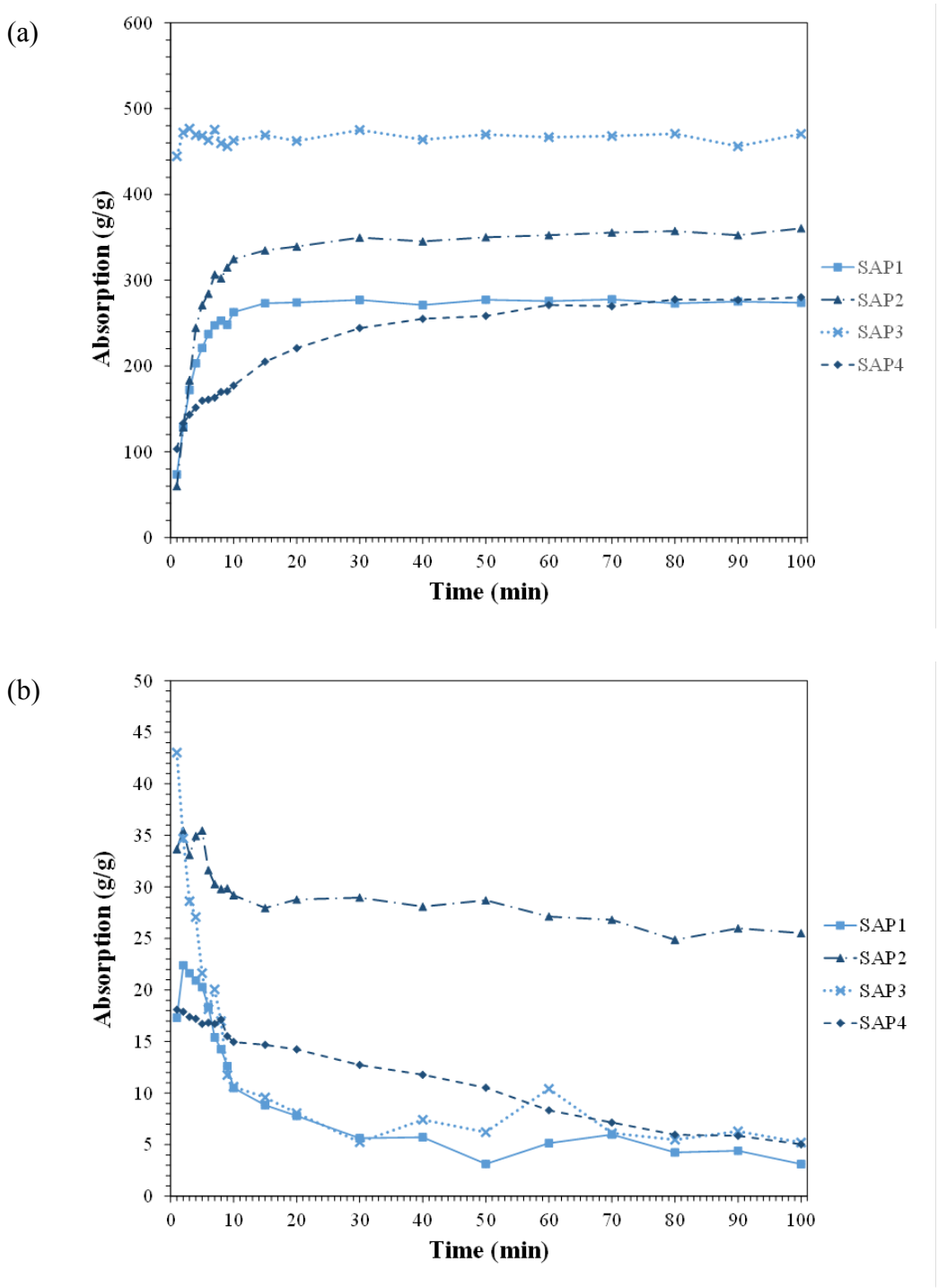

Figure 3-2 Absorption of SAPs in (a) distilled water and (b) an extracted cement pore solution. (Adapted from [44])

3.3 The effect of capillary forces on desorption of hydrogels in contact with porous ceramic (cement paste)

In the previous sections the importance of pressure and mechanical constraint was mentioned. Here in these sections, the mechanical effect related to the capillary forces, is explained in detail. As an initial observation a set of experimental tests are performed to obtain insight into plausible processes affecting the desorption of hydrogels in contact with cementitious matrix. In these set of experiments, cement paste substrates are considered as a porous ceramic with a very wide range of pore size distribution from nano to micro and macro scale. For comparison purposes, a micro-porous ceramic is also considered as a substrate.

The results of desorption of fully swollen block of hydrogels with contact with porous substrates are presented. The images showing the desorption of hydrogel blocks at various times are shown in Figure 3-3 (a). The images corresponding to the desorption of a hydrogel block without contact with a porous substrate is also included for comparison (the hydrogel sample is placed on top of a plastic mesh which is covered with a small amount of silicon oil in order to avoid any planar constraint). The variation of desorption with time is plotted in Figure 3-3 (b). It is interesting to note the significant difference in desorption between the hydrogel block with contact with the cementitious substrate and that with contact with microporous ceramic or without any contact. The change in the morphology of hydrogel block during desorption reveals interesting features. It is noted that the desorption of hydrogel block with contact with cementitious substrate occurs mainly in the thickness direction and the other dimensions of the block do not experience notable changes. On the other hand, the hydrogel block without contact and only exposed to air

undergoes changes in all three dimensions as a free deswelling situation. The hydrogel block with contact with cementitious substrate is subjected to the capillary forces at the interface and these forces provide adhesion between the hydrogel block and the substrate, thereby constraining the deformation in the planar dimension normal to the thickness direction. The significantly higher desorption rate of the hydrogel block with contact with the cementitious substrate compared to that without contact is attributed to the capillary effect. This can be evidence that the Laplace pressure developed on the hydrogel at the interface accelerates the desorption of the hydrogel block. Since the capillary force decreases with increasing pore size, higher capillary forces are expected to develop in cementitious substrate with nanoscale pores than in the ceramic substrate with microscale pores. Also, it is seen from Figure 3-3 (a) that the hydrogel block with contact with the microporous ceramic exhibits some changes in the planar dimension. This indicates a smaller adhesion at the interface due to smaller capillary forces as discussed previously. The hydrogel which is used in these tests is H-A which is fully swollen in distilled water. Substrates (both ceramic and cement paste) are polished using SiC sand papers with varying grit sizes of 80, 180, 320, 600, and 1200 and the experiments are carried out in a drybox with fixed RH-value and no air flow. Duplicated samples are used which are in a great agreement.

As observed from these sets of experiments, the effect of interfacial bonding and boundary constraint can be very critical in regard to desorption behavior of hydrogels in cementitious materials. In order to gain an in-depth understanding of the desorption behavior of hydrogels in cementitious materials further investigations were performed which are explained in detail in the next sections [185].

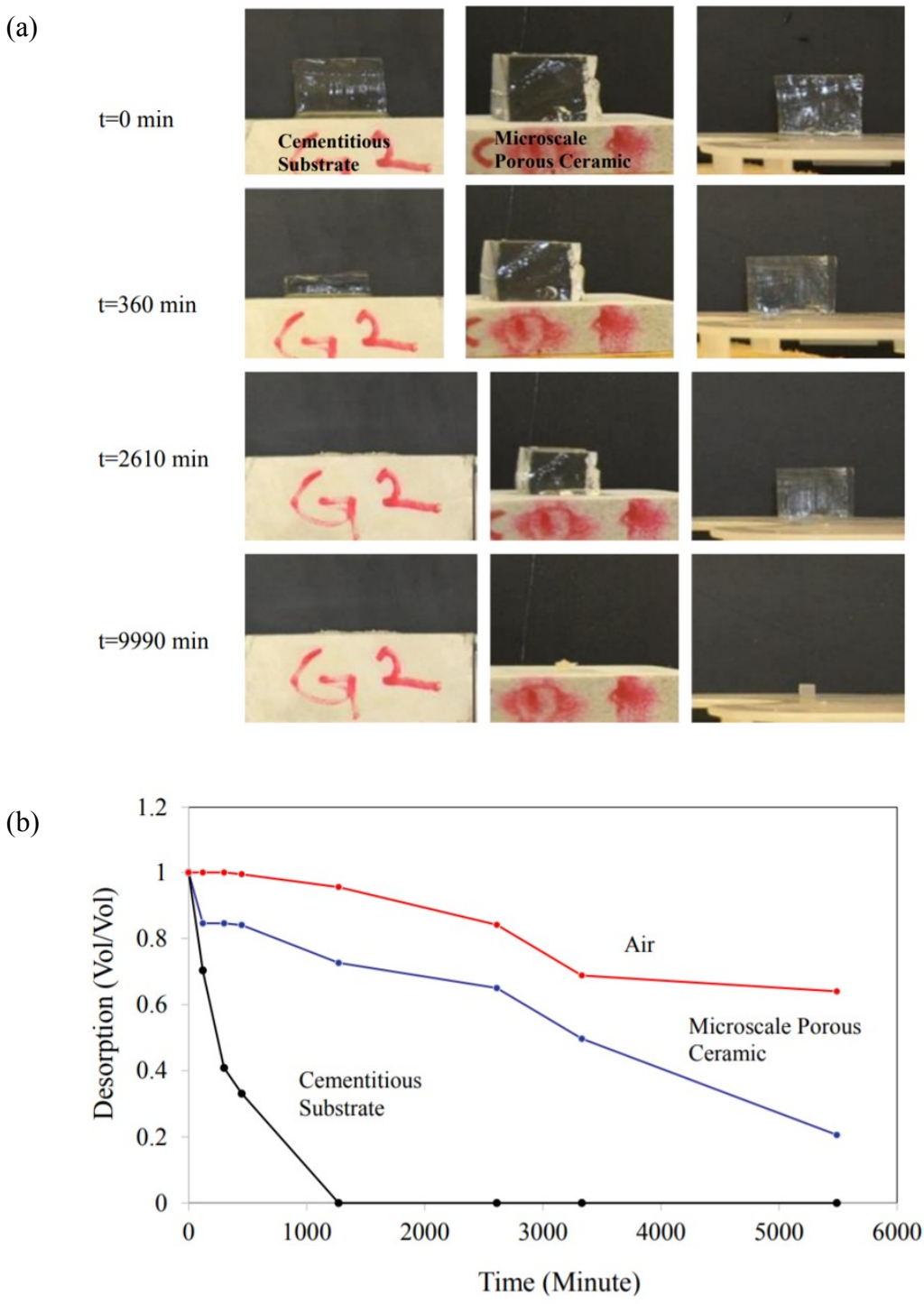

Figure 3-3 (a) Images showing the desorption with time of hydrogel blocks with contact with a cementitious substrate (left), a microscale porous ceramic (middle), and without contact with a porous substrate (right). (b) Desorption of hydrogel blocks indicating the effect of capillary forces. (Adapted from [185])

3.3.1 Desorption of hydrogel layers

The height profiles of H-O, H-0.25, H-0.45, and H-0.65 along a line bisecting the hydrogel layers, corresponding to the initial and final desorption in the 95% relative humidity level, are shown in Figure 3-4 (a-d). The hydrogel used in this section is H-A and in order to simplify name designation, they are referred to their substrate i.e. H-0.25 referred to H-A placed on top of the cement paste substrate with water to cement ratio of 0.25 (H-O is referred to H-A placed on top of the plastic mesh). A 3D reconstruction of H-0.65 at the initial time is shown in Figure 3-4 (e). The line used in extracting the height profiles is marked with a dashed line in Figure 3-4 (e). It is noted from Figure 3-4 (a-d) that desorption in H-O occurred uniformly in all dimensions, while H-0.25, H-0.45, and H-0.65 remains adhered to the substrate in all relative humidity levels and the desorption is primarily in the thickness direction. The desorption - volume change normalized with respect to the initial absorbed volume - of the hydrogel layers as a function of time measured using optical profilometry is given in Figure 3-5 (a-c). It is seen from Figure 3-5 (a-c) that desorption is fast in the beginning and then reaches a final value after which no significant changes are observed. The final desorption of H-O is lower than that of H-0.25, H-0.45, and H-0.65 in all relative humidity levels. As mentioned earlier, desorption in H-O occurred only from one side (the top surface) via evaporation and the bottom surface is insulated as a result of contact with the Teflon substrate. This difference in boundary conditions is expected to affect only desorption rate in the early stage. However, the final equilibrium desorption of H-O is not expected to be affected by this. The difference observed in the final desorption between the hydrogel layers with contact and without contact with a cementitious material has an important implication in the design of

hydrogels as internal curing agents. This is particularly important as desorption of hydrogels is usually characterized in controlled relative humidity conditions [186,187]; however, in applications where hydrogels are embedded in a porous cementitious matrix, this can lead to inaccuracies in the characterization of the desorption behavior of hydrogels.

The adhesion between the hydrogel layers and cementitious material substrates is mainly attributed to the capillary suction at the interface between the hydrogel layers and the porous substrates. In the hydrogels with contact with the cementitious material substrates, the capillary suction is large enough to produce an adhesion force preventing changes in the in-plane dimensions of the hydrogel layers. It should be noted that other physical or chemical bonds between the hydrogel layers and the solid portion of the cementitious material substrate can exist. As discussed later, an increase in the adhesion force with increasing capillary pores and concomitant decreasing solid portion of the cementitious substrate is observed, indicating the dominant role of the capillary adhesion compared to other types of bonds.

The effect of the in-plane constraint, as a result of capillary adhesion, on the desorption of hydrogel layers can be discussed using a mechanistic analysis of the desorption of free and constrained hydrogel layers. A detailed analysis comparing the swelling of free and constrained hydrogel layers was discussed in [188] and is not repeated here. Adapting their analysis to a case where deswelling rather than swelling occurs, the ratio of equilibrium volumetric desorption in constrained condition to that in free condition can be estimated from the following equation:

$$\text{Constrained Desorption/Free Desorption} = (1 + \upsilon) / [3(1 - \upsilon)] \quad (5)$$

where υ is the Poisson's ratio of the hydrogel. It is seen from the above equation that the ratio of constrained to free desorption is about 2/3 assuming a typical value of 1/3 for the Poisson's ratio of the hydrogels. It is realized from this ratio that the desorption of a constrained hydrogel layer is lower than that of a free hydrogel layer. Thus, in light of this result, it is expected that the hydrogel layers in contact with the cementitious material substrate undergo a lower desorption than the hydrogel layers without contact at equilibrium. However, as noted previously, the experimental results presented in Figure 3-5 (a-c) indicate an opposite trend and show a higher desorption of the hydrogel layers with contact with the cementitious material substrates.

Now, we try to explain the increase in the desorption of the hydrogel layers with contact with the cement paste substrates. The final desorption value of the hydrogel layers is determined by the thermodynamics of equilibrium of hydrogels interacting with the surrounding medium. We propose the capillary adhesion as the reason for the increased final desorption of H-0.25, H-0.45, and H-0.65, compared to H-O. Due to the Laplace pressure P_{Lap} in the pore fluid as a result of a meniscus formation, a contact pressure is developed between the hydrogel and the solid skeleton of the porous cementitious substrate squeezing the hydrogel. A schematic showing the Laplace pressure and contact pressure developed at the interface between the hydrogel layer and the cementitious material substrate is depicted in Figure 3-6. Since the hydrogels consist of polymeric networks and water, the Laplace pressure in the meniscus acts inside the hydrogel attempting to pull water out of the hydrogel. This means that in the presence of the Laplace pressure the equilibrium osmotic pressure occurs at a lower concentration of the fluid in the hydrogel than when there is no Laplace pressure. This mechanism is proposed to be the driving force

for the increased desorption of the hydrogel layers with contact with the cement paste substrate. Our attempt to detach similar hydrogel layers from the substrates resulted in fracture in the bulk of the hydrogel layers indicating strong adhesion at the interface. The influence of the capillary forces on the adhesion of a hydrogel sphere to a solid substrate and resulting desorption due to the Laplace pressure is theoretically studied recently [189].

It is noted that the ionic composition of the pore solution plays an important role in the absorption/desorption behavior of hydrogels, as demonstrated in the previous studies [34,42,43,120,122,132]. However, the main focus here is to examine, in detail, the effect of the capillary forces on the desorption of hydrogels and highlight the mechanisms involved at the interface between the hydrogel and a porous cementitious material. The general observations regarding the role of the capillary forces on accelerating the desorption, the final desorption value, and the adhesion at the interface can be applied to general hydrogels in contact with a cementitious porous substrate. Of course, the magnitude of the influence of the capillary forces on desorption is affected by the water content of hydrogels, the chemical composition of hydrogels, the ionic composition and pH of the solution, and other factors. In addition, our desorption results of hydrogels swollen in cement pore solutions (not shown here) indicates a similar accelerating effect of the capillary forces on the desorption of hydrogels as shown in Figure 3-5 (a-c).

It should be mentioned that in addition to its effect on the thermodynamic equilibrium of the hydrogel desorption, the Laplace pressure may also affect the diffusion rate of the fluid in the hydrogels near the interface during desorption. The effect of mechanical stress on the diffusion process in hydrogels and other material systems has been investigated in the past [190].

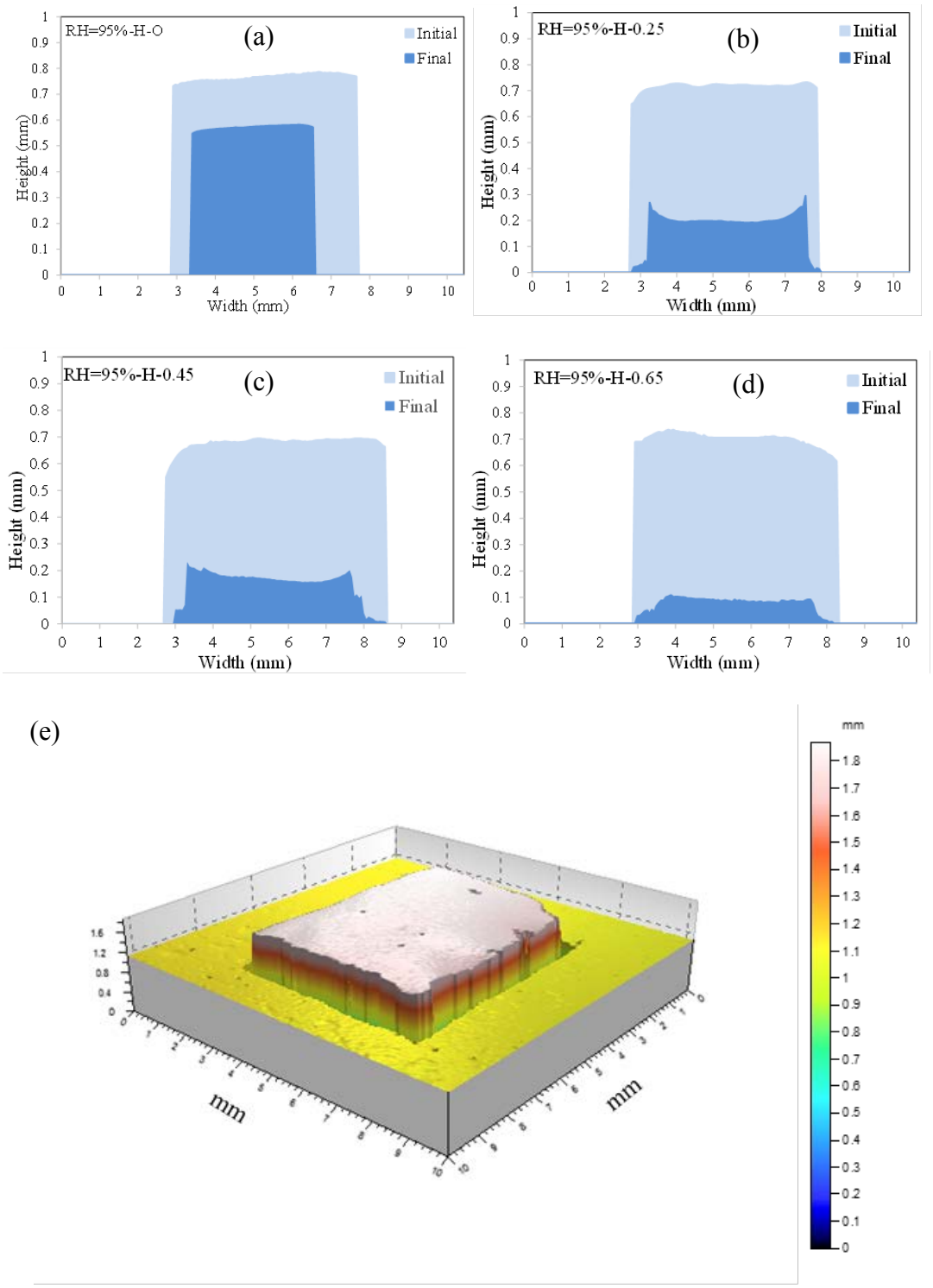

Figure 3-4 Initial (light colored) and final (dark colored) profiles of (a) H-O, (b) H-0.25, (c) H-0.45, and (d) H-0.65 during desorption in the relative humidity level of 95% obtained using optical profilometry. (e) 3D reconstruction of H-0.65 at the initial stage. (Adapted from [191])

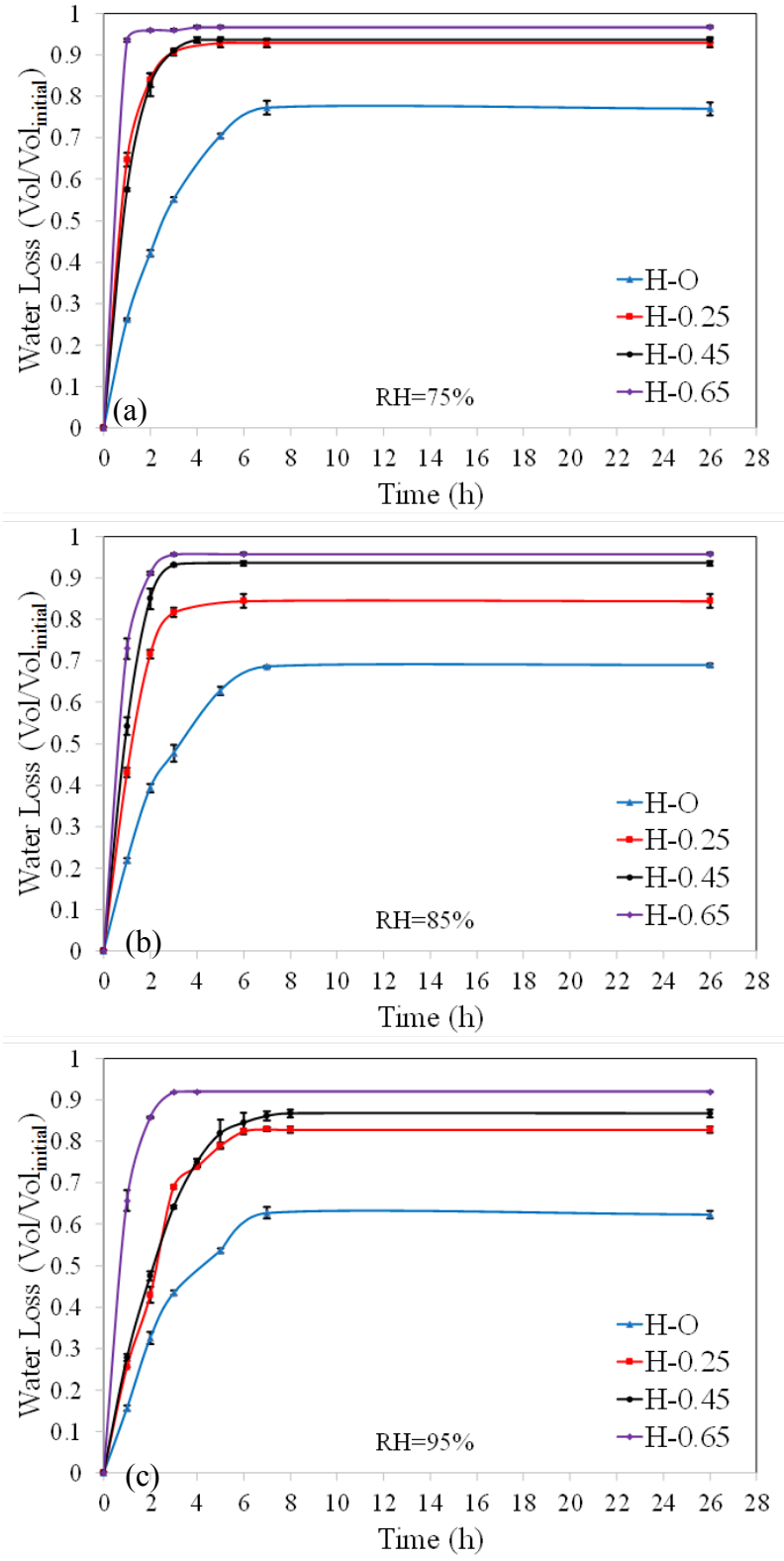

Figure 3-5 Variation of water loss with time of the hydrogel layers in the (a) 75%, (b) 85%, and (c) 95% relative humidity levels. The error bars represent standard errors. (Adapted from [191])

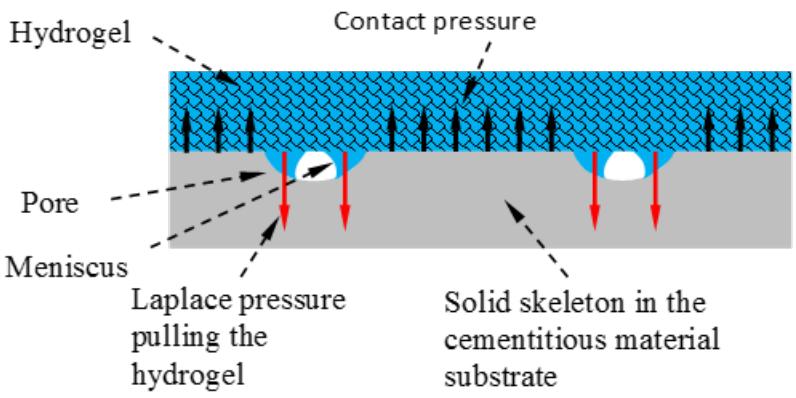

Figure 3-6 Schematic showing the development of the capillary adhesion at the interface between the hydrogel layer and substrate. The Laplace pressure pulls the hydrogel and provides the adhesion force at the interface. (Adapted from [191])

In Figure 3-7 (a-c), the effect of relative humidity is illustrated. The results that is measured and indicated in Figure 3-5 (a-c) are rearranged to elucidate the effect of relative humidity. As it is expected, the desorption of hydrogel on each specific cement paste substrate (CM-0.25, CM-0.45 and CM-0.65) is affected by relative humidity as another motivation. By increasing the relative humidity the both kinetics and final thermodynamic equilibrated state of desorption is decreased. It is interesting that by increasing the cement paste substrate water to cement ratio from 0.25 to 0.65, the difference between varied relative humidity are getting less. In other word, by increasing the water to cement ratio as a motivation force (capillary forces), the effect of relative humidity as another motivation get less pronounced. This evidence can show the importance of capillary pressure as a motivation for desorption.

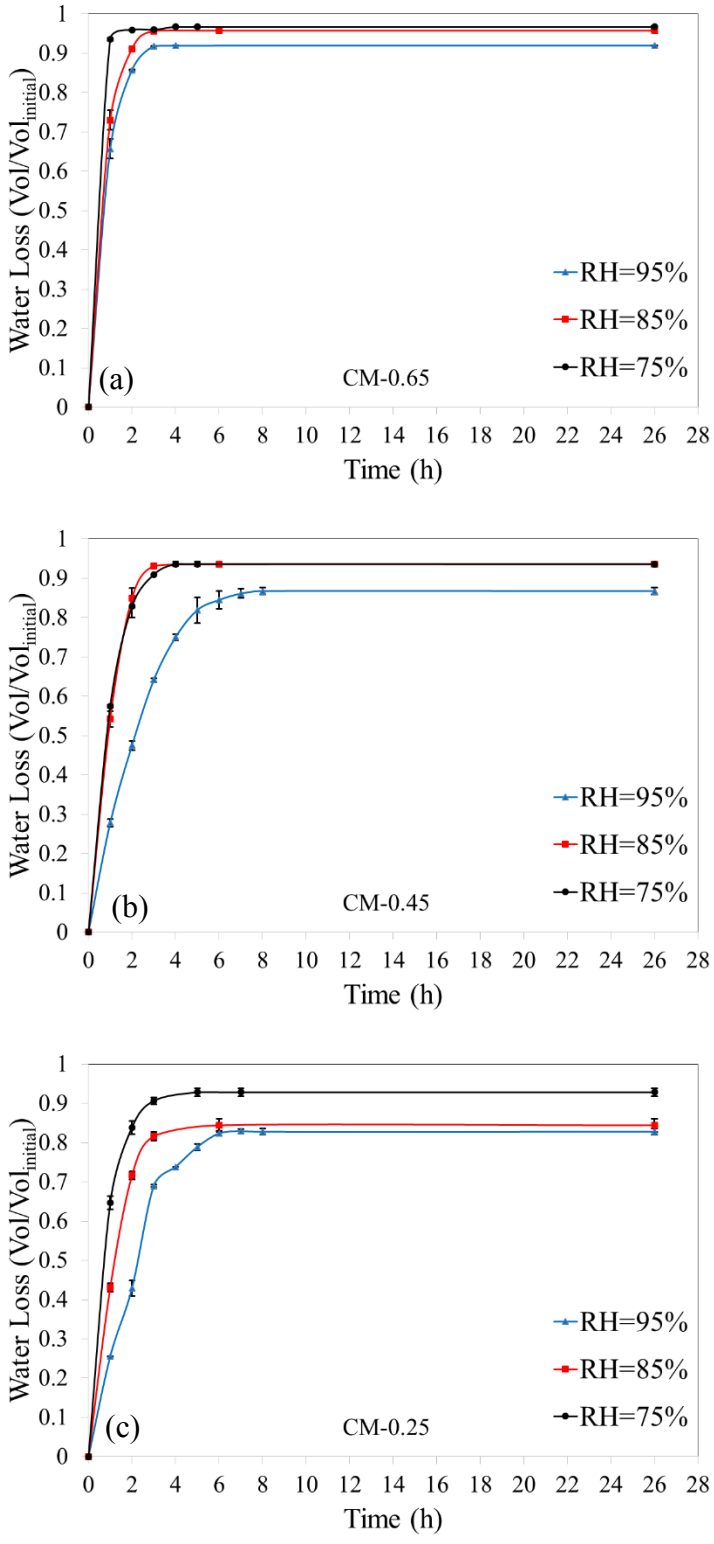

Figure 3-7 Variation of water loss with time of the hydrogel layers on the (a) CM-0.65, (b) CM-0.45, and (c) CM-0.25 for different RH. The error bars represent standard errors.

3.3.2 Effect of microstructure and relative humidity

The effect of the microstructure and relative humidity of cementitious materials on the desorption of hydrogels is discussed here. A reduction in the final desorption with increasing relative humidity level is evident from Figure 3-5 (a-c) and Figure 3-7 (a-c). It appears from Figure 3-5 (a-c) and Figure 3-7 (a-c) that the difference between the desorption of H-0.25, H-0.45, and H-0.65 decreases with decreasing relative humidity level.

The Laplace equation for a circular cylindrical pore with a radius of r is written as $\sigma = 2\gamma/r$. It can be seen from this equation that the Laplace pressure drops with increasing pore size. Pore size distribution can be used to relate the dependence of capillary forces on the microstructure of the cementitious materials with varied water to cement ratios. The bulk porosity of the cementitious substrates with a water to cement ratio of 0.65, 0.45, and 0.25 is measured to be 38%, 33%, and 18%, respectively, using MIP. The results indicate that the density of the capillary pores in the range of 100-300 nm reduces with decreasing water to cement ratio of the substrates. Thus, at a constant relative humidity level, the number of capillary pores that can exert the capillary suction is expected to increase with increasing water to cement ratio resulting in higher desorption in H-0.65 than in H-0.45 and H-0.25. This is in agreement with the observations made from Figure 3-5 (a-c).

With a reduction in relative humidity, finer pores are gradually emptied and contribute to the capillary suction on the hydrogels, and as a result increase the desorption of hydrogels. An increase in desorption with decreasing relative humidity levels can be realized from the results shown in Figure 3-5 (a-c).

It is important to note that the rate of water transport through the porous substrates is much faster than the hydrogel desorption rates shown in Figure 3-5 (a-c). A water reservoir of the same dimensions as the hydrogel layers is measured to desorb and disappear in the substrates in about five minutes. Therefore, the difference in the desorption rate of the hydrogel layers in contact with different substrates is controlled by the capillary suction at the interface rather than the water transport rate through the substrates. The results of MIP experiments is illustrated in Figure 3-8.

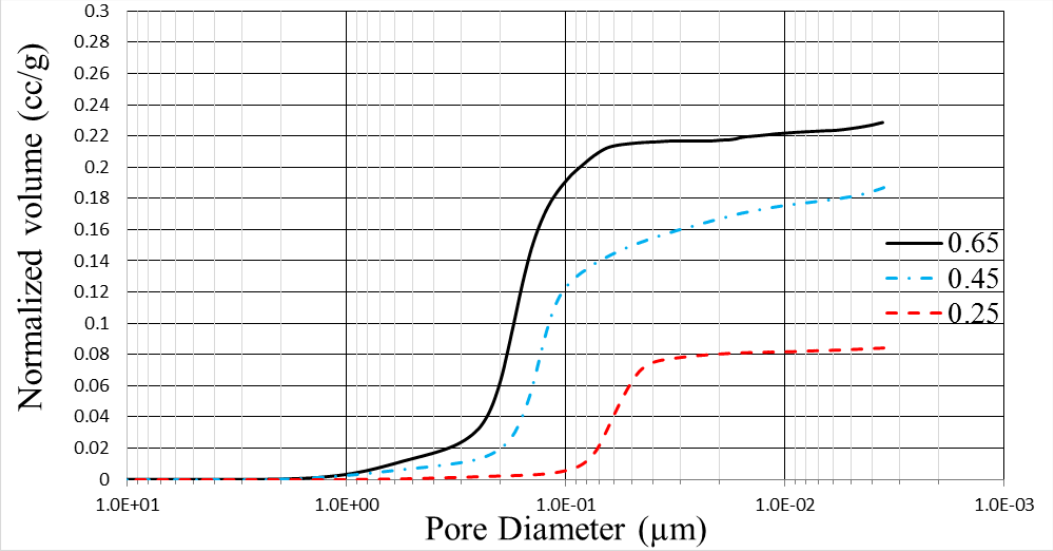

Figure 3-8 Normalized volume vs pore diameter for CM-0.25, CM-0.45 and CM-0.65

The results corresponding to the desorption of the hydrogel layers in contact with cementitious material substrates with SRA, as described before, in 75% relative humidity indicated a reduction in both final desorption value and desorption rate compared to the substrates without SRA. The reduction in desorption was 6 ± 1%, 12 ± 1.2%, and 13 ± 1.5% corresponding to H-0.25, H-0.45, and H-0.65, respectively. The reduction increased with increasing water to cement ratio. The reduction in the desorption of the hydrogel layers in the presence of SRA is attributed to a decrease in the surface tension of the pore

fluid. It should be noted that the concentration and ionic strength of the pore solution could affect the capillary forces [14,192]; however, these effects are not investigated in this study.

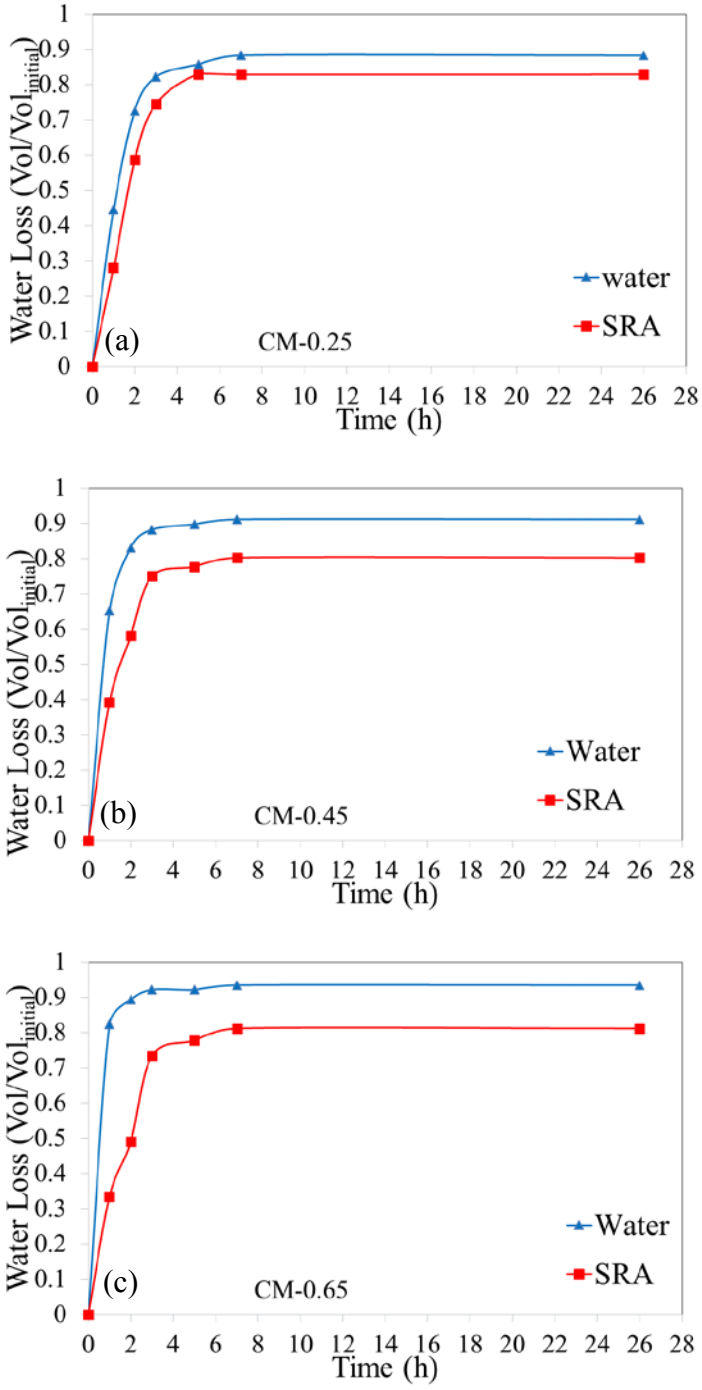

Figure 3-9 Variation of water loss with time of the hydrogel layers on the (a) CM-0.25, (b) CM-0.45, and (c) CM-0.65 for water and SRA substrate samples.

3.3.3 Effect of thickness

In this section, the effect of thickness on the desorption of the hydrogel layers is discussed. The desorption behavior of the hydrogel layers with a 3 mm thickness (in swollen state) in contact with CM-0.25 and CM-0.65, as well as without contact with the cementitious material substrate is shown in Figure 3-10. The results correspond to a relative humidity level of 95%. The desorption results of the thin hydrogel layers with a thickness of 0.7 mm are also included in this figure for comparison. Only the desorption results during the first 26 h are presented in Figure 3-10 since the thick hydrogel layers required a long time to reach the final equilibrium desorption. It can be seen that the rate of desorption exhibits a noticeable reduction after about 3 h in the case of the thick hydrogel layers with contact with cementitious material substrates (3mm-H-0.25 and 3mm-H-0.65), and about 8 h in the case without contact with a cementitious material substrate (3mm-H-O).

The difference in the desorption of the hydrogel layers with different thicknesses is evident from this figure. The desorption rate of thick hydrogel layers (3mm) is lower than that of the thin hydrogel layers (0.7mm). This is to be expected from the size dependence of bulk diffusion in the hydrogel layers. The desorption of the hydrogel layers without contact with a cementitious material substrate can be used to infer the effect of size on the diffusion of fluid in the hydrogel layers during desorption. The final equilibrium desorption of both 0.7mm-H-O and 3mm-H-O was close about 0.63 (Vol/Vol_{intial}). The former reached this equilibrium desorption after about 26 h and the latter after 360 h. The hydrogel layers with contact with the cementitious material substrates reveal interesting differences in the behavior of these hydrogel layers besides the effect of size on bulk diffusion. It is observed that the difference between the desorption of thin and thick layers appeared to be

larger in the case of CM-0.25 than CM-0.65. This observation can be attributed to the larger number of capillary pores that can exert suction at the interface in the case of the hydrogel layers with contact with CM-0.65 than that with contact with CM-0.25, thereby resulting in higher desorption. More interestingly, debonding is observed to occur in the thick layer with contact with CM-0.25, as shown in Figure 3-10. A noticeable change in the desorption rate of this hydrogel layer is noticed when the debonding initiated. The onset of debonding is marked in the figure. This reduction in the desorption rate can be realized in view of the fact that the Laplace pressure no longer contributed to the desorption of the debonded portion of the hydrogel layer. It is noted that after the initiation of debonding the desorption rate of 3mm-H-0.25 and 3mm-H-O appeared to be parallel indicating a similar desorption rate after the debonding. No debonding is observed in the thin or thick hydrogel layers with contact with CM-0.65, due most likely to stronger capillary adhesion at the interface.

The observed debonding of the thick hydrogel layer and its influence on desorption highlight the importance of size effect and interfacial bonding in the desorption of hydrogels and this can have implications in the design of superabsorbent hydrogels for internal curing. The effect of size and interfacial bonding can be explained by fracture mechanics. The energy release rate G_d associated with a debonding crack at the interface of a hydrogel layer bonded to a rigid substrate is given by

$$G_d = \frac{(1-\upsilon^2)\sigma_{xx}{}^2 h}{2E} \tag{6}$$

where σ_{xx} is the biaxial stress in the layer, h is the layer thickness, and E and υ are the Young's modulus and Poisson's ratio of the layer, respectively. It is seen from this equation that debonding occurs if $G_d > \Gamma$, where Γ is the interfacial toughness at the interface. The size dependence of G_d can be realized from this equation as G_d increases with increasing

thickness of the hydrogel layer. Therefore, it is expected that at the same desorption state, and therefore the same stress level, a thick hydrogel layer has a higher propensity to debonding than a thin hydrogel layer. This result provides an explanation for the debonding of the thick hydrogel layer as observed in the experiment and shown in Figure 3-10.

The thick hydrogel layer in contact with CM-0.65 remains adhered to the substrate and does not experience debonding at the interface. However, in the case of the thick hydrogel layer in contact with CM-0.25 debonding is observed after about 3 h from the start of desorption. Therefore, it can be inferred that the interfacial strength is higher in the case of the thick hydrogel layer with contact with CM-0.65 than the thick hydrogel layer with contact with CM-0.25. Since the interfacial toughness is directly related to the capillary adhesion at the interface, the above observation indicates stronger capillary adhesion in the case of the hydrogel layers with contact with CM-0.65 than the hydrogel layers with contact with CM-0.25. Thin hydrogel layers with contact with CM-0.25 and CM-0.65 remains adhered to the substrate. Thus, it is expected that the energy release rate is lower than interfacial toughness in thin layers with contact with substrates in both CM-0.25 and CM-0.65. This is conceivable due to the small thickness of the hydrogel layers. In addition to the size effect, the influence of mechanical properties e.g., E and ν, can also be appreciated from the above equation. The experimental observations coupled with the fracture mechanics analysis presented above highlight the potential effect of size on the desorption of hydrogels beyond the known size dependent diffusion behavior of hydrogels.

It should be noted that the shape of hydrogels can affect the analysis presented above; however, the size dependent fracture argument can be generalized to different geometries.

The emphasis here is to demonstrate, from a mechanics point of view, how the interplay between size and interfacial bonding strength could influence the desorption of hydrogels.

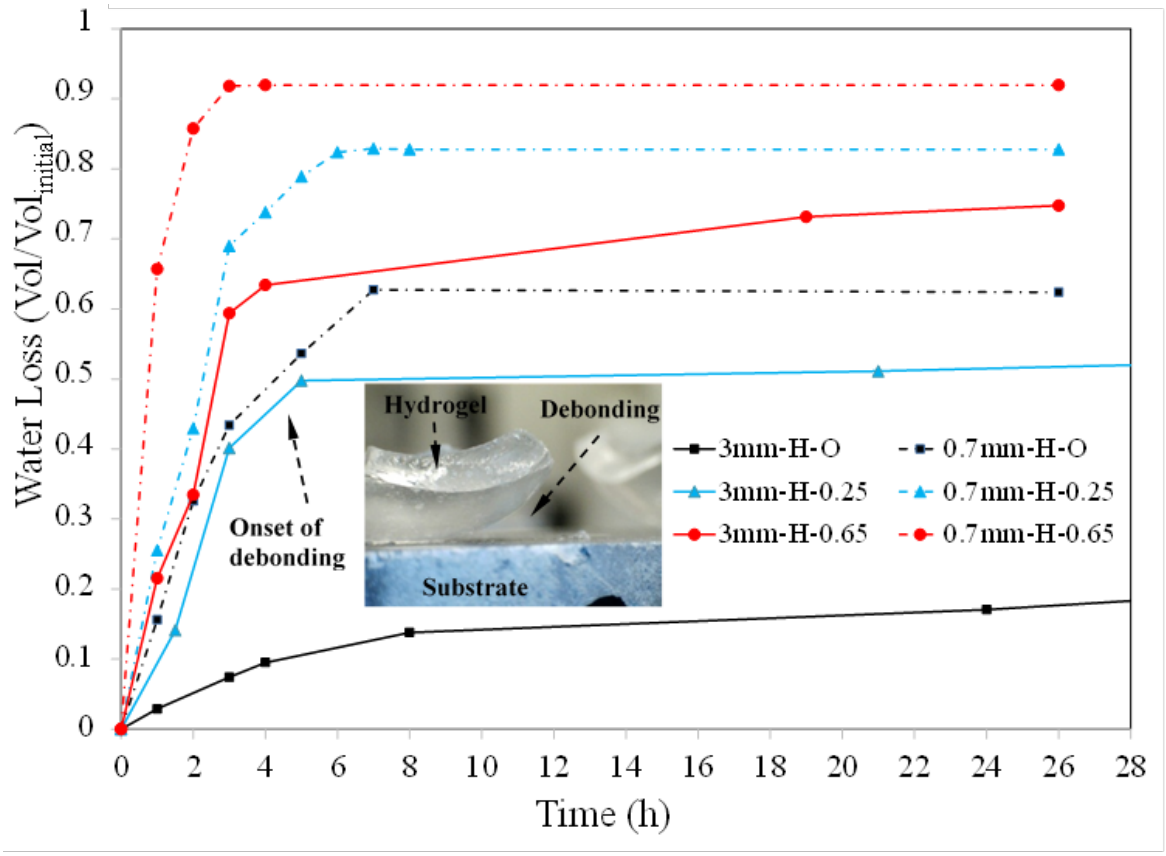

Figure 3-10 Effect of size on the desorption of the hydrogel layers with contact with cementitious material substrates. Debonding at the interface between the thick hydrogel layer (3mm-H-0.25) and the substrate is illustrated. (Adapted from [191])

3.3.4 Desorption of embedded hydrogels in cementitious materials

The SEM examination of hydrogel particles in a cementitious material matrix reveals interesting features worth noting. The majority of the desorbed hydrogel particles exhibits a shell-like morphology where the desorbed hydrogel particles appeared to remain bonded to the cementitious matrix while reducing size during desorption. A SEM image showing

a desorbed hydrogel particle in the cementitious matrix is presented in Figure 3-11 (a). The shell-like morphology is also observed in the SEM images of several other regions in the microstructure to obtain a realistic representation of the microstructure. This morphology of desorbed hydrogel particles in the cementitious matrix is in contrast with that of initially dry hydrogel particles possessing a solid morphology. The size of the voids surrounding hydrogel particles in the cementitious matrix can be used to infer the maximum absorption of the hydrogel particles in the cementitious matrix during hydration and before setting. It appears from the SEM image that the reduction in size as a result of desorption occurs through formation of a fracture (cavity formation) in the hydrogel particle and subsequently, reduction in volume continued while the particle remained mostly bonded to the cementitious matrix. Tensile stress developed during the reduction in size of the hydrogel particle bonded to the cementitious matrix is most likely responsible for the observed fracture. A schematic showing the observed desorption of hydrogel particles in a cementitious matrix is shown in Figure 3-11 (b) (top row). The morphology of the desorbed hydrogel particles would be different if the hydrogel particles become debonded at the interface with the cementitious matrix and an isotropic reduction in the size of the hydrogel particles would be expected (see Figure 3-11 (b), bottom row). In this case, the desorbed hydrogel particles would be expected to return to a size similar to their initial size before fluid absorption and desorbed hydrogel particles would not take a shell-like morphology and rather have a solid morphology. It should be noted that the initial shape of solid hydrogel particles before absorption is expected to influence the morphology of desorbed hydrogel particles. In addition, the view orientation of hydrogel particles in SEM images could affect the appearance of desorbed hydrogel particles and this should be taken with

care in the interpretation of images. In this study, a large number of desorbed hydrogel particles (more than 30) are imaged to account for this variability in the discussion presented above.

The SEM micrographs showing the cross section of the two hydrogel micro-strip, namely Hydrogel A and Hydrogel B, are shown in Figure 3-12 (a) and (b), respectively. SEM examination is conducted on six replicates for each hydrogel and similar features are observed. These images correspond to near desorbed state of hydrogels. The following observations are made:

- It is interesting to note the sharp contrast in the morphology of the two hydrogels. The cross section of Hydrogel A shows a solid morphology with a relatively uniform reduction in size in both directions. On the other hand, Hydrogel B shows a thin shell-like morphology. The cross section of Hydrogels A and B is delimited with a dashed red line to aid in visual examination. The thickness of the shell-like hydrogel B is about 50 μm. The morphology of Hydrogels A and B resembles the two desorption modes illustrated in the top and bottom rows, respectively, of Figure 3-11 (b). It is observed that debonding occurred between Hydrogel A and the cementitious matrix and the desorption continued with a relatively uniform reduction in size. On the other hand, Hydrogel B appears to have maintained bonding, over a portion of its surface, to the matrix.
- As shown previously in Figure 3-5 and Figure 3-10, the contact between hydrogels and a cementitious matrix plays an important role in the desorption of the hydrogels. Thus, it is expected that the different desorption modes and

interaction at the interface between the hydrogels and cementitious matrix influence their desorption behavior. To ensure that the shell-like morphology of Hydrogel B is due to interaction with the cementitious matrix, the two hydrogels are first swollen in a synthetic pore solution with a pH of 13.7 and compositions of $[Na^+]$=400 mM, $[K^+]$=400 mM, $[Ca^{2+}]$=1 mM. Then the hydrogels are dried in 55% relative humidity for two days and then in an oven at 40℃ until no change in mass was realized. Both hydrogels show a similar solid morphology and no indication of a shell-like morphology is observed.

- The reason for the observed debonding in Hydrogel A and bonding in Hydrogel B is expected to be attributed to the difference in the chemical composition of the two hydrogels. A potential reason for the observed debonding in Hydrogel A could be early desorption due to the interaction between the hydrogel and the pore solutions before the onset of setting and loss of relative humidity in the matrix. The dependence of hydrogels' chemical composition on the interaction between hydrogels and a pore solution has been examined in the previous studies [34,42,43,120,122,132]. It is shown that hydrogels with a higher relative concentration of acrylic acid to acrylamide tend to show a rapid release in a pore solution. In a recent study [164], the desorption of two hydrogels with different chemical compositions is studied using neutron radiography. Their results indicated an early desorption of the hydrogel with only acrylic acid as the main monomers and retention of water in the hydrogel with both acrylic acid and acrylamide monomers up to the percolation threshold of the cementitious matrix. Similar desorption behaviors of the same two hydrogel

types are realized using rheological measurements [28]. However, the dependence of bonding between the hydrogels and a cementitious matrix on chemical composition is not addressed in the previous studies.

- These investigations indicate a tendency to bond between the hydrogel and a cementitious matrix with increasing relative concentration of acrylamide in the hydrogels. A systematic study on the relation between the chemical composition of hydrogels and their desorption in a cementitious matrix is explained in the next chapter and will be presented in details. The different mechanisms of desorption highlighted above can certainly have important implications in the behavior of hydrogel particles as internal curing agents. As mentioned previously, desorption of hydrogels is typically investigated in air under controlled relative humidity levels. The results presented in this section clearly emphasize the potential errors that can arise from neglecting the effect of interfacial bonding between hydrogels and a cementitious matrix. Therefore, a coupled chemo-mechanical model is needed in order to predict the behavior of hydrogel in cementitious material.

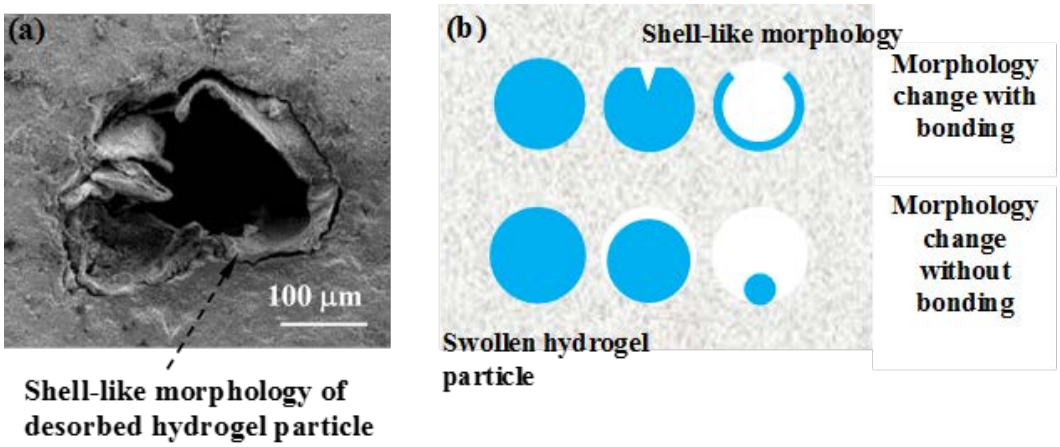

Figure 3-11 (a) SEM image of a desorbed hydrogel particle showing a shell-like morphology in the microstructure of a cementitious material. (b) Schematic depicting the desorption of a hydrogel particle with bonding to a cementitious matrix resulting in a shell-like morphology (top row) and a hydrogel particle without bonding to a cementitious matrix (bottom row). In latter case, the desorbed hydrogel particle will return to a solid morphology similar to before absorption. (Adapted from [191])

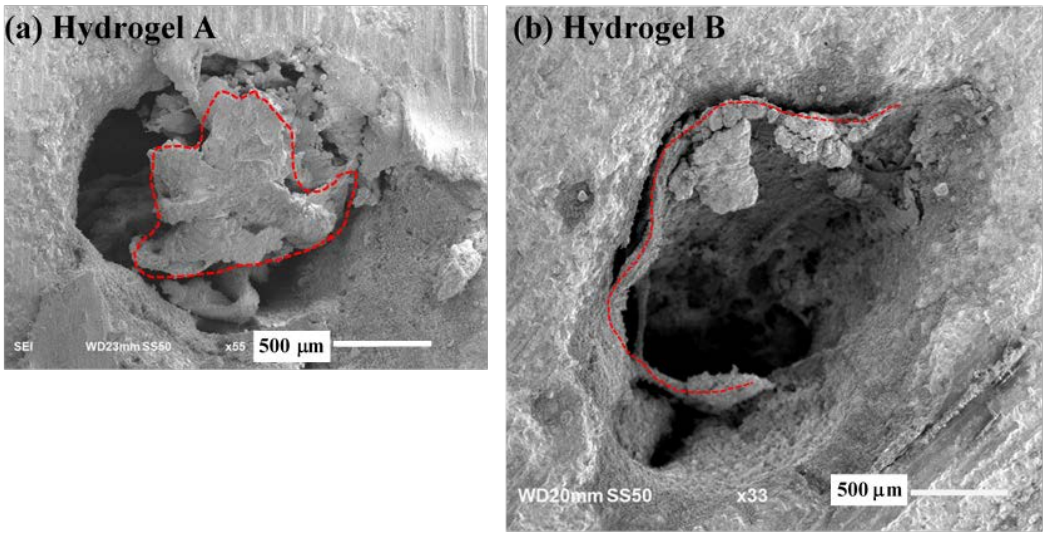

Figure 3-12 SEM images showing the cross section of (a) Hydrogel A and (b) Hydrogel B. A relatively uniform reduction in size in Hydrogel A and a shell-like morphology in Hydrogel B are evident. The morphology of hydrogels is delimited with a red dash line. (Adapted from [191])

Chapter 4: The effect of cement paste chemistry on absorption/desorption behavior of hydrogels with varied chemical compositions

The hydrogels used in cementitious materials are typically polyelectrolytes, and as a result, are sensitive to the pH and ionic composition of the environment [21,42,43,133]. The hydrogels used in the cementitious materials are primarily composed of poly(acrylate-co-acrylamide) copolymers [5,28,42,43,193]. When they are exposed to distilled water, the repulsion between the anionic groups on the polymer backbones results in a large absorption of water in the hydrogel increasing its volume [30,42,54]. In the presence of cations, a reduction in the absorption of hydrogels occurs due to the screening effect of cations and also complexation between cations and anionic groups of the polymeric networks [7,29,42,54]. An increase in pH promotes deprotonation of acidic groups of the polymer as well as hydrolysis of certain groups and crosslinks in the polymer networks, thereby affecting the repulsive forces within the polymer networks as well as the structural stiffness of the polymer networks [133].

The thermodynamics and kinetics of hydrogels are directly dependent on the molecular composition of the polymeric networks; thus, the absorption capacity and rate of absorption/desorption of hydrogels can be tuned to adapt to the chemistry of the cementitious materials to achieve desired characteristics. The free energy of hydrogels comprises contributions from the polymer networks stretching, mixing of the networks and solvent, and the ionic effects [194].

Understanding the behavior of hydrogels in cementitious materials is necessary for the optimum design of internal curing. The hydrogel absorption/desorption and the associated kinetics are important factors affecting the performance and microstructure of cementitious

materials. The amount of retained water in hydrogels governs the size of macrovoids in the microstructure and, thus, plays an important role in mechanical properties. In addition, the rate of water release from hydrogels is a critical parameter governing the effect of hydrogels on the autogenous shrinkage and other properties of cementitious materials [7,21].

Before the initiation of setting and the formation of a solid skeleton in cementitious materials, the behavior of hydrogels is primarily governed by the chemistry of the pore solution. In the initial stage of hydration, the microstructure is saturated with water and capillary forces are not yet developed. With continued hydration, the water continues to be consumed and replaced by vapor-filled pores resulting in a reduction in relative humidity. As a result of meniscus formation between the fluid and vapor phase, capillary forces are gradually increased in the microstructure [14]. With decreasing relative humidity and increasing the capillary forces, the role of capillary forces on the desorption of hydrogel is expected to become more dominant [191]. In the previous chapter, the role of capillary force on the desorption of hydrogel in contact with a porous ceramic (cement paste substrate) was investigated. It should be noted that the behavior of hydrogels can still be affected by the evolving chemistry of the pore solution even after the start of the self-desiccation and development of capillary forces in the microstructure; however, the influence of the pore solution is more pronounced in the initial stage of the hydration.

The relation between the chemical composition of hydrogels, chemistry of the environment and the absorption behavior of hydrogels have been extensively investigated in the past [21,42,43,122,133]. Most of these studies were limited to the behavior of hydrogels in an extracted pore solution or synthetic pore solution. There have been few

studies aimed at in-situ examination of the behavior of hydrogels in cementitious materials [163,164,195].

The morphology of two SAP particles with a size of about 2.3-2.5 mm at the swollen state in a cement paste was investigated using neutron tomography [163]. The authors examined partial debonding of one of the SAP particles from the cement paste and the formation of a cavity in the other one. Recently, neutron radiography [164] was utilized to investigate the desorption behavior of two hydrogels with different chemical compositions. An early desorption was observed in the hydrogel composed mainly of acrylic acid, while the hydrogel with both acrylic acid and acrylamide showed higher water retention until the percolation threshold of the matrix. Rheological studies of the same two hydrogels indicated a similar desorption behavior [28].

In spite of a large body of prior studies on the influence of chemical environment on the absorption behavior of hydrogels [21,42,43,122,133], the desorption of hydrogels due to the capillary action has not received attention and is currently not fully understood. Recently, few papers examined the desorption of hydrogels in pore solutions or in air with controlled relative humidity [34,196]; however, the role of the capillary forces at the interface between the hydrogels and cementitious materials was not studied. More importantly, the coupling effect of cement slurry chemistry, hydrostatic pressure due to boundary constraint and capillary forces was not investigated in the past.

Thus, this chapter is aimed at elucidating the interactions between hydrogels and a cementitious matrix with a focus on the mechanisms affecting the desorption of hydrogels in a porous cementitious matrix. In order to reveal the relation between the desorption behavior and the chemical composition of hydrogels, hydrogels with varied compositions

are synthesized and used in this study. The effect of cement mixture chemistry on the absorption and mechanical response of hydrogels is investigated. Fourier transform infrared spectroscopy (FTIR) is utilized to examine the possible alterations in the chemical structure of the hydrogels as a result of interaction with the cement mixture. After investigating the effect of the cement mixture chemistry on different types of hydrogels' absorption/desorption behavior, all the mechanical (capillary forces and hydrostatic pressure) and chemical effects are coupled back together in order to make a model for the behavior of hydrogel in cementitious based materials. The desorption of different synthesized hydrogels under the effect of capillary action is studied and compared to that without the effect of the capillary action. Due to the importance of the hydrogel surface characteristics on the interactions between the hydrogels and the cementitious matrix, the surface characteristics including roughness, elastic stiffness and adhesion force of the hydrogels are studied. Scanning electron microscopy (SEM) and the freeze drying technique are employed to monitor the evolution of the hydrogels' size and morphology in a hydrating cementitious matrix during early stage of hydration as an in situ experiments. At the end of this chapter, main parameters which can effect on the absorption/desorption behavior of hydrogels in cement mixture are identified, analyzed and coupled together in order to predict the behavior of hydrogels in cement paste as a model. This model allows us to have an optimized and effective mixed design for internal curing agents [53].

4.1 Hydrogel absorption

In order to have better understanding of the effect of the pore solution chemistry on the absorption capacity and kinetics, in the first step, ionic solution with varied chemical compositions in two different pH level (below 9.5 and above 11.5) are prepared, as it is

shown in Table 3. Absorption of two extreme types of hydrogel in terms of AA to AM ratio is examined in all the solutions which is illustrated in Figure 4-1. As expected, by increasing the acrylamide (AM) concentration the hydrogel sensitivity to ionic strength especially Ca^{2+} is decreased, which is critical for internal curing mixed design. Due to higher concentration of anionic group in H-1 which is related to AA concentration, we observe higher swelling capacity, as expected [42,197]. Anionic carboxylic groups in the polymer network (COO-) increases the absorption capacity of hydrogel by electrostatic repulsion force. The existence of Na^{+} and K^{+} in the solutions can be the reason for decrease on this repulsion. In general the absorption capacity in both hydrogels increase by increasing pH-value, but it is more dominant in H-1 compared with H-3 which shows that increasing in pH-value prevent monovalent alkaline cations to effect on anionic carboxylic groups [133]. The existence of Ca^{2+} ions in some of the ionic solutions (number 2, 4, 5 and 6) causes complexation with carboxylate groups which is the reason for sharp decrease in absorption capacity [122,164,198]. A potential ionic crosslink formation with Ca^{2+} ions is observed which hinders absorption capacity, the possibility of ionic crosslink formation will be examined in section 4.2. This complexation effect most likely the anionic part (corresponding to AA monomer), therefore the dramatic decrease in absorption capacity is observed in H-1 compared with H-3.

After free swelling of hydrogels in diluted cement mixture, drastic change in morphology, color and absorption capacity of hydrogels especially H-1 is observed compared with free swelling in ionic solutions or extracted pore solution as shown in Figure 4-2 (b) and (c). This can be due to the physical and chemical effect of hydrating cement particles on hydrogels. The absorption results of the hydrogels with different

compositions swollen in the diluted cement mixture are shown in Figure 4-2 (a). Images of these hydrogels are shown in Figure 4-2 (b). All hydrogels demonstrated the formation of a skin with a distinct color and texture compared to the bulk interior hydrogels. A cross sectional view of H-2 showing the contrast between the skin and the interior bulk of the hydrogels is also illustrated in Figure 4-2 (b). The skin on H-1 is clearly more pronounced compared to H-2 and H-3 and seemed to be notably stiff. The mass of the skin in H-1 contributed to the absorption measurement presented in Figure 4-2 (a) and the actual water content is expected to be less than that shown in this figure. It is noted that H-3 shows a different behavior from H-2 and H-1. The absorption of H-3 increases rapidly in the first hour with a slower increase after this time. H-2 and H-1 show a rapid increase in the first ½ h followed by a reduction. H-2 shows a slightly higher absorption compared to H-1 at 12 h. The final absorption of H-1, H-2 and H-3 in distilled water was measured to be 400, 315, and 165, respectively. Such a reduction in absorption is due to the screening effect of the positively charged cations as well as complexation between anionic groups of the hydrogels and divalent ion Ca^{2+} in the pore solution [28,30,44,133]. The reduction in the absorption of H-1 and H-2, which contains a higher concentration of acrylic acid (AA), is attributed to a more pronounced effect of ion screening and complexation between the anionic groups of AA and the positively charged cations on the absorption of these hydrogels. The formation of a relatively thick skin on H-1 with the highest concentration of AA (90%) is an evidence of such complexation. The physical and chemical interactions between the hydrogel and the hydrating cement particles can also contribute to the changes in the surface characteristics of the hydrogels. More information about the chemical structure of the skin is provided from the FTIR analysis in section 4.3.

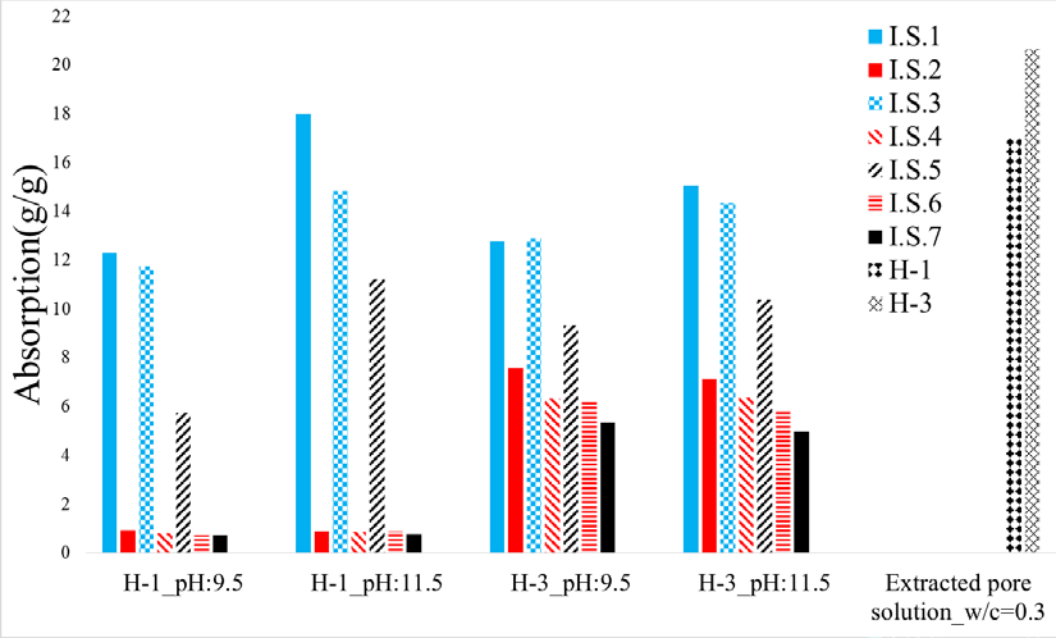

Figure 4-1 Absorption capacity of H-1 and H-3 in seven ionic solution and extracted pore solution with water to cement ratio of 0.3

Table 3 Ionic solution chemical composition at two pH levels

Ionic Solution	***NaCl***	***KCl***	***$CaCl_2$***	***Low pH-level***	***High pH-level***
I.S.1	400	0	0	8.32	11.58
I.S.2	0	0	400	9.54	11.66
I.S.3	0	400	0	7.54	11.86
I.S.4	0	400	400	9.60	11.52
I.S.5	400	400	0	7.13	11.90
I.S.6	400	0	400	9.72	11.88
I.S.7	400	400	400	9.51	12.33

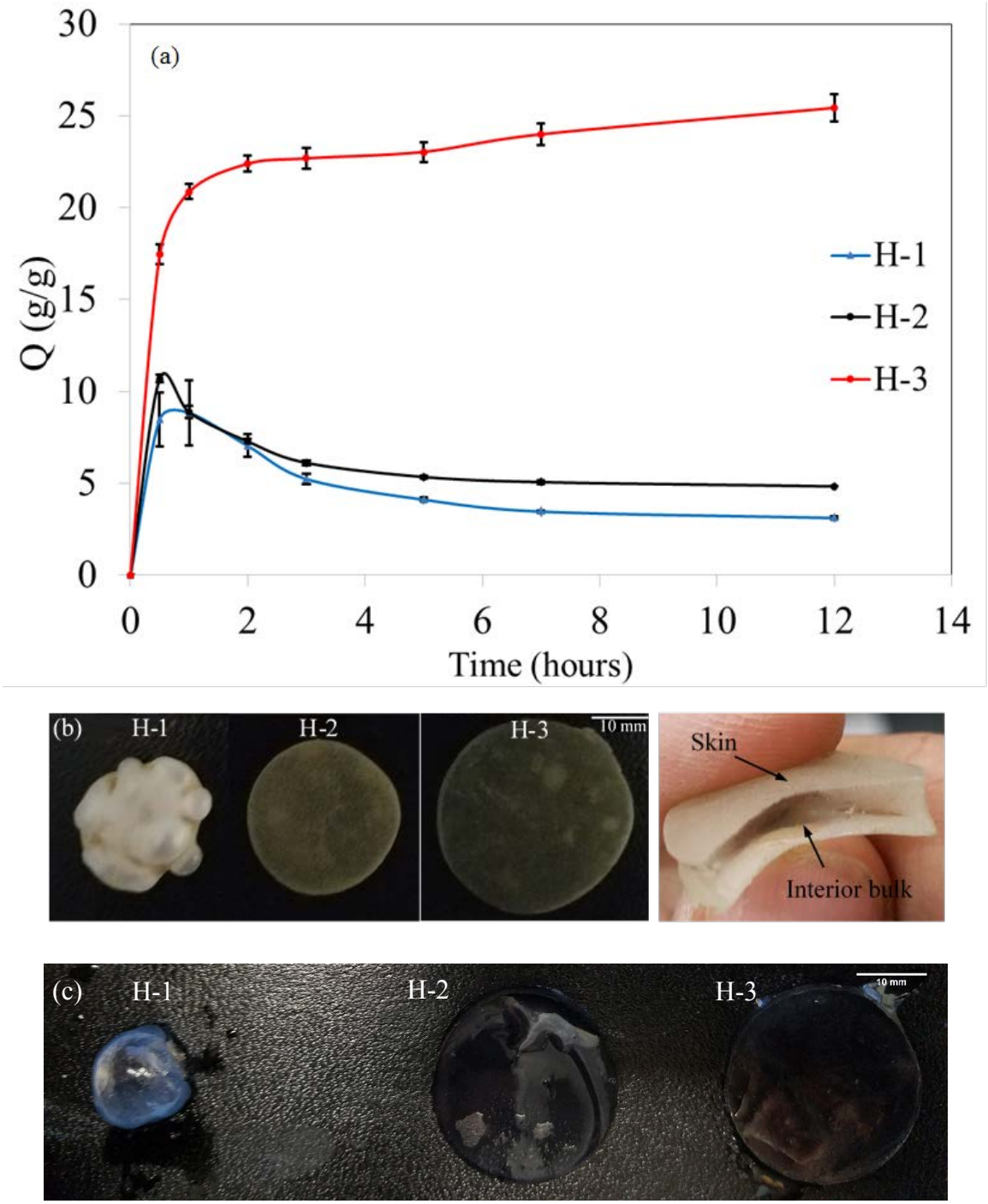

Figure 4-2 (a) Absorption of different hydrogels in a diluted cement mixture. (b) Images showing the swollen state of the hydrogels highlighting formation of a skin and different surface characteristics of the hydrogels in diluted cement mixture (c) Hydrogels swollen in extracted pore solution. (Adapted from [191])

4.2 Elastic shear modulus

The nominal stress vs nominal strain curves of the hydrogels are shown in Figure 4-3. The elastic shear modulus of H-1, H-2, and H-3 is 20 kPa, 6 kPa, and 1 kPa, respectively. The notably higher elastic shear modulus of H-1 compared to H-2 and H-3 is in part due to the formation of a relatively stiff skin on the surface of this hydrogel. Comparing the curves of H-2 and H-3 indicates a lower stiffness in H-3, which can be related to a higher water content in H-3. The elastic shear modulus of hydrogels is affected by the primary covalent crosslink density and the ionic crosslink density of the polymeric networks [121,125,199–201]. Thus, the elastic stiffness of hydrogels is intimately dependent on the water absorption of hydrogels as the number of crosslinks per unit volume of hydrogels decreases with increasing water content. Since the concentration of crosslinking agent MBA is the same in H-2 and H-3, an increase in water content results in a reduction in the density of the crosslinks as a result of increased volume of the hydrogel. However, according to theory of rubber elasticity, the elastic modulus is given by $G = G_0\varphi^{1/3}$ where $G_0 = RTA\nu$ is a constant and referred to as un-swollen state of rubber (hydrogel), R is the gas constant, T is the absolute temperature, A is a constant of the order of unity, ν is the concentration of network chain and φ is the volume fraction of polymer [135]. We calculated G_0 from experimental results and observed that G_0 of H-2 is approximately 3.5 times larger than that of H-3. This can imply that the number of crosslinks in H-2 is higher than in H-3, in spite of the same concentration of MBA in the synthesis of H-2 and H-3. Creation of ionic crosslinks as a result of complexation between anionic carboxylate groups of hydrogels and positively charged ions could also contribute to the increased stiffness of H-2,

compared to H-3. However, a more comprehensive study is necessary to systematically investigate this hypothesis.

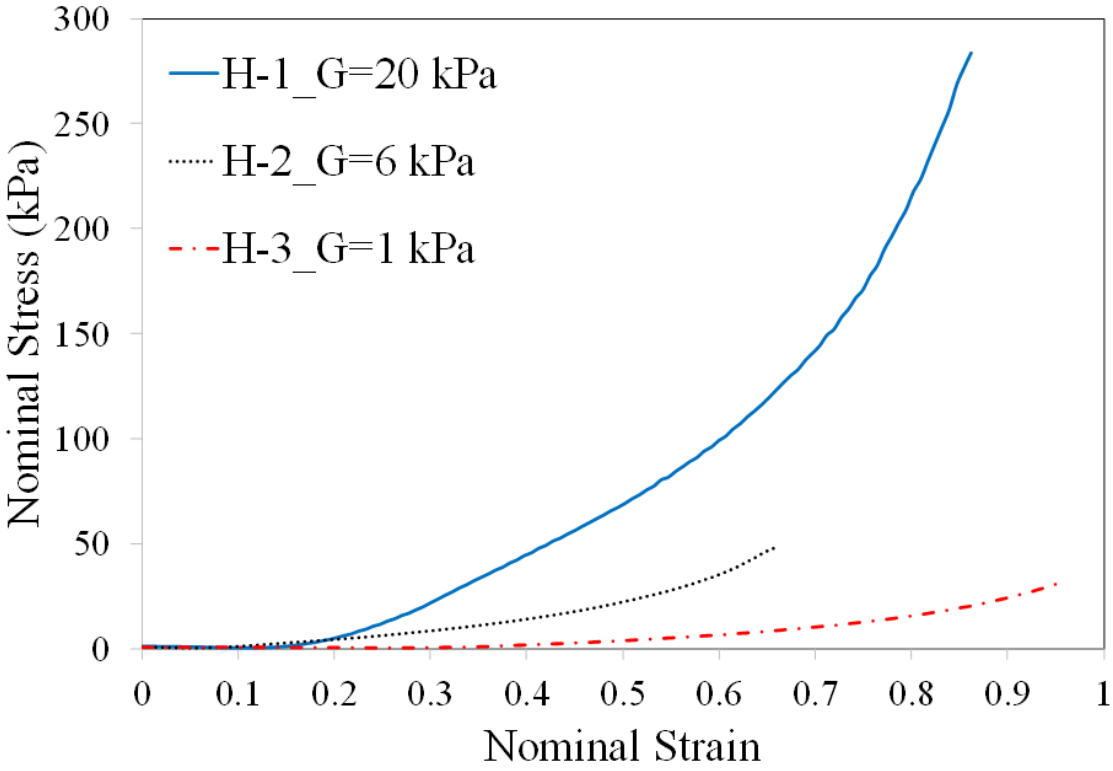

Figure 4-3 Nominal stress-Nominal strain curves of the hydrogels. (Adapted from [53])

4.3 FTIR analysis

The FTIR spectra of H-1, H-2, and H-3 swollen in diluted cement mixture are illustrated in Figure 4-4. The spectra of the interior bulk of H-1, H-2, and H-3 generally show similar features [202]. The peak at 1638 cm^{-1} is related to the presence of amide group [203]. The characteristic band at 1560 cm^{-1} can be attributed to asymmetric stretching of carboxylate groups ($–COO^-$) and the peak at 1408 cm^{-1} is due to symmetric stretching of carboxylate groups; the band at 1560 cm^{-1} can be attributed to hydrolysis of amide groups and conversion of them to carboxylate groups [34,133,197].

However, there are noticeable differences between the skin and bulk FTIR spectra. The high possibility of calcium carbonate formation on the skin was observed, which was more pronounced in H-1 compared with H-3 probably due the higher ratio of AA/AM. The spectrum of H-2 seems to show features in between that of H-1 and H-3. The major peaks observed on skins were illustrated in Table 4. The peak at 874 cm^{-1} is related to out-of-plane bending of CO_3^{-2} [204]. The next major difference on skin is the peak at 1110 cm^{-1} which is related to symmetric stretching of CO_3^{-2} and attributed to vaterite or/and aragonite, two polymorphs of calcium carbonate [141,205]. The peak around 1413 cm^{-1} observed on the H-1 and H-2 skins corresponds to asymmetric stretch of CO_3^{-2} [34,141]. Finally, the increase in the peaks at 2920 cm^{-1} and 2850 cm^{-1} can be attributed to C-H stretching, which is more intense at H-1 and H-2 on the skin; this may confirm the existence of strong chemical bonds between calcium carbonate formed on the hydrogel surface and hydrogel [204].

Table 4 Characteristic signals of FTIR of the swollen hydrogels (skin & interior bulk) in diluted cement mixture. (Adapted from [53])

	H-1		H-2		H-3	
Wavenumber (cm^{-1})	Skin	Bulk	Skin	Bulk	Skin	Bulk
2920	+	-	+	-	-	-
2850	+	-	+	-	-	-
1638	+	+	+	+	+	+
1530-1560	+	+	+	+	-	+
1413	+	-	+	-	-	-
1408	+	+	+	+	+	+
1110	+	-	+	-	+	-
874	+	-	+	-	+	-

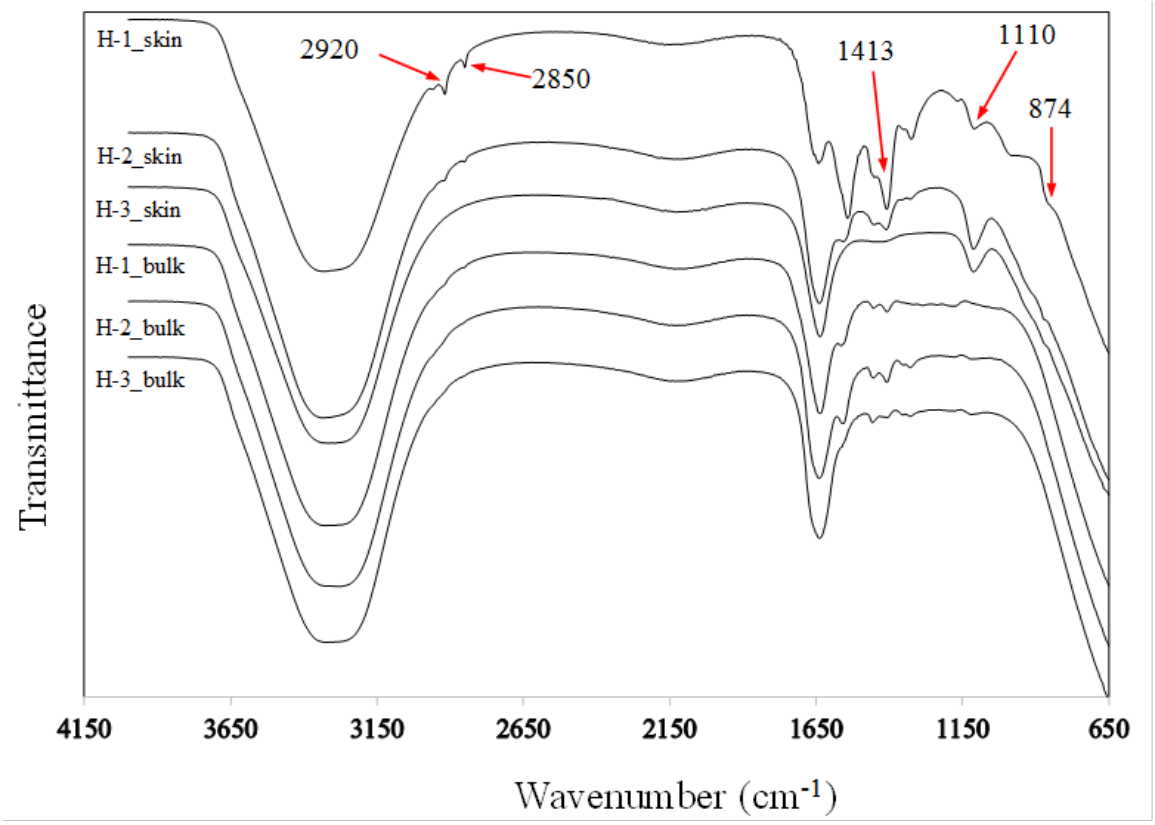

Figure 4-4 FTIR spectra of different hydrogels (skin & interior bulk) swollen in diluted cement mixture. (Adapted from [53])

4.4 Desorption of hydrogels in contact with cementitious substrates

The desorption behavior of hydrogel disks H-1, H-2 and H-3 with and without contact with cementitious substrates is depicted in Figure 4-5 (a). It is seen from Figure 4-5 (a) that the desorption rate of the hydrogels with contact with cementitious substrates is higher than hydrogels without contact. The increase in the desorption rate when in contact with the cementitious substrate is due to the capillary effect at the interface between the hydrogels and the cementitious substrate. At the interface, the Laplace pressure developed in the capillary pore liquid pulls the hydrogel against the rigid cementitious substrate squeezing a thin layer of the hydrogel near the interface. The Laplace pressure decreases the osmotic

pressure of the hydrogel near the interface resulting in an increase in desorption in the hydrogel near the interface. The effect of the capillary forces on accelerating the desorption of hydrogels is also investigated and shown in our prior study [191]. In addition, the rate of water transport due to capillary sorption in the cementitious substrate is expected to be higher than the rate of evaporation from the surface of the hydrogels. Thus, the two mechanisms proposed above provide an explanation for the increased desorption rate of hydrogels in contact than without contact with cementitious substrates. In a recent study, Sokoloff [189] gave an analytical treatment of desorption of a hydrogel sphere compressed against a rigid surface due to the capillary forces. The effect of mechanical stress on the behavior of hydrogels has also been studied by [44,206]. It is seen that H-2 and H-3 shows a noticeable difference in desorption and desorption rate in the first 8 h with H-3 demonstrating faster desorption. This is interesting in view of a relatively similar desorption behavior in the first 8 h of H-2 and H-3 without contact with a cementitious substrate. The similar desorption behavior of the two hydrogels, H-2 and H-3, without contact with a cementitious substrate indicates the similar bulk diffusivity of the two hydrogels. The results of the hydrogels without contact allow us to decouple the effect of the interactions occurring at the interface between the hydrogel and the cementitious substrate from the effect of the bulk of hydrogels on desorption. It is realized from these results that measuring hydrogel desorption in air can lead to significant errors and does not provide a realistic desorption behavior of hydrogels.

H-1 shows a similar desorption in both with and without contact with the substrate. Thus, only the desorption curve corresponding to without contact with cementitious substrate is included in the figure. The similar desorption behavior of H-1 with and without

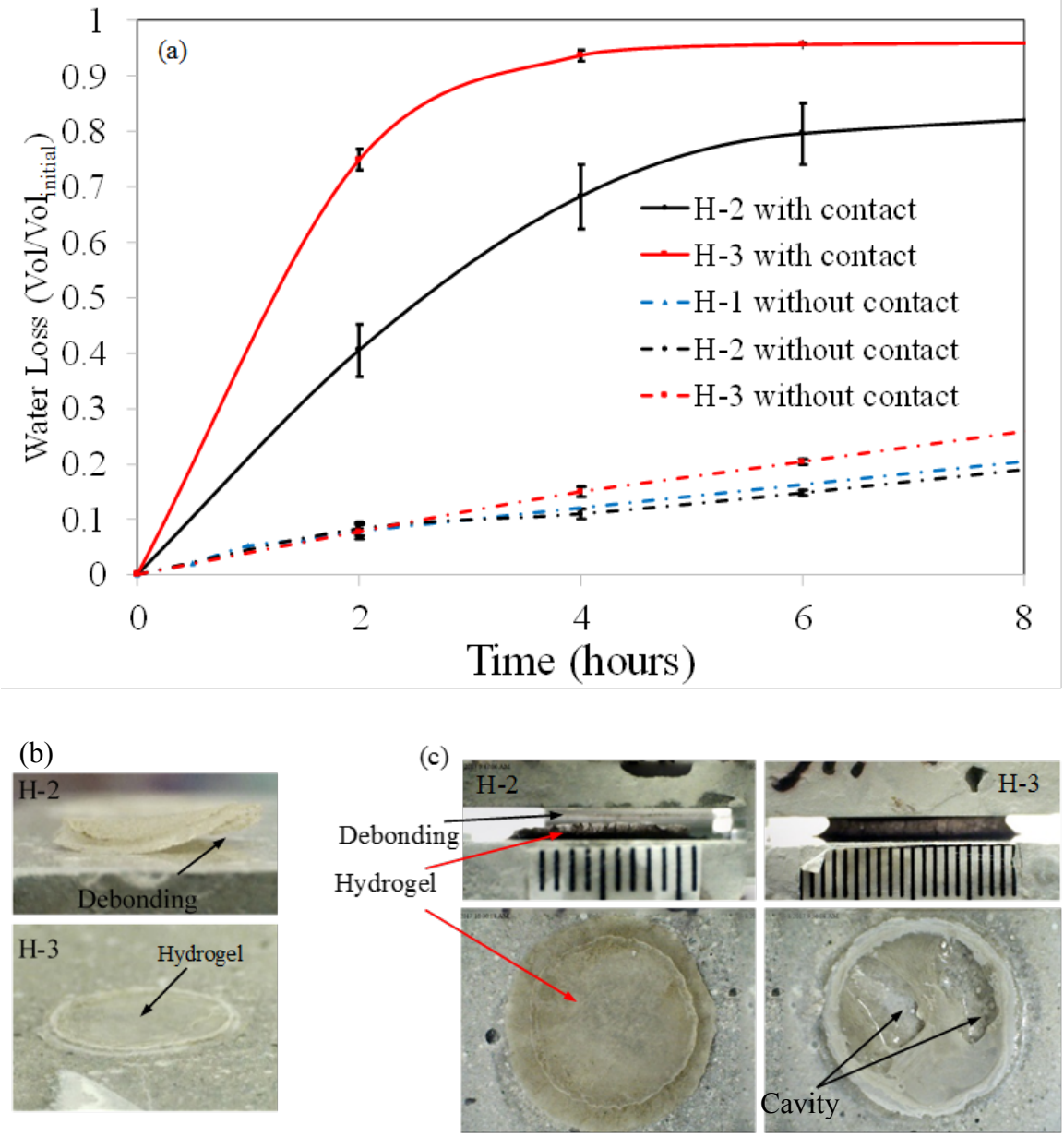

Figure 4-5 (a) Desorption of different hydrogels with and without contact with a cementitious substrate. *Note that the results of H-1 with and without contact with a cementitious substrate were similar; thus, only the results corresponding to without contact are shown here.* (b) Images showing the debonding of H-2 from and bonding of H-3 to the cementitious substrate. (c) Images showing the debonding of H-2 from the top block and bonding of H-3 to both top and bottom blocks. The scale markings are 1 mm in each image. Cavities are seen in the interior of H-3 as a result of tensile stress generated due to bonding to the top and bottom blocks during volume reduction of H-3. (Adapted from [53])

contact with cementitious blocks is attributed to the surface characteristics and lack of contact between the hydrogel and the substrate. As shown previously in Figure 4-2 (b), H-1 exhibits a thick skin with large deformity. This stiff skin prevents contact between the hydrogel and the cementitious substrate and as a result, the effect of the capillary forces is significantly reduced.

In order to investigate the reason for the observed difference in the desorption of H-2 and H-3 with contact with cementitious substrate in spite of a small difference between the desorption of the two hydrogels when not in contact with cementitious substrate, the interaction between these two hydrogels and the cementitious substrate is examined.

4.5 Surface roughness and contact adhesion measurement

The roughness of two interacting surfaces influences the contact mechanics between the two surfaces and has been studied in the past [207]. An increase in surface roughness can potentially decrease the contact surface between the hydrogel and a porous cementitious matrix thereby decreasing the desorption rate. Roughness (R_a) of the surface of H-2 and H-3 measured over an area of 2×2 mm^2 is 3.34 μm and 5.32 μm, respectively. It is noted that both hydrogels exhibit a somewhat similar roughness on their surface. Thus, surface roughness is not expected to significantly contribute to the difference in the desorption behavior of the two hydrogels in contact with a cementitious substrate as shown in Figure 4-5 (a). The 3D topography of diluted H-3 surface is illustrated in Figure 4-6.

In order to further investigate the effect of the hydrogel surface characteristics on their desorption behavior; AFM-based contact adhesion measurement is carried out. The average Young's modulus of the skin of H-2 and H-3 swollen in the diluted cement mixture

is measured to be 1.89 ± 0.15 MPa and 1.79 ± 0.27 MPa, respectively. Comparing the Young's modulus of the skin obtained from AFM measurement and those shown in Figure 4-3, clearly indicates a higher elastic stiffness in the skin. Prior studies [208] on the capillary adhesion between a soft elastic solid and a rigid substrate with asperities indicated a reduction in the capillary adhesion with an increase in the elastic modulus of the soft elastic solid. The mechanical behavior of hydrogels is commonly modelled as that of a soft elastic solid [121,135]; thus, it seems logical to expect that with a reduction in the Young's modulus of hydrogels, hydrogels are more easily deformed and pulled into the capillary pores increasing the real contact area at the interface. This increase in contact area can potentially improve the desorption of hydrogels. However, the difference in the Young's modulus of the skin of H-2 and H-3 is not significant; therefore, the different surface stiffness is not likely to result in the increased desorption of H-3 compared to H-2, as observed from Figure 4-5 (a).

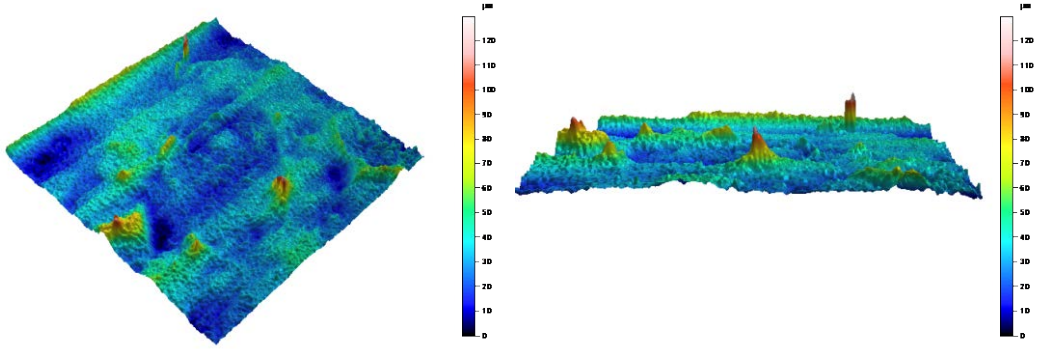

Figure 4-6 3D topography of diluted H-3 surface

On the other hand, the adhesion forces are measured to be 74.1 ± 16.7 nN and 156.07 ± 28.03 nN for H-2 and H-3, respectively. It is interesting to see the notably higher adhesion

force in the case of H-3 than H-2. The nature of the adhesion force in the contact adhesion measurement can be chemical and physical bonds between the hydrogel surface and the glass microsphere. The details of these bonds and the relative contribution of each to the total adhesion force measured in the experiments are currently not known. It should be noted that the microsphere surface characteristics are different from those of hydrating cement particles. Thus, caution should be exercised in the interpretation of the results. Nonetheless, the results of the adhesion measurements are used here to aid in understanding the potential mechanisms underlying the interaction between hydrogels and cementitious materials. An accurate adhesion force measurement requires the use of a hydrating cement particle with a geometry and surface characteristics similar to the glass microsphere used in this study. Due to the highly heterogeneous surface characteristics and irregular shape of hydrating cement particles, a microsphere is instead used in the adhesion measurement.

The higher adhesion force between the hydrogels and cementitious matrix can have important implications in the desorption of hydrogels. The higher desorption of H-3 than H-2 in contact with the cementitious substrate as shown in Figure 4-5 (a) can be attributed to stronger bonding in the case of H-3 than H-2. It seems probable that stronger bonding enhances the effect of the capillary forces on the desorption of hydrogels.

4.6 Effect of adhesion on desorption and macro-scale observation

An observation is made of the bonding between the hydrogels and the cementitious substrate near the end of the desorption test. As seen in Figure 4-5 (b), it is observed that H-2 could be easily detached from the surface of the cementitious block, while a strong bonding existed between the H-3 and the substrate so that a blade has to be used to detach

H-3 from the surface of the block. This points to a stronger bonding between H-3 and the substrate and this bonding remains until the end of desorption. Since improved bonding promotes the capillary-driven transport of water at the interface, this provides an explanation for the increased desorption of H-3 compared to H-2.

The desorption of H-2 and H-3 in contact with two cementitious blocks with a constant distance between the blocks is also examined. The main reason for this test is to simulate the behavior of the hydrogels surrounded by a macrovoid in a cementitious material. This situation qualitatively resembles the desorption of hydrogels and their interaction with the macrovoid created in the cementitious matrix as a result of hydrogel initial absorption.

Figure 4-5 (c) shows the images of H-2 and H-3 and the cementitious blocks with a gap width equal to the initial thickness of the hydrogels at the swollen state. The top and bottom images are the side view and top view of the hydrogels, respectively. It is seen that H-2 seems to have debonded from the top block; on the other hand, H-3 remains bonded to both top and bottom cementitious blocks as seen from the figure. In order to investigate the interior of H-3, the top block was removed using a plyer, as the bonding force is relatively large. Cavities are observed in the bulk of H-3 as indicated in Figure 4-5 (c). The debonding of H-2 from the top block could be a result of a low adhesion force. Once debonded from the top block, the hydrogel is allowed to simply sit on the bottom block and it is only in contact with the bottom block. This is a direct consequence of the experimental setup used in this study; if the entire setup is such that the blocks and the hydrogel are parallel to the gravitational force, then the debonding from two blocks can result in a total loss of contact from both sides. A different mechanism is observed to occur during the desorption of H-3. It is shown that H-3 maintains bonding to the top and bottom blocks; in this scenario, the

reduction in size during desorption develops tensile stress in the hydrogel, which ultimately results in cavity formation in the interior of H-3. The different mechanics involved in the desorption of the two hydrogels can have important implications in the desorption rate of the two hydrogels. In the case of H-3, the continued bonding between the hydrogel and blocks most likely results in an enhanced desorption rate compared to the case where debonding occurs. In addition, the formation of fractures and cavities reduces the relevant diffusion length of the hydrogel during desorption. The two mechanisms discussed above, are proposed to have important influences on the desorption of hydrogels in a cementitious matrix. The quantitative measurement of desorption is not possible due to a lack of visual access to the dimensional change of the hydrogels during desorption.

The above observations related to the interactions between hydrogels and a cementitious material in the setup studied here can vary from that in a real situation due to the assumption made in the experiments. The evolution in the morphology and chemical characteristics of the phases produced during hydration in the early age can affect the interaction between the hydrogel and the surrounding cementitious matrix. It has been shown that hydration products, primarily consisting of $Ca(OH)_2$, can intrude into the macrovoids surrounding SAP [209]. Nonetheless, the main focus here is to shed light, for the first time, on the processes affecting the desorption of hydrogels in an unsaturated porous solid, which can contribute to our understanding of the behavior of hydrogels in cementitious materials.

4.7 Morphology evolution of embedded hydrogels in a hydrating cementitious matrix as an index for in situ absorption/desorption behavior of hydrogel

The results of the hydrogel absorption and desorption in a hydrating cementitious matrix at early age are discussed in this section. The desorption of H-1, H-2, and H-3 at various times is shown in Figure 4-7. Six replicates for each hydrogel type and at each time are used to account for the statistical variability. Images showing the cross section of the hydrogels at different times are demonstrated in Figure 4-8. The hydrogels are delimited with a yellow dashed line to aid in visual identification of hydrogels.

The desorption measurement of the hydrogels in the cement paste is started 4 h after mixing since the cement paste before 4 h is too fragile and crumbled so that imaging is not possible before this time. It is seen that H-1 has desorbed a large amount at even 4 h. The desorption of H-1 continues at a low rate until 16 h at which point the hydrogel seems to reach its final desorption. H-3 exhibits a small desorption at 4 h as seen from Figure 4-7, followed by a steep increase in desorption between 8 h and 12 h. After 12 h, the desorption of H-3 continues at a lower rate. H-2 shows a different desorption behavior from that of H-1 and H-3. At 4 h, H-2 experienced a desorption more than H-3 but significantly smaller than H-1 at this time. Compared to H-1 and H-3, the desorption of H-2 seems to be more uniform and does not show any steep changes.

A close examination of the different desorption observations of hydrogels highlights the role of different mechanisms governing the desorption of hydrogels. At early age before the start of depercolation of the pores in the microstructure, the chemical interaction between the hydrogels and the pore solution and the hydrating cement particles is responsible for the possible desorption. The effect of chemical interaction can also be

recognized from the desorption of H-1 in the diluted cement slurry as shown in Figure 1. With continued hydration and a reduction in relative humidity, the capillary forces are developed and provide the primary driving force for desorption. This can be noted from an increased rate of desorption in H-3, at about 8 h, which more likely corresponds to the beginning of the setting in the cement paste. The observed behavior can be explained in view of the role of contact between the hydrogel and the cementitious matrix. In case of H-1, the hydrogel gives back most of the retained water at early age and consequently reduced in size, inevitably decreasing its contact surface with the surrounding cementitious matrix. This can be seen from the SEM images in Figure 4-8. On the other hand, H-3 does not desorb much and maintains a larger contact area with the cementitious matrix at the early age. The bonding between the hydrogel and the cementitious matrix is expected to increase the desorption rate of the hydrogel and drive the hydrogel to take a shell-like morphology as seen from Figure 4-8 (H-3, 12 h). The shell-like morphology is the direct influence of the adhesion during desorption of hydrogels; the shell-like morphology of H-3 is in a stark contrast with the solid-like morphology of H-1, which suggests a relatively uniform reduction in size during the desorption of H-1 indicating a smaller contact surface with the cementitious matrix. A schematic in Figure 4-8 (b) shows the two different mechanisms of morphology changes during the desorption of H-1 and H-3. In case of H-2, the effect of capillary forces on desorption is smaller than in H-3 due to a slightly higher desorption before 8 h, due to chemical interactions, and consequently smaller contact area with the cementitious matrix at the start of the Laplace pressure development in the matrix. In addition, as discussed previously and shown in Figure 4-5 (b) and (c), the bonding between H-3 and the cementitious block is shown to be stronger than that between H-2 and

the block. Thus, it is plausible that H-3 had stronger bonding to the cementitious matrix than H-2; consequently, the influence of the capillary suction is anticipated to be more effective in H-3 than in H-2. The main observation here is the competition between the chemical interaction and the capillary forces on the desorption kinetics of hydrogels in cementitious materials. This competition between these two factors are strongly dependent on the chemical composition of the hydrogels and possibly on the mix design of the cementitious matrix. As demonstrated in Figure 4-5 (a), when there is a contact between the hydrogel and the cementitious matrix, the capillary forces can accelerate the desorption of the hydrogels compared to hydrogels without contact. This is evident from a comparison of the rate of desorption of H-1 and H-3 in the time interval of 8 h-12 h, as demonstrated in Figure 4-7. Therefore, the chemical interactions between the hydrogels and a cementitious matrix and how they affect bonding at the interface are important factors determining the desorption behavior of hydrogels in cementitious materials.

It is worthwhile to compare the desorption behavior of H-2 and H-3 in the cement paste, Figure 4-7, and absorption behavior of diluted cement mixture, Figure 4-2 (a). It is seen that while H-3 demonstrates a higher water retention than H-2 in the diluted cement mixture early on, it desorbs at a higher rate than H-2 in the cement paste after the start of setting and development of the capillary forces in the cementitious material. The water retention behavior of hydrogels is usually studied in an extracted pore solution. The SEM observation shown above clearly illustrates the inability of measurement in an extracted pore solution to accurately predict the behavior of hydrogels in cementitious materials.

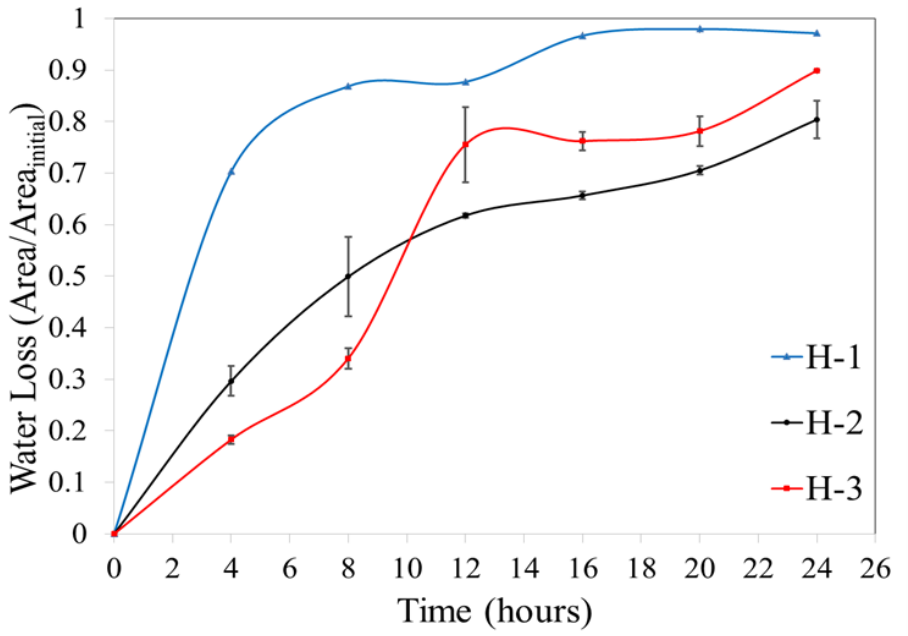

Figure 4-7 Desorption behavior (water loss) of hydrogels embedded in cement pastes.

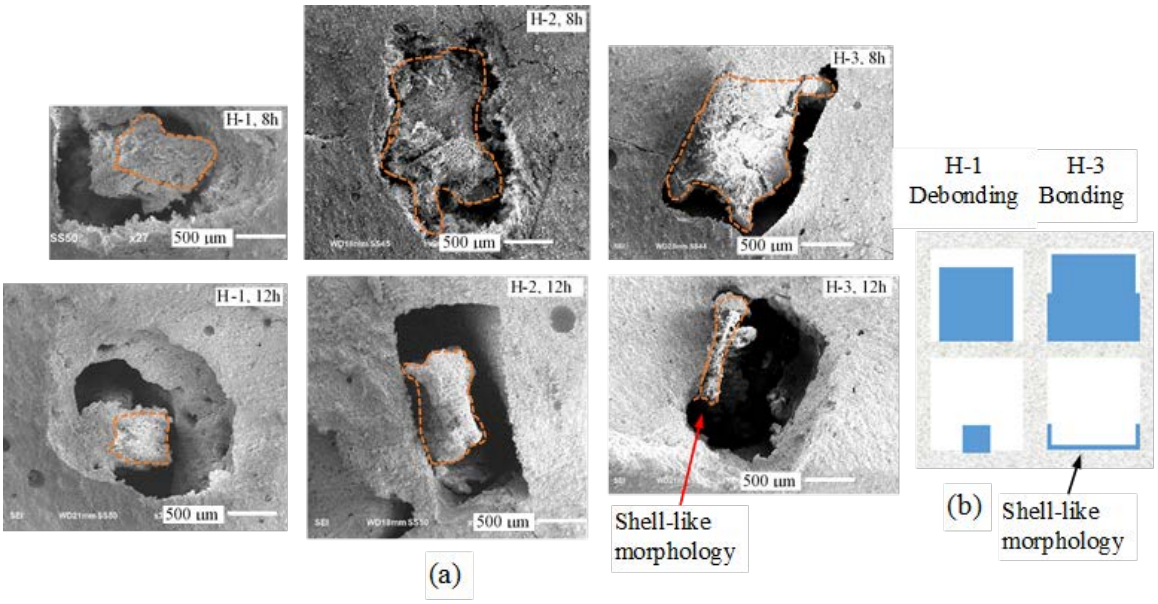

Figure 4-8 (a) SEM images showing the morphology changes during the desorption of H-1, H-2 and H-3, at 8 h (top row) and 12 h (bottom row). The cross section of the hydrogel microstrip is delimited with a dashed yellow line. (b) Schematic showing the different morphology evolutions of H-1 and H-3. (Adapted from [53])

Chapter 5: The effect of supplementary cementitious materials (SCMs) on the desorption of superabsorbent hydrogels and the effect of hydrogels on microstructure of cement matrix

It is well recognized that the use of supplementary cementitious materials (SCM), such as silica fume (SF), slag and fly ash (FA), are necessary in order to enhance the durability of HPC [210,211]. Since many mineral admixtures are by-products of other industries, these waste by-products can be used to reduce the amount of cement, thus reducing greenhouse gas emissions generated as a result of cement production [212–220].

In this chapter, the main focus is to investigate the effect of SCMs on the desorption behavior of hydrogels in cementitious materials. In order to achieve this goal, five different SCMs (Slag, silica fume, Fly ash, Glass powder CS400 and Glass powder VCAS) are used as a replacement of cement.

5.1 Pore solution chemistry of blended cement paste with SCM

The chemistry of supplementary cementitious materials is generally characterized by lower calcium content than Portland cement as it is mentioned in Table 5. Thus there are differences in the hydrates formed during hydration, which influence strength and durability. Also, the understanding of the reaction kinetics in blended systems is complicated by the fact that the hydration of the cement and SCMs may interact and measuring their individual effects on the reaction rate is difficult [215]. The partial replacement of cement with SCMs influences hydration kinetics, pore solution pH level and chemistry, released heat, microstructure, RH drop rate, etc [130,215,221]. These parameters can have significant impacts on the absorption/desorption behavior of hydrogel in blended cement containing SCMs. In this chapter, some of general factors which may

influence the interaction between hydrogel and blended cement mixture are reported from literatures which are useful to interpret the hydrogel behavior in blended cement paste. Of course, the main focus of this investigation is on the very early age pore solution chemistry, since this period of time is more effective on absorption behavior of hydrogel; for the desorption behavior of hydrogel other parameters in addition to pore solution chemistry should be considered as well.

The effect of different types of SCMs on the pore solution chemistry has been studied intensively in the past [216,221–227]. Common trends are summarized as follows:

- Alkali concentrations (such as potassium and sodium) generally decrease with increasing replacement of Portland cement (PC) by SCMs. Alkali concentrations in the pore solution depend strongly on the total alkali content of the PC. Partial replacement by SCMs thus reduces alkali concentrations as the alkalis from the cement are released faster than the alkalis in the SCMs. In general, silica fume is more effective in decreasing the alkali concentration of the pore solution. This reduction of alkali concentration is more pronounced in the very early age (before 6 hours) which is more important for hydrogel and blended cement interaction.
- The decreased alkali concentrations in the pore solution lead to reduced OH^- concentrations. In the case of slag negatively charged sulfur species such as sulfide or thiosulfate can additionally decrease the OH- concentrations of the pore solution. The reduction of OH- concentration can affect the absorption/desorption behavior of hydrogel in cementitious materials. But, it should be noted that at very early age (before 4 hours) there is not a major

difference in pH level which can affect the hydrogels properties. However, after 4 hours up to 3 days this reduction is more pronounced.

- Sulfate concentrations are not significantly affected by slag or fly ash. Calcium concentrations tend to decrease at very high fly ash and slag replacement levels.
    - Reported measured silicon and aluminum concentrations are few. Because of the low concentrations, the precise concentrations are difficult to detect. Therefore some of the very low measurements given in literature may not be reliable. The available data do not show changes in the silicon and aluminum concentrations of slag and silica fume blends compared to pure PC pastes; however, for fly ash blends the aluminum concentration tends to increase over time and with an increasing replacement ratio which can be effective on the desorption behavior of hydrogels with higher acrylic acid concentration.

Table 5 Composition of Cement, Fly Ash, GP1, GP2 and SF [1] [228,229]

Composition(% by mass)	Cement	FA	GP2	GP1	SF
Silica (SiO_2)	20.6	54	57.5	63.3	85-95
Alumina (Al_2O_3)	4.8	28	12.7	6.4	0.5-1.7
Iron oxide (Fe_2O_3)	3.5	7	0.06	0.31	
Calcium oxide (CaO)	64	1.4	22.7	17.1	0.1-0.9
Magnesium oxide (MgO)	0.9	1	3.6	4.5	
Sodium oxide (Na_2O)	0.1	0.3	0.62	6.1	0.15-0.2
Potassium oxide (K_2O)	0.3	2.4	0.06	0.07	0.15-1
Sulfur trioxide (SO_3)	3.4	0.1	0.22	0.19	
Titanium dioxide (TiO_2)	0.3		0.98	0.44	
Boron trioxide (B_2O_3)			0-6	0-5	
Loss on ignition (%)	2.75	3.4	0.5	1	1.5-2.5
Specific gravity		2.31	2.6	2.5	2.21
Passing sieve #325 (%)		81	98	>99	
Median particle size (μm)		13.1	8.4	8.4	

[1] SF composition is obtained from literature reviews

In general, there is a lack of investigations for the precise measurement of very low concentration elements in pore solution at very early age. This low concentrations can be effective based on the types of the elements and hydrogels.

5.2 Hydrogel absorption/desorption behavior in blended cements containing SCMs and diluted slurry

The absorptions of H-2 and H-3 are investigated in hydrating cement paste and in diluted slurry which are illustrated in Figure 5-2 and Figure 5-3, respectively. The absorption in hydrating cement paste was calculated by $Q = (D_{macrovoid}/D_{initial})$ ^3, where $D_{macrovoid}$ is the thickness of macrovoid as the maximum absorption capacity of hydrogel and $D_{initial}$ is the thickness of dried hydrogel before embedding in blended cement paste. The absorption kinetics of H-2 and H-3 in diluted slurry are shown in Figure 5-3 and it is calculated by dividing the hydrogel mass at each time by initial dry mass of hydrogel. The main reason for these set of experiments is to show the effect of hydrostatic constraint on the absorption capacity. As it is illustrated the hydrogels' absorption capacities in different blended cement pastes are closer together compared with in the diluted slurry. Since in diluted slurry the concentration of some ions are less, this absorption should have more tolerance compared with hydrating cement paste.

The modified freeze drying technique which is explained in detail in section 2.2.8 is utilized to examine the absorption/desorption behavior of hydrogels in situ. Also, absorption/desorption kinetics of H-2 and H-3 in diluted slurry is investigated and compared with in situ results. This comparison indicates the effect of constraint and pore chemistry on absorption capacity simultaneously. The desorption results of the hydrogels

in various cement pastes are shown in Figure 5-4 (a) and (b). SEM images of the hydrogels in cement pastes are depicted in Figure 5-5.

The results cover the first 24 hours of the desorption from the time of mixing. It is observed that all hydrogels show a desorption value of about 0.15-0.25 as seen from Figure 5-4 (a) and (b). The H-2 in the control paste showed a relatively uniform desorption rate until 12h after which time the hydrogel appeared to reach its final desorption value. H-2-GP1 and H-2-S[2] also show a similar behavior with their final desorption occurring being delayed until 16 h. H-2-SF, H-2-FA and H-2-GP2 showed a relatively sharp rate of desorption regime in part of their desorption history. This increased desorption rate initiated at 4 h for H-2-SF leading to a faster desorption compared to other samples. In H-2-FA and H-2-GP2, the initiation of the fast desorption is shifted to a later time at 8 h. It is seen that after 16 h no significant change in desorption of all hydrogels can be observed.

The desorption behavior of hydrogel H-3 also revealed a regime of fast desorption in the pastes and this regime is also more pronounced in H-3-Ctrl, H-3-GP1 and H-3-S compared to H-2 in the respective pastes. Once again, it is noted the hydrogel in paste with SF (H-3-SF) exhibited a higher desorption rate compared to other pastes and the hydrogel in paste with FA (H-3-FA) showed the lowest desorption compared to other pastes. It is seen that all hydrogels except H-3-GP2 reached their final desorption at about 16 h.

The desorption of hydrogels is influenced by the capillary forces exerted by the surrounding porous matrix as well as chemical interactions between the hydrogels and pore solutions and between the hydrogels and the surrounding matrix. The effect of capillary forces on desorption of hydrogels in contact with cementitious materials was studied in our

[2] In order to simplify writing, GP1 and GP2 are referred to GP CS400 and GP VCAS, respectively. Also, S, SF, FA and Ctrl are referred to Slag, Silica fume, Fly ash and Control, respectively.

prior studies [53,185,191]. Our prior examination indicated that the effect of chemical interactions on desorption is more dominant in hydrogels with high acrylic acid (AA) concentrations. In this study, H-2 and H-3 were used so that the desorption behavior of the hydrogels is not dominated by chemical interactions and the effect of capillary forces is expected to play a major role.

The increase in the desorption rate of the hydrogels in cement paste with SF is attributed to the evolution of the microstructure surrounding the hydrogel. The presence of SF enhances the hydration rate and formation of a solid skeleton in the matrix. The effect of SF on the hydration and microstructure of cementitious materials has been examined in [230]. In addition, SF can serve as a fine filler filling the space between the hydration products resulting in creation of larger number of fine pores that are effective in providing capillary pressure. The delay in the desorption of hydrogel in the paste with FA can also be explained in light of delay in hydration as a result of replacement of cement with FA. Prior investigations have documented the retarding effect of FA on hydration of cement pastes at early in room temperature [231]. Thus, it is expected that in the paste with FA, the formation of solid skeleton and percolation threshold take place later compared to other cement pastes. Therefore, hydrogels in paste with FA are subjected to the capillary forces of the matrix at a later time. However, once capillary forces start to develop, the desorption of hydrogels accelerates as seen in Figure 5-4 (a) and (b). Narmluk and Nawa [231] showed that FA retards the very early age hydration rate up to 10 hours, but after 10 hours it accelerates the hydration of cement paste, which is in a good agreement with our results. SEM images of the control paste and the paste with SF and FA are shown in Figure 5-1 (a-c).

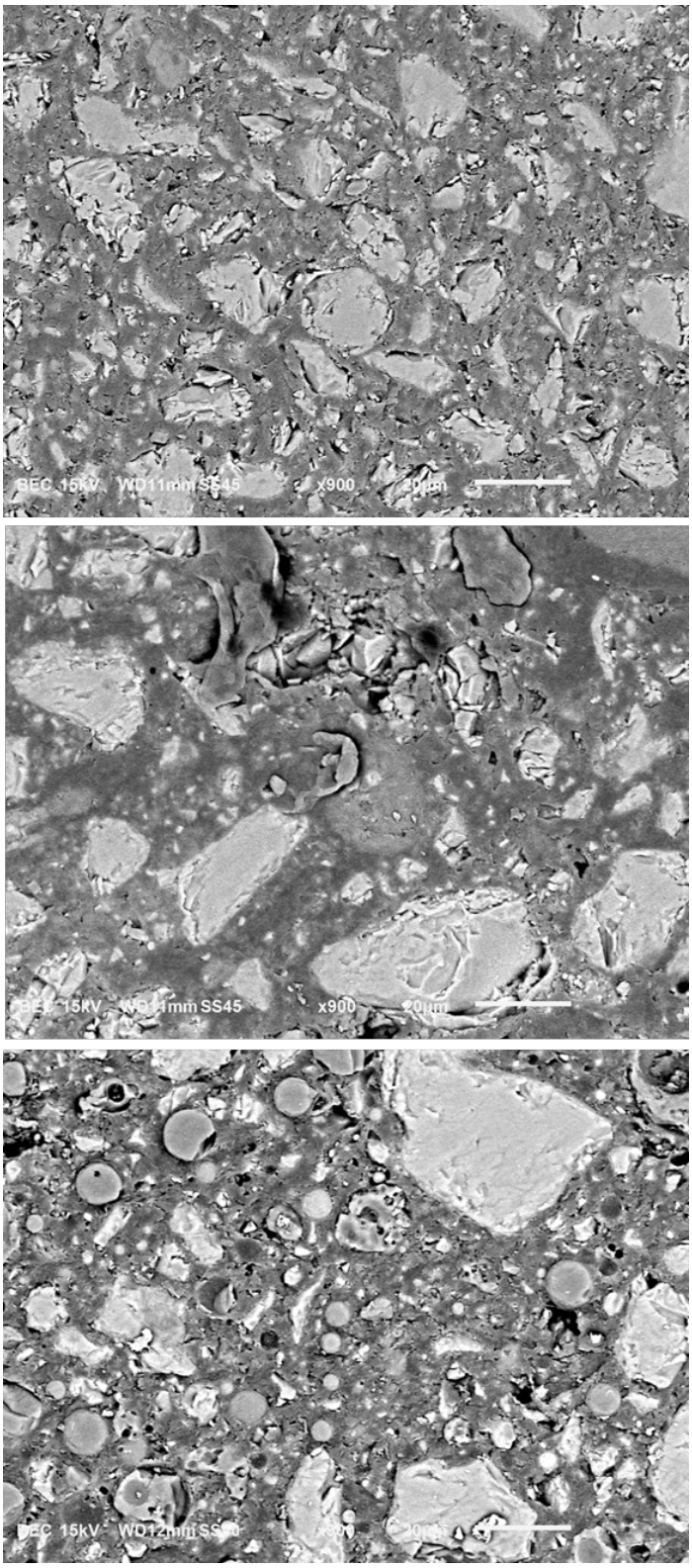

Figure 5-1 Microstructure analysis: hydration degree and porosity; (a) H-1-Ctrl (b) H-1-SF (c) H-1-FA, all at 8 hours.

The SEM images reveal a more densified pore structure in the cement paste with SF and the cement paste with FA appears to be the least densified. A reduction in the desorption of H-3 in cement paste with S, GP1 and GP2 compared to the control cement paste in the time interval of 8-12 h can be observed; however, this reduction was less pronounced in the case of H-2 compared to H-3.

One reason for greater reduction in desorption rate of hydrogels in paste with FA compared to cement pastes with other SCMs can be attributed to more pronounced delay in early hydration of cement in cement paste with FA compared to other SCMs used here. Prior studies [231] regarding the effect of FA and other SCMs have shown such an effect on the early hydration of cement. In addition, since the particle size of S, GP1 and GP2 is smaller than that of FA, it is possible that these fine particles occupy the space within the solid skeleton of the hydration product more effectively than FA resulting in a larger number of fine capillary pores. Therefore, the hydrogels in paste with S, GP1 and GP2 see a larger influence of the capillary forces compared to the hydrogel in paste with FA.

It is worthwhile to discuss how the chemistry of hydrogel affects the desorption in various cement pastes. In the control paste and the pastes with GP1 and S, H-2 showed an initially higher desorption rate; however, at about 8 h, H-3 demonstrated a higher rate of desorption. The two hydrogels in the pastes with SF and GP2 showed a similar behavior. The initial increase in desorption of H-2 compared to H-3 could be due to chemical effect resulting from the interaction between ions and polymeric networks of the hydrogels. Since H-2 contains more acrylic acid monomers compared to H-3, it is logical to expect a greater reduction in retained water in H-2 than H-3 in the first few hours before the onset of solidification of the surrounding microstructure [53,185,191]. When solidification of the

microstructure and pore percolation starts, the capillary pressure is developed and the influence of capillary forces becomes more important. It has been shown in our prior work that the interfacial bond between the hydrogel and the cementitious matrix increases with increasing concentration of acrylamide in the hydrogels. The stronger bond between the hydrogel and the cementitious matrix allows for a more effective influence of the capillary forces on the hydrogels resulting in an increased desorption rate of the hydrogels. This explanation provides a rationale for higher desorption rate of H-3 compared to H-2 as seen in the control paste and the paste with GP1 and S.

An opposite observation was made of the behavior of H-2 and H-3 in the paste with FA. It is seen that H-3 initially desorbed faster but later H-2 exhibited a faster desorption as seen from Figure 5-4 (a) and (b).

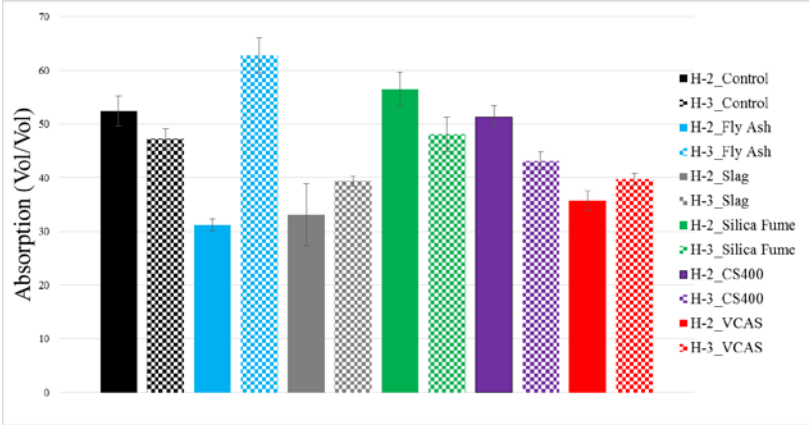

Figure 5-2 Absorption of H-2 and H-3 in different blended cement

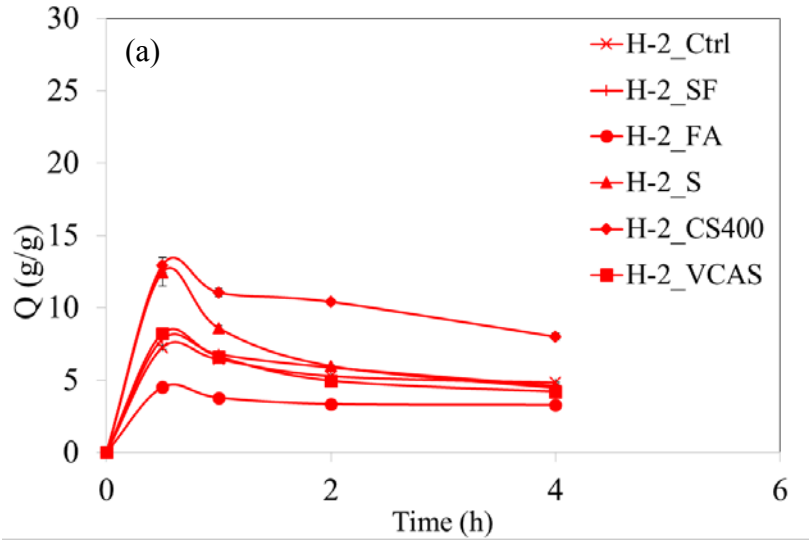

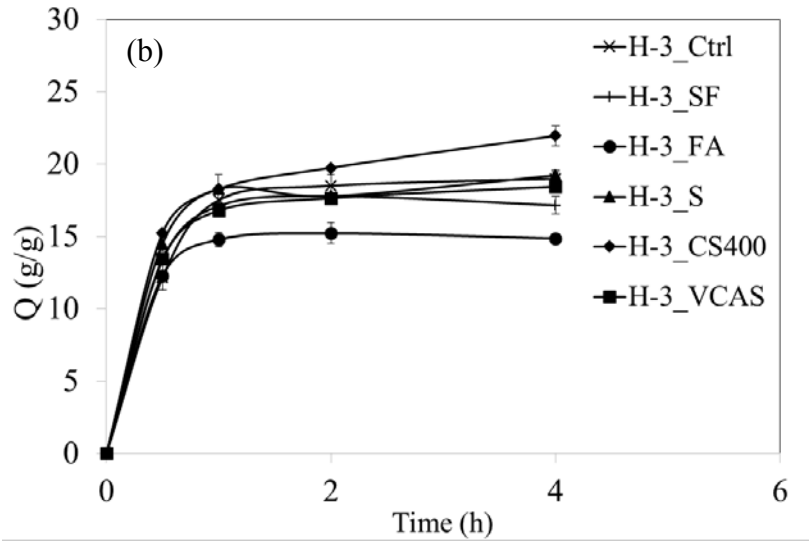

Figure 5-3 Absorption of Hydrogel in diluted slurry (a) H-2 (b) H-3

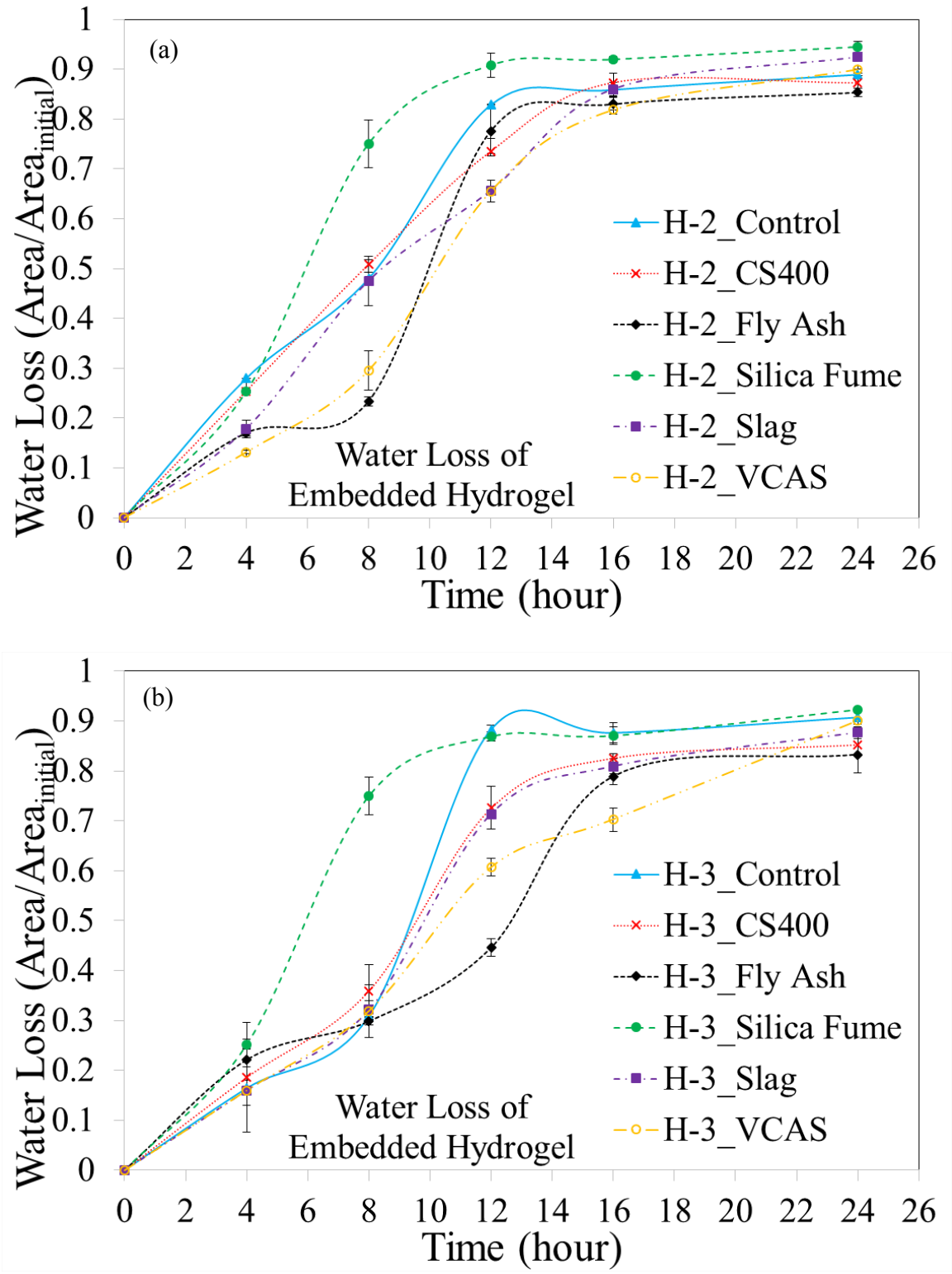

Figure 5-4 the desorption results of the hydrogels in various blended cement pastes (a) H-2 and (b) H-3

5.3 Hydrogel morphology investigation

Investigation on morphology evolution of hydrogel in cement paste is important in elucidating the processes affecting the desorption of hydrogels. Such an investigation shows the release mechanisms and reveals the possible chemical and physical interaction between hydrogel and cement paste. As expected, H-3 generally has more tendency to create shell like morphology. This morphology difference is due to higher adhesion between solid skeleton and H-3 compared with H-2 which has higher acrylic acid concentration. This increased adhesion is shown in 12 hours SEM images in Figure 5-5. The change in the morphology of desorbing hydrogel or sticking to more than one side of the macrovoid show the higher adhesion between H-3 and cement skeleton in general. In contrast, H-2 generally shows lower adhesion and the cross section morphology has less deformation and change compared to initial cross section morphology. This can indicate different mechanisms of desorption and show the lower effect of capillary forces on H-2 due to less adhesion. However, partially adhered H-2 samples are observed in the cases for FA, GP1 and Ctrl; which can be due to chemical effect on the hydrogel skin, drop in RH, pore microstructure or hydration rate.

An interesting mechanism is observed in the morphology studying for the H-3-FA samples which are illustrated in Figure 5-6. In these samples, H-3 shows a tendency to adhere to all sides of the macrovoid. Due to this boundary condition (hydrogel is fixed on all sides) and the change in the surrounding chemical potential which leads to water release from hydrogel and consequent shrinkage a form of cavity nucleated. This is a very interesting phenomenon which is observed in all the H-3-FA samples. These samples either

form a cavity in the middle portion or get ruptured from a corner, which is due to very high adhesion. The fundamental reasons for this high adhesion is not fully known yet.

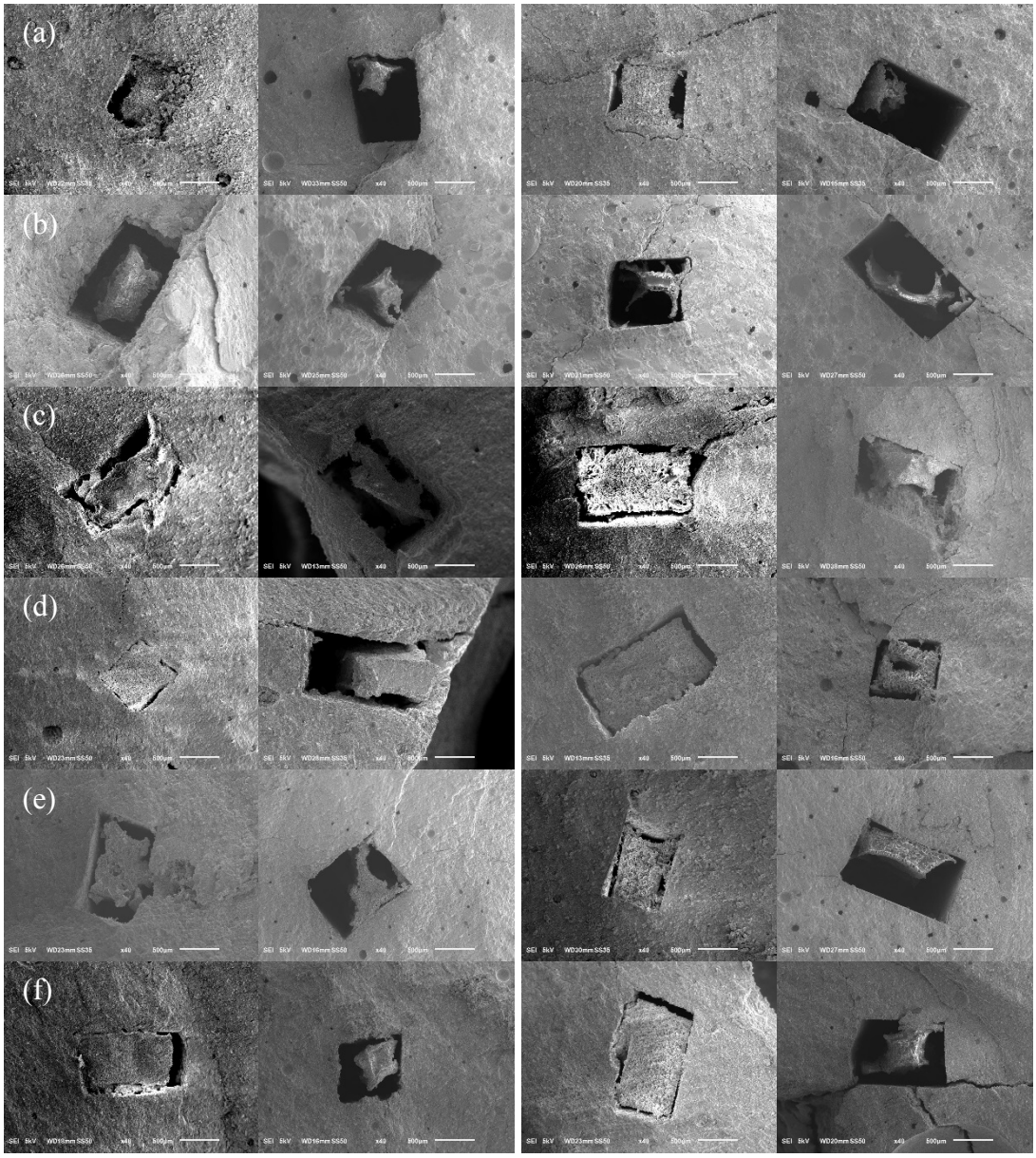

Figure 5-5 Hydrogel morphology evolution in different blended cement paste: Rows (a-f) are: Ctrl, SF, S, FA, GP1 and GP2, respectively. From left to right: 1th and 2nd columns are H-2 at 8 and 12 h, respectively; 3rd and 4th columns are H-3 at 8 and 12 h, respectively.

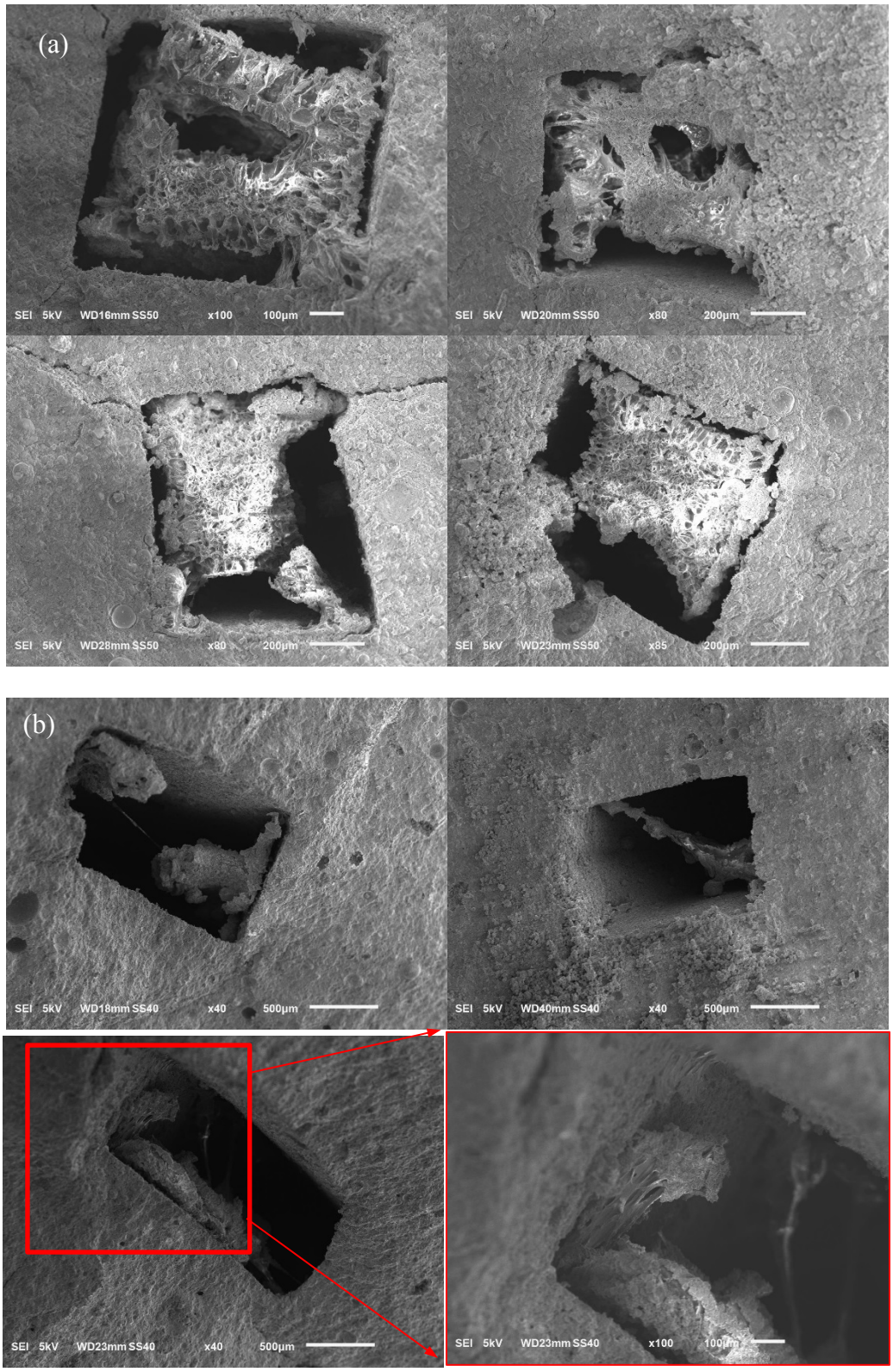

Figure 5-6 (a) H-3-FA at 12 h, two samples with cavity and two are ruptured, (b) H-3-FA at 16 h, three sample, ruptured and shell like morphology with high magnification.

5.4 FTIR analysis

The FTIR experiments and analysis are performed in order to clarify the possible chemical effect of SCMs on the chemical structure of hydrogels. In the previous chapter, a difference between skin and interior bulk of hydrogels was observed, which has a major effect on the interfacial interaction between hydrogels and matrix. The FTIR spectra of H-2 and H-3 in six different diluted mixtures are shown in Figure 5-7.

H-2 and H-3 generally show similar features in the spectra of the interior bulk [53,202]. The peak at 1638 cm^{-1} is related to the presence of amide group [203]. The characteristic band at 1560 cm^{-1} can be referred to asymmetric stretching of carboxylate groups ($–COO^–$) and the peak at 1408 cm^{-1} is due to symmetric stretching of carboxylate groups; the band at 1560 cm^{-1} can be attributed to hydrolysis of amide groups and conversion of them to carboxylate groups [34,133,197]. These observations show no specific differences between different blended cement mixtures.

However, like in the cement paste and hydrogels in previous chapter, there are noticeable differences between the skin and bulk FTIR spectra in all the blended cement mixture. The evidence of calcium carbonate formation on the skin was observed. The peak at 874 cm^{-1} is related to out-of-plane bending of CO_3^{-2} [204]. The next major difference on skin is the peak at 1110 cm^{-1} which is related to symmetric stretching of CO_3^{-2} and attributed to vaterite or/and aragonite, two polymorphs of calcium carbonate [141,205]. The peak around 1413 cm^{-1} which was observed in previous chapter related to the H-1 and H-2 skins corresponds to asymmetric stretch of CO_3^{-2} [34,141] and is not pronounced here. Finally, the increases in the peaks at 2920 cm^{-1} and 2850 cm^{-1} are observed to be more noticeable on the skin compared with bulk for H-2, however they are only observed on skin

for H-3, which can be attributed to C-H stretching; this may confirm the existence of strong chemical bonds between calcium carbonate formed on the hydrogel surface and hydrogel [204]. No significant effect from SCMs on the hydrogel skin is observed, which can be the cause for high adhesion mentioned in previous section, specifically for fly ash mixture.

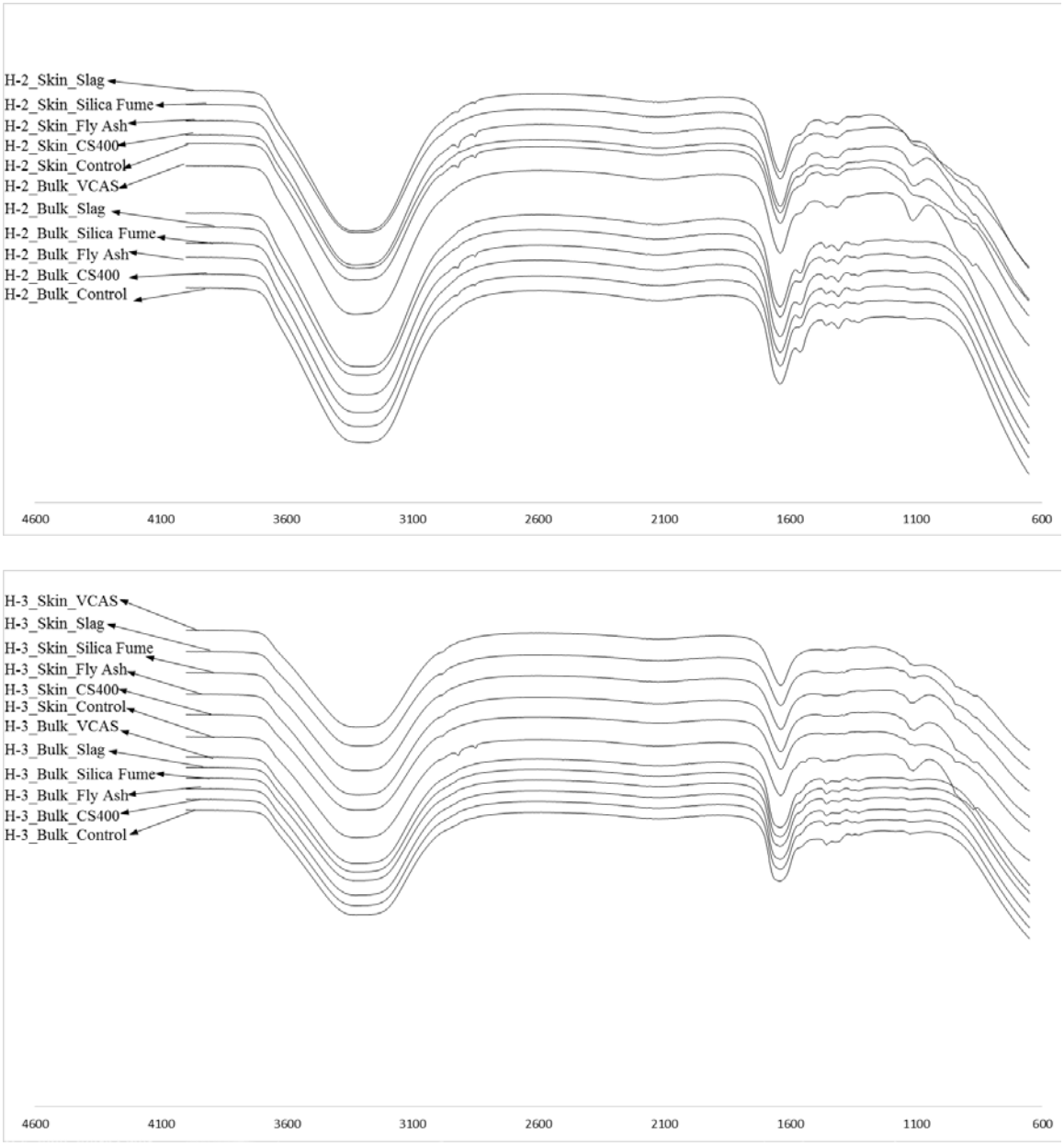

Figure 5-7 FTIR analysis on the H-2 and H-3, bulk and skin.

5.5 Microstructure investigation

In this section, the back scatter SEM imaging is used to study the microstructure of the surrounding matrix and regions far away from hydrogel. The hydration degree of cement paste adjacent to hydrogel and far away at different time can be different which is also investigated. It is necessary to note that the SEM imaging does not give us enough resolution for nano-scale analysis, hydration degree and porosity at the micro-scale is the main focus.

The backscatter SEM images of matrix adjacent to hydrogel and far away at the age of 8 h are illustrated in Figure 5-8 (a) and (b). As shown in the images the cement paste degree of hydration next to hydrogel is higher compared with far away from hydrogel, since there are less unhydrated particles in Figure 5-8 (a) compared with Figure 5-8 (b). This can be explained by existence of extra water in the region close to hydrogel which can be effective on increasing the rate of hydration. It is also noticed that the number of large capillary pores are increased close to hydrogel.

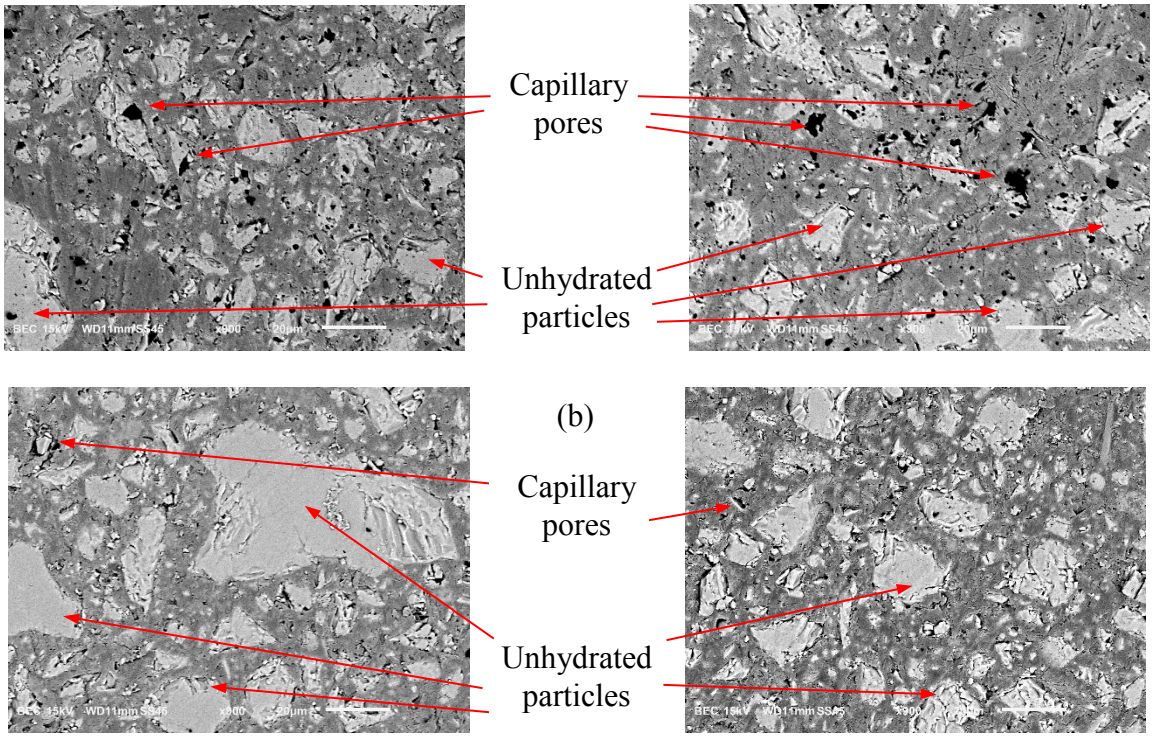

Figure 5-8 Backscatter SEM imaging of cement paste samples freeze dried at 8 h; (a) H-2-Ctrl adjacent to hydrogel (b) H-2-Ctrl far away from hydrogel

Chapter 6: Conclusion and future work

6.1 Conclusion

This study is performed to obtain a fundamental understanding of the interaction between cementitious materials and superabsorbent hydrogels. For the past two decades, efforts have been focused primarily on the effect of hydrogels on the performance characteristics of cementitious materials. This study presented a systematic and fundamental experimental study on the absorption/desorption behavior of hydrogels in cementitious materials. A significant aspect of this study is the fact that the hydrogel synthesis was performed in house, which allows us to control the chemical and physical properties of the hydrogels and to establish the link between the molecular structure of hydrogels and their behavior in cementitious materials. In this investigation, chemical and mechanical interactions between hydrogels and cementitious material are considered. These interactions were decoupled in order to have better insight into the desorption behavior of hydrogels.

In this research, the effect of capillary pressure on the desorption behavior of hydrogels in contact with porous ceramics was discussed and presented for the very first time. Also, the investigation of hydrogels in cement paste revealed the importance of the interfacial bonding between hydrogels and cement matrix on the desorption behavior of hydrogels. A brief summary of the main findings of this investigation is listed as follows:

- The effect of mechanical pressure on the absorption of SAP hydrogels was evaluated and shown to notably influence the absorption behavior; this indicates

the importance of considering the constraint effect of the cementitious matrix on SAPs' behavior during initial mixing.

- The desorption of hydrogels under the action of capillary forces was investigated and related to the microstructure and internal relative humidity in pores. The capillary adhesion developed at the interface between hydrogels and cementitious materials was shown to increase the desorption of hydrogels.
- The effect of hydrogel size and interfacial bonding strength on the desorption of hydrogels interacting with a cementitious matrix was elucidated and explained on the basis of fracture mechanics. It was proposed that with increasing size of hydrogels and decreasing interfacial bonding strength, the tendency to interface debonding increases resulting in a decrease of desorption due to the loss of the Laplace pressure at the interface.
- SEM microscopy of two hydrogels with different chemical compositions embedded in cement paste indicated a significant contrast in their desorption morphology. It was shown that the hydrogel with a higher concentration of acrylamide showed a tendency to bond to the cementitious matrix. The results from this study provide new insight into the underlying mechanisms determining the desorption of hydrogels in cementitious materials and help in the development of design guidelines for the internal curing applications. These results showed the influence of chemical structure of hydrogels on interfacial bonding between hydrogels and cement paste, which can effect on the desorption mechanisms.

- The desorption of hydrogels with different chemical compositions was systematically investigated under the effect of the capillary forces. The chemical interactions between the hydrogels and pore solutions and hydrating cement particles were studied. The influence of chemical interactions on hydrogels' surface characteristics and how the surface characteristics affect desorption due to the capillary forces are highlighted.
- The desorption test of swollen hydrogels in contact with cementitious materials indicated a larger effect of the capillary forces on the desorption rate of hydrogels with lower concentration of acrylic acid. This behavior was explained in light of the changes in the surface characteristics of the hydrogels. In the hydrogel with a very high concentration of acrylic acid (H-1), a relatively thick and stiff skin was formed, which prevents a close contact between the hydrogel and the cementitious substrate at the interface thereby reducing the effect of capillary forces on the hydrogel. It was shown that with an increase in the concentration of acrylamide the hydrogel showed a stronger adhesion to the cementitious material, which accelerated the desorption of the hydrogel due to the capillary suction.
- The freeze drying technique was used for the first time to investigate the absorption/desorption behavior of hydrogels in a hydrating cement mixture. This technique compared to other techniques such as neutron radiography and tomography is very cost effective and can provide better understanding of the behavior of hydrogel in a hydrating cement mixture. In addition, the evolution of the cement mixture microstructure can be tracked at the same time.

- The scanning electron microscopic examination of hydrogel microstrip in a hydrating cementitious material (using freeze drying technique) highlighted an interesting contrast in the morphology evolution of hydrogels during desorption. It was observed that the hydrogel with a low concentration of acrylic acid (H-3) showed a shell-like morphology while a solid morphology was examined in the hydrogel with a high concentration of acrylic acid (H-1 and H-2). The distinct contrast in the desorption morphology was attributed to the difference in the interface bonding of the two hydrogels. The interface bonding with the cementitious matrix is expected to influence the desorption rate of hydrogels. The results from this study help elucidate the fundamental processes affecting the desorption behavior of hydrogels in cementitious materials.
- Examination of the effect of SCMs on the desorption of hydrogels revealed the dependence of desorption kinetics on the rate of hydration and microstructure percolation. It was found that the cement paste with SF showed the fastest desorption among all the samples. On the other hand, the cement paste with FA was shown to start desorption later than the other cement pastes. Such desorption behavior can be explained in light of the effect of hydration and microstructure formation of the cementitious matrix.

6.2 Future work

The main focus in this research was to understand the absorption/desorption behavior of hydrogel in cementitious material in order to design the best internal curing agent and a suitable mixture design for HPC. Of course this research cannot answer all the questions

in regard to use of superabsorbent hydrogels as an admixture. To make hydrogel a practical internal curing agent, many investigations are needed to be performed; here are some of author's suggestions for future works:

- The hydrogels that are used in this study consist of two types of monomers: acrylic acid and acrylamide. It is important to mention that even though these hydrogels show completely different desorption behavior in cementitious material, it is still highly important to explore different types of monomers (such as Alginate) which can give us more alternatives.
- One of the main flaws of hydrogel is the reduction in compressive strength which is due to increasing the voids in concrete. Hydrogel encapsulated with bacteria can be effective to fill the macro-void created with hydrogel. There is a lack of knowledge for encapsulation and release mechanism of bacteria in and out of hydrogel.
- Mass transport phenomenon in porous media is highly complex. The effect of hydrogel on mass transport and the mechanisms of self-sealing need to be investigated. This can lead to major improvement in durability and sustainability of concrete.
- Hydrogel create macro-void which can be effective on freeze-thaw resistance. This can be an alternative for traditional air-entrainment technique to prevent damages caused by freeze-thaw. But, there is a lack of fundamental research in this area.

- Mixture design, type, shape and size of hydrogel are parameters which can effect on freeze-thaw, mass transport, change in relative humidity, self-healing and self-sealing aspects.
- All the effort that has been done in this study is on the interaction between hydrogel and cement, but these understandings need to be applied on concrete. The effect of hydrogel on concrete is vital which is not fully known.
- Geopolymers are considered as an alternative for cement. Internal curing is indeed an important component in the future of geopolymers. There is not enough knowledge in regard to hydrogel behavior in geopolymers. The interaction between hydrogel and geopolymer solution and microstructure is highly important which is poorly known.

References

[1] K.J. Folliard, N.S. Berke, Properties of high-performance concrete containing shrinkage-reducing admixture, Cem. Concr. Res. 27 (1997) 1357–1364.

[2] S. Zhutovsky, K. Kovler, Effect of internal curing on durability-related properties of high performance concrete, Cem. Concr. Res. 42 (2012) 20–26.

[3] P.K. Mehta, P.J.M. Monteiro, Concrete - Microstructure, Properties, and Materials., (2006) 684.

[4] G.R. de Sensale, A.F. Goncalves, Effects of fine LWA and SAP as internal water curing agents, Int. J. Concr. Struct. Mater. 8 (2014) 229–238.

[5] O.M. Jensen, P.F. Hansen, Water-entrained cement-based materials II. Experimental observations, Cem. Concr. Res. 32 (2002) 973–978.

[6] K. Kovler, O.M. Jensen, Internal curing of concrete, state-of-the-art report of RILEM technical committee 196-ICC, 2007.

[7] M.G. Christof Schröfl, Viktor Mechtcherine, Relation between the molecular structure and the efficiency of superabsorbent polymers (SAP) as concrete admixture to mitigate autogenous shrinkage, (2012).

[8] E. ichi Tazawa, S. Miyazawa, T. Kasai, Chemical shrinkage and autogenous shrinkage of hydrating cement paste, Cem. Concr. Res. 25 (1995) 288–292.

[9] G. Sant, P. Lura, J. Weiss, Measurement of volume change in cementitious materials at early ages: review of testing protocols and interpretation of results, Transp. Res. Rec. 1979 (2006) 21–29.

[10] E.E. Holt, Early age autogenous shrinkage of concrete, VTT Publ. (2001) 2–184.

[11] R. Henkensiefken, D. Bentz, T. Nantung, J. Weiss, Volume change and cracking in internally cured mixtures made with saturated lightweight aggregate under sealed and unsealed conditions, Cem. Concr. Compos. 31 (2009) 427–437.

[12] D. Cusson, T. Hoogeveen, Internal curing of high-performance concrete with pre-soaked fine lightweight aggregate for prevention of autogenous shrinkage cracking, Cem. Concr. Res. 38 (2008) 757–765.

[13] O.M. Jensen, P.F. Hansen, Autogenous deformation and RH-change in perspective, Cem. Concr. Res. 31 (2001) 1859–1865.

[14] P. Lura, O.M. Jensen, K. van Breugel, Autogenous shrinkage in high-performance cement paste: An evaluation of basic mechanisms, Cem. Concr. Res. 33 (2003) 223–232.

[15] A.G.A. Saul, Principles underlying the steam curing of concrete at atmospheric pressure, Mag. Concr. Res. 2 (1951) 127–140.

[16] W.F. Price, Curing concrete, Concr. 32 (1998) 9–10.

[17] H.M.Z. Al-Abidien, J.H. Allred, R. Bouclin, C.A. Carbonell, R.J. Ferrell, R.P. Furick, R.D. Gaynor, J. Gendrich, G.R.U. Burg, F.K. Gibbe, G.T. Harris, G.W. Hollon, R.H. Keck, F. Kozeliski, D.B. McCaulley, M.B. Mittelacher, Hot weather concreting, ACI Mater. J. 88 (1991) 417–436.

[18] E.A. Kay, Hot and cold weather concreting, in: Adv. Concr. Technol., 2003: pp. 1–18.

[19] A.A. Ramezanianpour, M.H. Khazali, P. Vosoughi, Effect of steam curing cycles on strength and durability of SCC: A case study in precast concrete, Constr. Build. Mater. 49 (2013) 807–813.

[20] American Society of Testing and Materials (ASTM), Standard Specification for Sheet Materials for Curing Concrete - C171-01, (2001).

[21] M.J. Krafcik, K.A. Erk, Characterization of superabsorbent poly (sodium-acrylate acrylamide) hydrogels and influence of chemical structure on internally cured mortar, Mater. Struct. 49 (2016) 4765–4778.

[22] A.M. Soliman, M.L. Nehdi, Effect of drying conditions on autogenous shrinkage in ultra-high performance concrete at early-age, Mater. Struct. 44 (2011) 879–899.

[23] M. Şahmaran, M. Lachemi, K.M. a. Hossain, V.C. Li, Internal curing of engineered cementitious composites for prevention of early age autogenous shrinkage cracking, Cem. Concr. Res. 39 (2009) 893–901.

[24] A. Bentur, S. Igarashi, K. Kovler, Prevention of autogenous shrinkage in high-strength concrete by internal curing using wet lightweight aggregates, Cem. Concr. Res. 31 (2001) 1587–1591.

[25] V. Mechtcherine, H.-W. Reinhardt, Application of Super Absorbent Polymers (SAP) in Concrete Construction, Springer, 2012.

[26] H. Beushausen, M. Gillmer, M. Alexander, The influence of superabsorbent polymers on strength and durability properties of blended cement mortars, Cem. Concr. Compos. 52 (2014) 73–80.

[27] M.T. Hasholt, O.M. Jensen, Chloride migration in concrete with superabsorbent polymers, Cem. Concr. Compos. 55 (2015) 290–297.

[28] V. Mechtcherine, E. Secrieru, C. Schröfl, Effect of superabsorbent polymers (SAPs) on rheological properties of fresh cement-based mortars — Development of yield stress and plastic viscosity over time, Cem. Concr. Res. 67 (2015) 52–65.

[29] D. Snoeck, D. Schaubroeck, P. Dubruel, N. De Belie, Effect of high amounts of superabsorbent polymers and additional water on the workability, microstructure and strength of mortars with a water-to-cement ratio of 0.50, Constr. Build. Mater. 72 (2014) 148–157.

[30] O.M. Jensen, P.F. Hansen, Water-entrained cement-based materials I . Principles and theoretical background, Cem. Concr. Res. 31 (2001) 647–654.

[31] A. Mignon, D. Snoeck, P. Dubruel, S. Van Vlierberghe, N. De Belie, Crack mitigation in concrete: superabsorbent polymers as key to success?, Materials (Basel). 10 (2017) 237.

[32] I. De La Varga, J. Castro, D. Bentz, J. Weiss, Application of internal curing for mixtures containing high volumes of fly ash, Cem. Concr. Compos. 34 (2012) 1001–1008.

[33] D.P. Bentz, W.J. Weiss, Internal Curing : A 2010 State-of-the- Art Review, Natl. Inst. Stand. Technol. Rep. 7765. (2011) 82.

[34] A. Mignon, D. Snoeck, D. Schaubroeck, N. Luickx, P. Dubruel, S. Van Vlierberghe, N. De Belie, pH-responsive superabsorbent polymers: A pathway to self-healing of mortar, React. Funct. Polym. 93 (2015) 68–76.

[35] H.X.D. Lee, H.S. Wong, N.R. Buenfeld, Self-sealing of cracks in concrete using superabsorbent polymers, Cem. Concr. Res. 79 (2016) 194–208.

[36] J.Y. Wang, D. Snoeck, S. Van Vlierberghe, W. Verstraete, N. De Belie, Application of hydrogel encapsulated carbonate precipitating bacteria for approaching a realistic self-healing in concrete, Constr. Build. Mater. 68 (2014) 110–119.

[37] G. Souradeep, H.W. Kua, Encapsulation technology and techniques snself-healing concrete, J. Mater. Civ. Eng. 25 (2016) 864–870.

[38] B.L. Cope, G.E. Ramey, Reducing drying shrinkage of concrete, Concr. Int. (2001) 76–82.

[39] D.P. Bentz, Influence of shrinkage-reducing admixtures on early-age properties of cement pastes, J. Adv. Concr. Technol. 4 (2006) 423–429.

[40] Z. He, Z.J. LI, M.Z. Chen, W.Q. Liang, Properties of shrinkage-reducing admixture-modified pastes and mortars, Mater. Struct. 39 (2006) 445–453.

[41] S.P. Shah, M.E. Karaguler, M. Sarigaphuti, Effect of shrinkage reducing admixtures on restrained shrinkage cracking of concrete, ACI Mater. J. 89 (1992) 289–295.

[42] Q. Zhu, C.W. Barney, K.A. Erk, Effect of ionic crosslinking on the swelling and mechanical response of model superabsorbent polymer hydrogels for internally cured concrete, Mater. Struct. 48 (2015) 2261–2276.

[43] L.P. Esteves, Superabsorbent polymers: On their interaction with water and pore fluid, Cem. Concr. Compos. 33 (2011) 717–724.

[44] K. Farzanian, K. Pimenta Teixeira, I. Perdigão Rocha, L. De Sa Carneiro, A. Ghahremaninezhad, The mechanical strength, degree of hydration, and electrical resistivity of cement pastes modified with superabsorbent polymers, Constr. Build. Mater. 109 (2016) 156–165.

[45] A. Assmann, H.W. Reinhardt, Tensile creep and shrinkage of SAP modified concrete, Cem. Concr. Res. 58 (2014) 179–185.

[46] B. Craeye, M. Geirnaert, G. De Schutter, Super absorbing polymers as an internal curing agent for mitigation of early-age cracking of high-performance concrete bridge decks, Constr. Build. Mater. 25 (2011) 1–13.

[47] V. Mechtcherine, M. Gorges, C. Schroefl, A. Assmann, W. Brameshuber, D. Ribeiro, Anto´nio Bettencourt Cusson, et al., Effect of internal curing by using superabsorbent polymers (SAP) on autogenous shrinkage and other properties of a high-performance fine-grained concrete : results of a RILEM round-robin test, (2014) 541–562.

[48] P. Lura, F. Durand, A. Loukili, K. Kovler, Compressive strength of cement pastes and mortars with superabsorbent polymers, in: Int. RILEM Conf. Vol. Chang. Hardening Concr. Test. Mitig. 20-23 August, 2006: pp. 117–125.

[49] S. Igarashi, a Watanabe, O.M. Jensen, P. Lura, K. Kovler, Experimental study on prevention of autogenous deformation by internal curing using super-absorbent polymer particles, Int. RILEM Conf. Vol. Chang. Hardening Concr. Test. Mitig. (2006) 77–86.

[50] O.M. Jensen, Use of superabsorbent polymers in construction materials, in: H.C. W. Sun, K. van Breugel, C. Miao, G. Ye (Ed.), Int. Conf. Microstruct. Relat. Durab. Cem. Compos., RILEM Publications, 2008: pp. 757–764.

[51] K.S. Sikora, A.J. Klemm, Effect of Superabsorbent Polymers on Workability and Hydration Process in Fly Ash Cementitious Composites, J. Mater. Civ. Eng. 27 (2015) 4014170.

[52] D. Snoeck, L.F. Velasco, A. Mignon, S. Van Vlierberghe, P. Dubruel, P. Lodewyckx, N. De Belie, The effects of superabsorbent polymers on the microstructure of cementitious materials studied by means of sorption experiments, Cem. Concr. Res. 77 (2015) 26–35.

[53] K. Farzanian, A. Ghahremaninezhad, Desorption of superabsorbent hydrogels with varied chemical compositions in cementitious materials, Mater. Struct. (2017).

[54] A. Pourjavadi, S.M. Fakoorpoor, P. Hosseini, Alireza Khaloo, Interactions between superabsorbent polymers and cement-based composites incorporating colloidal silica nanoparticles, (2013).

[55] Y. Wehbe, A. Ghahremaninezhad, Combined effect of shrinkage reducing admixtures (SRA) and superabsorbent polymers (SAP) on the autogenous shrinkage and properties of cementitious materials, Constr. Build. Mater. 138 (2017) 151–162.

[56] V. Mechtcherine, M. Gorges, C. Schroefl, A. Assmann, Effect of internal curing by using superabsorbent polymers (SAP) on autogenous shrinkage and other properties of a high-performance fine-grained concrete : results of a RILEM round-robin test, Mater. Struct. (2014) 541–562.

[57] World Energy Council, Efficient Use of Energy Utilizing High Technology: An Assessment of Energy Use in Industry and Building, World Energy Council, London, 1995.

[58] EPA (Environmental Protection Agency), Available and Emerging Technologies for Reducing Greenhouse Gas Emissions from the Portland Cement Industry, Washington D.C., 2010.

[59] USGS (US Geological Survey), Background Facts and Issues Concerning Cement and Cement Data, Reston, VA, 2005.

[60] D. Snoeck, O.M. Jensen, N. De Belie, The influence of superabsorbent polymers on the autogenous shrinkage properties of cement pastes with supplementary cementitious materials, Cem. Concr. Res. 74 (2015) 59–67.

[61] P. Termkhajornkit, T. Nawa, M. Nakai, T. Saito, Effect of fly ash on autogenous shrinkage, Cem. Concr. Res. 35 (2005) 473–482.

[62] O. Mejlhede Jensen, P. Freiesleben Hansen, Autogenous deformation and change of the relative humidity in silica fume-modified cement paste, ACI Mater. J. 93 (1996) 539–543.

[63] K.M. Lee, H.K. Lee, S.H. Lee, G.Y. Kim, Autogenous shrinkage of concrete containing granulated blast-furnace slag, Cem. Concr. Res. 36 (2006) 1279–1285.

[64] E. Dunstan, The effect of fly ash on concrete alkali-aggregate reaction, Cem. Concr. Aggregates. 3 (1981) 101.

[65] H. Kizhakkumodom Venkatanarayanan, P.R. Rangaraju, Decoupling the effects of chemical composition and fineness of fly ash in mitigating alkali-silica reaction, Cem. Concr. Compos. 43 (2013) 54–68.

[66] K. Harish, P. Rangaraju, Effect of blended fly ashes in mitigating alkali-silica reaction, Transp. Res. Rec. J. Transp. Res. Board. 2240 (2011) 80–88.

[67] M.H. Shehata, M.D.. Thomas, The effect of fly ash composition on the expansion of concrete due to alkali–silica reaction, Cem. Concr. Res. 30 (2000) 1063–1072.

[68] J.S. Lumley, The ASR expansion of concrete prisms made from cements partially replaced by ground granulated blastfurnace slag, Constr. Build. Mater. 7 (1993) 95–99.

[69] D. Hester, C. McNally, M. Richardson, A study of the influence of slag alkali level on the alkali–silica reactivity of slag concrete, Constr. Build. Mater. 19 (2005) 661–665.

[70] A. Beglarigale, H. Yazici, Mitigation of detrimental effects of alkali-silica reaction in cement-based composites by combination of steel microfibers and ground-granulated blast-furnace slag, J. Mater. Civ. Eng. 26 (2014) 4014091.

[71] M. Kamali, A. Ghahremaninezhad, Effect of glass powders on the mechanical and durability properties of cementitious materials, Constr. Build. Mater. 98 (2015) 407–416.

[72] J. Flores, M. Kamali, A. Ghahremaninezhad, An investigation into the properties and microstructure of cement mixtures modified with cellulose nanocrystal, Materials (Basel). 10 (2017) 1–16.

[73] M. Kamali, A. Ghahremaninezhad, An investigation into the influence of superabsorbent polymers on the properties of glass powder modified cement pastes, Constr. Build. Mater. 149 (2017).

[74] Y. Shao, T. Lefort, S. Moras, D. Rodriguez, Studies on concrete containing ground waste glass, Cem. Concr. Res. 30 (2000) 91–100.

[75] T.D. Dyer, R.K. Dhir, Chemical reactions of glass cullets used as cement component, J. Mater. Civ. Eng. 13 (2001) 412–417.

[76] Z. Wang, C. Shi, J. Song, Effect of glass powder on chloride ion transport and alkali-aggregate reaction expansion of lightweight aggregate concrete, J. Wuhan Univ. Technol. Sci. Ed. 24 (2009) 312–317.

[77] N. Schwarz, H. Cam, N. Neithalath, Influence of a fine glass powder on the durability characteristics of concrete and its comparison to fly ash, Cem. Concr. Compos. 30 (2008) 486–496.

[78] R.-U.-D. Nassar, P. Soroushian, Green and durable mortar produced with milled waste glass, Mag. Concr. Res. 64 (2012) 605–615.

[79] R.-U.-D. Nassar, P. Soroushian, Strength and durability of recycled aggregate concrete containing milled glass as partial replacement for cement, Constr. Build. Mater. 29 (2012) 368–377.

[80] K. Pettersson, Effects of silica fume on alkali-silica expansion in mortar specimens, Cem. Concr. Res. 22 (1992) 15–22.

[81] A.M. Boddy, R.D. Hooton, M.D.A. Thomas, The effect of the silica content of silica fume on its ability to control alkali–silica reaction, Cem. Concr. Res. 33 (2003) 1263–1268.

[82] W. Aquino, D.. Lange, J. Olek, The influence of metakaolin and silica fume on the chemistry of alkali–silica reaction products, Cem. Concr. Compos. 23 (2001) 485–493.

[83] T. Ramlochan, M. Thomas, K. a Gruber, The effect of metakaolin on alkali–silica reaction in concrete, Cem. Concr. Res. 30 (2000) 339–344.

[84] E.M. Ahmed, Hydrogel: Preparation, characterization, and applications: A review, J. Adv. Res. 6 (2015) 105–121.

[85] K.S. Soppimath, T.M. Aminabhavi, A.M. Dave, S.G. Kumbar, W.E. Rudzinski, Stimulus-responsive smart'' hydrogels as novel drug delivery dystems, Drug Dev. Ind. Pharm. 28 (2002) 957–974.

[86] A.Z. Zardad, Y.E. Choonara, L.C. du Toit, P. Kumar, M. Mabrouk, P.P. Demarco Kondiah, V. Pillay, A review of thermo- and ultrasound-responsive polymeric systems for delivery of chemotherapeutic agents, Polymers (Basel). 8 (2016) 1–22.

[87] K. Vats, D.S.W. Benoit, Dynamic manipulation of hydrogels to control cell behavior: a review, Tissue Eng. Part B Rev. 19 (2013) 455–469.

[88] I. El-Sherbiny, M. Yacoub, Hydrogel scaffolds for tissue engineering: Progress and challenges, Glob. Cardiol. Sci. Pract. 2013 (2013) 316–42.

[89] J. Akhter, K. Mahmood, K.A. Malik, A. Mardan, M. Ahmad, M.M. Iqbal, Effects of hydrogel amendment on water storage of sandy loam and loam soils and seedling growth of barley, wheat and chickpea, Plant, Soil Environ. 50 (2004) 463–469.

[90] R. Vundavalli, S. Vundavalli, M. Nakka, D.S. Rao, Biodegradable nano-hydrogels in agricultural farming - alternative source for water resources, Procedia Mater. Sci. 10 (2015) 548–554.

[91] J.L. Drury, D.J. Mooney, Hydrogels for tissue engineering: Scaffold design variables and applications, Biomaterials. 24 (2003) 4337–4351.

[92] R. Landers, U. Hübner, R. Schmelzeisen, R. Mülhaupt, Rapid prototyping of scaffolds derived from thermoreversible hydrogels and tailored for applications in tissue engineering, Biomaterials. 23 (2002) 4437–4447.

[93] K.T. Nguyen, J.L. West, Photopolymerizable hydrogels for tissue engineering applications, Biomaterials. 23 (2002) 4307–4314.

[94] Y. Qiu, K. Park, Environment-sensitive hydrogels for drug delivery, Adv. Drug Deliv. Rev. 64 (2012) 49–60.

[95] T.R. Hoare, D.S. Kohane, Hydrogels in drug delivery: Progress and challenges, Polymer (Guildf). 49 (2008) 1993–2007.

[96] G.R. Cosgrove, J.B. Delashaw, J.A. Grotenhuis, J.M. Tew, H. van Loveren, R.F. Spetzler, T. Payner, G. Rosseau, M.E. Shaffrey, L.N. Hopkins, R. Byrne, A. Norbash, Safety and efficacy of a novel polyethylene glycol hydrogel sealant for watertight dural repair, J. Neurosurg. 106 (2007) 52–58.

[97] K.D. Kim, N.M. Wright, Polyethylene glycol hydrogel spinal sealant (duraseal spinal sealant) as an adjunct to sutured dural repair in the spine, Spine (Phila. Pa. 1976). 36 (2011) 1906–1912.

[98] J. Höpfner, C. Klein, M. Wilhelm, A novel approach for the desalination of seawater by means of reusable poly(acrylic acid) hydrogels and mechanical force, Macromol. Rapid Commun. 31 (2010) 1337–1342.

[99] J. Höpfner, A new method of seawater desalination via acrylic acid based hydrogels, Karlsruher Institut für Technologie (KIT), 2013.

[100] H.M. Shewan, J.R. Stokes, Review of techniques to manufacture micro-hydrogel particles for the food industry and their applications, J. Food Eng. 119 (2013) 781–792.

[101] A.S. Hoffman, Hydrogels for biomedical applications, Adv. Drug Deliv. Rev. 64 (2012) 18–23.

[102] D. Seliktar, Designing cell-compatible hydrogels for biomedical applications, Science (80-.). 336 (2012) 1124–1128.

[103] J. Berger, M. Reist, J.M. Mayer, O. Felt, N.A. Peppas, R. Gurny, Structure and interactions in covalently and ionically crosslinked chitosan hydrogels for biomedical applications, Eur. J. Pharm. Biopharm. 57 (2004) 19–34.

[104] B. Vázquez, J. San Roman, C. Peniche, M.E. Cohen, Polymeric hydrophilic hydrogels with flexible hydrophobic chains. control of the hydration and interactions with water molecules, Macromolecules. 30 (1997) 8440–8446.

[105] M. Pekar, Hydrogels with micellar hydrophobic (nano)domains, Front. Mater. 1 (2015) 1–14.

[106] Y. Tabata, Biomaterial technology for tissue engineering applications, J. R. Soc. Interface. 6 (2009) S311–S324.

[107] H. Omidian, J.G. Rocca, K. Park, Advances in superporous hydrogels, J. Control. Release. 102 (2005) 3–12.

[108] S. Kiatkamjornwong, Superabsorbent polymers and superabsorbent polymer composites, ScienceAsia. 33 (2007) 39–43.

[109] T. Ogata, K. Nagayoshi, T. Nagasako, S. Kurihara, T. Nonaka, Synthesis of hydrogel beads having phosphinic acid groups and its adsorption ability for lanthanide ions, React. Funct. Polym. 66 (2006) 625–633.

[110] D. Hunkeler, Synthesis and characterization of high molecular weight water-soluble polymers, Polym. Int. 27 (1992) 23–33.

[111] N. Watanabe, Y. Hosoya, A. Tamura, H. Kosuge, Characteristics of water???absorbent polymer emulsions, Polym. Int. 30 (1993) 525–531.

[112] A. Pourjavadi, M.J. Zohuriaan-Mehr, Modification of carbohydrate polymers via grafting in air. 1. Ceric-induced synthesis of starch-g-polyacrylonitrile in presence and absence of oxygen, Starch/Staerke. 54 (2002) 140–147.

[113] T. Qunyi, Z. Ganwei, Rapid synthesis of a superabsorbent from a saponified starch and acrylonitrile/AMPS graft copolymers, Carbohydr. Polym. 62 (2005) 74–79.

[114] B.V.O. Muir, D. Myung, W. Knoll, C.W. Frank, Grafting of cross-linked hydrogel networks to titanium surfaces, ACS Appl. Mater. Interfaces. 6 (2014) 958–966.

[115] Z. Ajji, G. Mirjalili, A. Alkhatab, H. Dada, Use of electron beam for the production of hydrogel dressings, Radiat. Phys. Chem. 77 (2008) 200–202.

[116] F. Khoylou, F. Naimian, Radiation synthesis of superabsorbent polyethylene oxide/tragacanth hydrogel, Radiat. Phys. Chem. 78 (2009) 195–198.

[117] L. Lazzeri, M.G. Cascone, P. Giusti, M. Laus, Physico-chemical and mechanical characterization of hydrogels of poly (vinyl alcohol) and hyaluronic acid, J. Mater. Sci. Mater. Med. 5 (1994) 862–867.

[118] S. Cai, Y. Hu, X. Zhao, Z. Suo, Poroelasticity of a covalently crosslinked alginate hydrogel under compression, J. Appl. Phys. 108 (2010) 1–8.

[119] P. Lura, K. Van Breugel, I. Maruyama, Effect of curing temperature and type of cement on early-age shrinkage of high-performance concrete, Cem. Concr. Res. 31 (2001) 1867–1872.

[120] C. Schröfl, V. Mechtcherine, M. Gorges, Relation between the molecular structure and the efficiency of superabsorbent polymers (SAP) as concrete admixture to mitigate autogenous shrinkage, Cem. Concr. Res. 42 (2012) 865–873.

[121] F. Horkay, F. Horkay, I. Tasaki, I. Tasaki, P.J. Basser, P.J. Basser, Osmotic swelling of polyacrylate hydrogels in physiological salt solutions, Biomacromolecules. 1 (2000) 84–90.

[122] W. Siriwatwechakul, J. Siramanont, W. Vichit-Vadakan, Behavior of superabsorbent polymers in calcium- and sodium-rich solutions, J. Mater. Civ. Eng. 24 (2012) 976–980.

[123] G. Sudre, D. Hourdet, F. Cousin, C. Creton, Y. Tran, Structure of surfaces and interfaces of poly(N,N-dimethylacrylamide) hydrogels, Langmuir. 28 (2012) 12282–12287.

[124] M.A. Haque, T. Kurokawa, J.P. Gong, Super tough double network hydrogels and their application as biomaterials, Polymer (Guildf). 53 (2012) 1805–1822.

[125] J.-Y. Sun, X. Zhao, W.R.K. Illeperuma, O. Chaudhuri, K.H. Oh, D.J. Mooney, J.J. Vlassak, Z. Suo, Highly stretchable and tough hydrogels, Nature. 489 (2012) 133–136.

[126] J.P. Gong, Y. Katsuyama, T. Kurokawa, Y. Osada, Double-network hydrogels with extremely high mechanical strength, Adv. Mater. 15 (2003) 1155–1158.

[127] A. Mignon, D. Snoeck, K. D'Halluin, L. Balcaen, F. Vanhaecke, P. Dubruel, S. Van Vlierberghe, N. De Belie, Alginate biopolymers: Counteracting the impact of superabsorbent polymers on mortar strength, Constr. Build. Mater. 110 (2016) 169–174.

[128] J. Castro, D. Bentz, J. Weiss, Effect of sample conditioning on the water absorption of concrete, Cem. Concr. Compos. 33 (2011) 805–813.

[129] R.P. Spragg, J. Castro, W. Li, M. Pour-Ghaz, P.T. Huang, J. Weiss, Wetting and drying of concrete using aqueous solutions containing deicing salts, Cem. Concr. Compos. 33 (2011) 535–542.

[130] F. Rajabipour, G. Sant, J. Weiss, Interactions between shrinkage reducing admixtures (SRA) and cement paste's pore solution, Cem. Concr. Res. 38 (2008) 606–615.

[131] A.B. Ribeiro, A. Gonçalves, A. Carrajola, Effect of shrinkage reducing admixtures on the pore structure properties of mortars, Mater. Struct. Constr. 39 (2006) 179–187.

[132] M.J. Krafcik, K.A. Erk, Characterization of superabsorbent poly (sodium-acrylate acrylamide) hydrogels and influence of chemical structure on internally cured mortar, Mater. Struct. 49 (2016) 4765–4778.

[133] A. Mignon, G.J. Graulus, D. Snoeck, J. Martins, N. De Belie, P. Dubruel, S. Van Vlierberghe, pH-sensitive superabsorbent polymers: a potential candidate material for self-healing concrete, J. Mater. Sci. 50 (2015) 970–979.

[134] C. Schröfl, D. Snoeck, V. Mechtcherine, A review of characterisation methods for superabsorbent polymer (SAP) samples to be used in cement-based construction materials: report of the RILEM TC 260-RSC, Mater. Struct. 50 (2017) 197.

[135] L.R.G. Treloar, The Physics of Rubber Elasticity (3rd Edition), Clarendon Press, Oxford, 2005.

[136] P.J. Flory, J. Rehner, Statistical mechanics of cross-linked polymer net works I. rubberlike elasticity, J. Chem. Phys. 11 (1943) 512–520.

[137] P.J. Flory, N. Rabjohn, M.C. Shaffex, Dependence of elastic properties of vulcanized rubber on the degree of cross linking, J. Polym. Sci. I (1949) 225–245.

[138] N.A. Peppas, P. Bures, W. Leobandung, H. Ichikawa, Hydrogels in pharmaceutical formulations, Eur. J. Pharm. Biopharm. 50 (2000) 27–46.

[139] K.S. Anseth, C.N. Bowman, L. Brannon-Peppas, Mechanical properties of hydrogels and their experimental determination, Biomaterials. 17 (1996) 1647–1657.

[140] L.R.G. Treloar, The elasticity and related properties of rubbers, Rubber Chem. Technol. 47 (1974) 625–696.

[141] L. Fernández-Carrasco, D. Torrens-Martín, L.M. Morales, Sagrario Martínez-Ramírez, Infrared spectroscopy in the analysis of building and construction materials, Infrared Spectrosc. – Mater. Sci. Eng. Technol. (2012) 369–382.

[142] J.B. Bates, Fourier transform infrared spectroscopy, Science (80-.). 191 (1976) 31–37.

[143] C. Berthomieu, R. Hienerwadel, Fourier transform infrared (FTIR) spectroscopy, Photosynth. Res. 101 (2009) 157–170.

[144] J. Schmitt, H.-C. Flemming, FTIR-spectroscopy in microbial and material analysis, Int. Biodeterior. Biodegradation. 41 (1998) 1–11.

[145] N. a Burnham, R.J. Colton, Measuring the nanomechanical properties and surface forces of materials using an atomic force microscope, J. Vac. Sci. & Technol. A (Vacuum, Surfaces, Film. 7 (1989) 2906–2913.

[146] N.J. Tao, S.M. Lindsay, S. Lees, Measuring the microelastic properties of biological material, Biophys. J. 63 (1992) 1165–1169.

[147] M. Radmacher, R.W. Tillmann, M. Fritz, H.E. Gaub, From molecules to cells: imaging soft samples with the atomic force microscope, Science (80-.). 257 (1992) 1900–1905.

[148] R.E. Mahaffy, C.K. Shih, F.C. MacKintosh, J. K??s, Scanning probe-based frequency-dependent microrheology of polymer gels and biological cells, Phys. Rev. Lett. 85 (2000) 880–883.

[149] E.K. Dimitriadis, F. Horkay, J. Maresca, B. Kachar, R.S. Chadwick, Determination of elastic moduli of thin layers of soft material using the atomic force microscope, Biophys. J. 82 (2002) 2798–2810.

[150] F. Variola, Atomic force microscopy in biomaterials surface science, Phys. Chem. Chem. Phys. 17 (2015) 2950–2959.

[151] H. Shinto, Y. Aso, T. Fukasawa, K. Higashitani, Adhesion of melanoma cells to the surfaces of microspheres studied by atomic force microscopy, Colloids Surfaces B Biointerfaces. 91 (2012) 114–121.

[152] K.L. Johnson, K. Kendall, A.D. Roberts, Surface Energy and the Contact of Elastic Solids, Proc. R. Soc. A Math. Phys. Eng. Sci. 324 (1971) 301–313.

[153] D.C. Lin, E.K. Dimitriadis, F. Horkay, Robust strategies for automated AFM force curve analysis-II: adhesion-influenced indentation of soft, elastic materials, J. Biomech. Eng. 129 (2007) 904–912.

[154] J.E. Sader, J.W.M. Chon, P. Mulvaney, Calibration of rectangular atomic force microscope cantilevers, Rev. Sci. Instrum. 70 (1999) 3967–3969.

[155] A.B. Abell, K.L. Willis, D.A. Lange, Mercury intrusion porosimetry and image analysis of cement-based materials, J. Colloid Interface Sci. 211 (1999) 39–44.

[156] R.A. Cook, K.C. Hover, Mercury porosimetry of hardened cement pastes, Cem. Concr. Res. 29 (1999) 933–943.

[157] C. Gallé, Effect of drying on cement-based materials pore structure as identified by mercury intrusion porosimetry - A comparative study between oven-, vacuum-, and freeze-drying, Cem. Concr. Res. 31 (2001) 1467–1477.

[158] S. Diamond, Mercury porosimetry: an inappropriate method for the measurement of pore size distributions in cement-based material, Cem. Concr. Res. 30 (2000) 1517–1525.

[159] Grzegorz Machowski, Porosimetry Laboratory, (n.d.). http://galaxy.agh.edu.pl/~k-se/x/en/team/the-porosimetry-laboratory/.

[160] M.A. Sutton, N. Li, D.C. Joy, A.P. Reynolds, X. Li, Scanning electron microscopy for quantitative small and large deformation measurements Part I: SEM imaging at magnifications from 200 to 10,000, Exp. Mech. 47 (2007) 775–787.

[161] K.D. Vernon-Parry, Scanning electron microscopy: an introduction, III-Vs Rev. 13 (2000) 40–44.

[162] M. Wyrzykowski, P. Lura, F. Pesavento, D. Gawin, Modeling of internal curing in maturing mortar, Cem. Concr. Res. 41 (2011) 1349–1356.

[163] P. Trtik, B. Muench, W.J. Weiss, G. Herth, A. Kaestner, E. Lehmann, P. Lura, Neutron tomography measurements of water release from superabsorbent polymers in cement paste, in: Int. Conf. Mater. Sci. 64th RILEM Annu. Week, 2010: pp. 175–185.

[164] C. Schroefl, V. Mechtcherine, P. Vontobel, J. Hovind, E. Lehmann, Sorption kinetics of superabsorbent polymers (SAPs) in fresh Portland cement-based pastes visualized and quantified by neutron radiography and correlated to the progress of cement hydration, Cem. Concr. Res. 75 (2015) 1–13.

[165] P. Trtik, B. Münch, W.J. Weiss, a. Kaestner, I. Jerjen, L. Josic, E. Lehmann, P. Lura, Release of internal curing water from lightweight aggregates in cement paste investigated by neutron and X-ray tomography, Nucl. Instruments Methods Phys. Res. Sect. A Accel. Spectrometers, Detect. Assoc. Equip. 651 (2011) 244–249.

[166] N. Nestle, A. Kuhn, K. Friedemann, C. Horch, F. Stallmach, G. Herth, Water balance and pore structure development in cementitious materials in internal curing with modified superabsorbent polymer studied by NMR, Microporous Mesoporous Mater. 125 (2009) 51–57.

[167] J. Justs, M. Wyrzykowski, F. Winnefeld, D. Bajare, P. Lura, Influence of superabsorbent polymers on hydration of cement pastes with low water-to-binder ratio: A calorimetry study, J. Therm. Anal. Calorim. 115 (2014) 425–432.

[168] H.T. Meryman, Principles of freeze-drying, Ann. N. Y. Acad. Sci. 85 (1960) 630–640.

[169] F. Franks, Freeze-drying of bioproducts: Putting principles into practice, Eur. J. Pharm. Biopharm. 45 (1998) 221–229.

[170] G.D.J. Adams, I. Cook, K.R. Ward, The principles of freeze-drying, Methods Mol. Biol. 1257 (2015) 121–143.

[171] C. Ratti, Freeze-Drying Process Design, in: Handb. Food Process Des., 2012: pp. 621–647.

[172] X. Tang, M.J. Pikal, Design of freeze-drying processes for pharmaceuticals: practical advice, Pharm. Res. 21 (2004) 191–200.

[173] S. Stokols, M.H. Tuszynski, Freeze-dried agarose scaffolds with uniaxial channels stimulate and guide linear axonal growth following spinal cord injury, Biomaterials. 27 (2006) 443–451.

[174] J. Xuemei Wu, Lindsay Black, Guido Santacana-Laffitte, Charles W. Patrick, Preparation and assessment of glutaraldehyde-crosslinked collagen–chitosan hydrogels for adipose tissue engineering, J Biomed Mater Res A. 81 (2006) 59–65.

[175] A. Korpa, R. Trettin, The influence of different drying methods on cement paste microstructures as reflected by gas adsorption: Comparison between freeze-drying (F-drying), D-drying, P-drying and oven-drying methods, Cem. Concr. Res. 36 (2006) 634–649.

[176] R. Ylmén, U. Jäglid, B.M. Steenari, I. Panas, Early hydration and setting of Portland cement monitored by IR, SEM and Vicat techniques, Cem. Concr. Res. 39 (2009) 433–439.

[177] R. Ylmén, U. Jäglid, I. Panas, Monitoring early hydration of cement by ex situ and in situ ATR-FTIR - a comparative study, J. Am. Ceram. Soc. 3675 (2014).

[178] G. Nireesha, L. Divya, C. Sowmya, N. Venkateshan, M. Niranjan Babu, V. Lavakumar, Lyophilization/Freeze Drying -An Review, Ijntps. 3 (2013) 87–98.

[179] N. Annabi, J.W. Nichol, X. Zhong, C. Ji, S. Koshy, A. Khademhosseini, F. Dehghani, Controlling the porosity and microarchitecture of hydrogels for tissue engineering., Tissue Eng. Part B. Rev. 16 (2010) 371–83.

[180] H.R. Oxley, P.H. Corkhill, J.H. Fitton, B.J. Tighe, Macroporous hydrogels for biomedical applications: methodology and morphology, Biomaterials. 14 (1993) 1064–1072.

[181] H.W. Kang, Y. Tabata, Y. Ikada, Fabrication of porous gelatin scaffolds for tissue engineering., Biomaterials. 20 (1999) 1339–1344.

[182] E. Sachlos, J.T. Czernuszka, Making tissue engineering scaffolds work. Review: the application of solid freeform fabrication technology to the production of tissue engineering scaffolds., Eur. Cell. Mater. 5 (2003) 29–40.

[183] Socratic.org, What does the phase diagram of water look like?, (n.d.). https://socratic.org/questions/what-does-the-phase-diagram-of-water-look-like.

[184] J. Li, Y. Hu, J.J. Vlassak, Z. Suo, Experimental determination of equations of state for ideal elastomeric gels, Soft Matter. 8 (2012) 8121.

[185] K. Farzanian, Y. Wehbe, A. Ghahremaninezhad, The effect of superabsorbent polymers (sap) on the performance of cementitious materials, 4th Int. Conf. Sustain. Constr. Mater. Technol. (2016).

[186] Z. Gu, P. Alexandridis, Drying of films formed by ordered poly(ethylene oxide)-poly(propylene oxide) block copolymer gels, Langmuir. 21 (2005) 1806–1817.

[187] M.E. Lyn, D. Ying, Drying model for calcium alginate beads, Ind. Eng. Chem. Res. 49 (2010) 1986–1990.

[188] J. Yoon, S. Cai, Z. Suo, R.C. Hayward, Poroelastic swelling kinetics of thin hydrogel layers: comparison of theory and experiment, Soft Matter. 6 (2010) 6004.

[189] J.B. Sokoloff, Effects of Capillary Forces on a Hydrogel Sphere Pressed against a Surface, Langmuir. 32 (2016) 135–139.

[190] Q. Liu, A. Robisson, Y. Lou, Z. Suo, Kinetics of swelling under constraint, J. Appl. Phys. 114 (2013) 64901.

[191] K. Farzanian, A. Ghahremaninezhad, The effect of the capillary forces on the desorption of hydrogels in contact with porous cementitious material, Mater. Struct. 50 (2017) 216.

[192] C. Villani, R. Spragg, M. Pour-Ghaz, J. Weiss, The influence of pore solutions properties on drying in cementitious materials, J. Am. Ceram. Soc. 97 (2014) 386–393.

[193] H. Lee, H.S. Wong, N.R. Buenfeld, Potential of superabsorbent polymer for self-sealing cracks in concrete, Adv. Appl. Ceram. 109 (2010) 296–302.

[194] J. Li, Z. Suo, J.J. Vlassak, A model of ideal elastomeric gels for polyelectrolyte gels., Soft Matter. 10 (2014) 2582–90.

[195] N. Toropovs, F. Lo Monte, M. Wyrzykowski, B. Weber, G. Sahmenko, P. Vontobel, R. Felicetti, P. Lura, Real-time measurements of temperature , pressure and moisture pro fi les in High-Performance Concrete exposed to high temperatures during neutron radiography imaging, Cem. Concr. Res. 68 (2015) 166–173.

[196] F. Wang, J. Yang, H. Cheng, J. Wu, X. Liang, Study on mechanism of desorption behavior of saturated superabsorbent polymers in concrete, ACI Mater. J. 112 (2015) 463–469.

[197] G.R. Mahdavinia, A. Pourjavadi, H. Hosseinzadeh, M.J. Zohuriaan, Modified chitosan 4. Superabsorbent hydrogels from poly(acrylic acid-co-acrylamide) grafted chitosan with salt- and pH-responsiveness properties, Eur. Polym. J. 40 (2004) 1399–1407.

[198] A. Richter, G. Paschew, S. Klatt, J. Lienig, K.-F. Arndt, H.-J.P. Adler, Review on hydrogel-based pH sensors and microsensors, Sensors. 8 (2008) 561–581.

[199] X. Zhao, N. Huebsch, D.J. Mooney, Z. Suo, Stress-relaxation behavior in gels with ionic and covalent crosslinks, J. Appl. Phys. 107 (2010) 1–5.

[200] S. Naficy, S. Kawakami, S. Sadegholvaad, M. Wakisaka, G.M. Spinks, Mechanical properties of interpenetrating polymer network hydrogels based on hybrid ionically and covalently crosslinked networks, J. Appl. Polym. Sci. 130 (2013) 2504–2513.

[201] F. Horkay, I. Tasaki, P.J. Basser, Effect of monovalent-divalent cation exchange on the swelling of polyacrylate hydrogels in physiological salt solutions, Biomacromolecules. 2 (2001) 195–199.

[202] F. Magalha˜es ASG, Neto MPA, Bezerra MN, Ricardo NMPS, JPA, Application of FTIR in the determination of acrylate content in poly(sodium acrylate- co-acrylamide) superabsorbent hydrogels, Quim. Nov. 35 (2012) 1464–1467.

[203] H. Chavda, R. Patel, I. Modhia, C. Patel, Preparation and characterization of superporous hydrogel based on different polymers, Int. J. Pharm. Investig. 2 (2012) 134.

[204] M. -s. Xia, Z. -t. Yao, L. -q. Ge, T. Chen, H. -y. Li, A potential bio-filler: The substitution effect of furfural modified clam shell for carbonate calcium in polypropylene, J. Compos. Mater. 49 (2014) 807–816.

[205] D.H. Chu, M. Vinoba, M. Bhagiyalakshmi, I.H. Baek, S.C. Nam, Y. Yoon, S.H. Kim, S.K. Jeong, CO2 mineralization into different polymorphs of CaCO3 using an aqueous-CO2 system, RSC Adv. 3 (2013) 21722–21729.

[206] J. Hopfner, C. Klein, M. Wilhelm, A novel approach for the desalination of seawater by means of reusable poly(acrylic acid) hydrogels and mechanical force, Macromulecular Rapid Commun. 31 (2010) 1337–1342.

[207] S. Banerjee, P. Mulder, J.M. Kleijn, M.A. Cohen Stuart, Effect of surface roughness and softness on water capillary adhesion in apolar media, J. Phys. Chem. A. 116 (2012) 6481–6488.

[208] B.N.J. Persson, Capillary adhesion between elastic solids with randomly rough surfaces, J. Phys. Condens. Matter. 20 (2008) 315007.

[209] J. Justs, M. Wyrzykowski, D. Bajare, P. Lura, Internal curing by superabsorbent polymers in ultra-high performance concrete, Cem. Concr. Res. 76 (2015) 82–90.

[210] A. Elahi, P.A.M. Basheer, S. V. Nanukuttan, Q.U.Z. Khan, Mechanical and durability properties of high performance concretes containing supplementary cementitious materials, Constr. Build. Mater. 24 (2010) 292–299.

[211] R. Duval, E.H. Kadri, Influence of silica fume on the workability and the compressive strength of high-performance concretes, Cem. Concr. Res. 28 (1998) 533–547.

[212] H. Toutanji, N. Delatte, S. Aggoun, R. Duval, A. Danson, Effect of supplementary cementitious materials on the compressive strength and durability of short-term cured concrete, Cem. Concr. Res. 34 (2004) 311–319.

[213] W.W.J. Chan, C.M.L. Wu, Durability of concrete with high cement replacement, Cem. Concr. Res. 30 (2000) 865–879.

[214] V.G. Papadakis, Effect of supplementary cementing materials on concrete resistance against carbonation and chloride ingress, Cem. Concr. Res. 30 (2000) 291–299.

[215] B. Lothenbach, K. Scrivener, R.D. Hooton, Supplementary cementitious materials, Cem. Concr. Res. 41 (2011) 1244–1256.

[216] M.D.A. Thomas, R.D. Hooton, A. Scott, H. Zibara, The effect of supplementary cementitious materials on chloride binding in hardened cement paste, Cem. Concr. Res. 42 (2012) 1–7.

[217] S.A. Bernal, M.C.G. Juenger, X. Ke, W. Matthes, B. Lothenbach, N. De Belie, J.L. Provis, Characterization of supplementary cementitious materials by thermal analysis, Mater. Struct. 50 (2017) 26.

[218] Y. Akkaya, C. Ouyang, S.P. Shah, Effect of supplementary cementitious materials on shrinkage and crack development in concrete, Cem. Concr. Compos. 29 (2007) 117–123.

[219] A. Aitcin, Pierre-Claude | Neville, High-performance concrete demystified., Concr. Int. 1 (1993) 21–26.

[220] P.C. Aïtcin, The durability characteristics of high performance concrete: A review, Cem. Concr. Compos. 25 (2003) 409–420.

[221] A. Vollpracht, B. Lothenbach, R. Snellings, J. Haufe, The pore solution of blended cements: a review, Mater. Struct. 49 (2016) 3341–3367.

[222] S. Diamond, Effects of two Danish flyashes on alkali contents of pore solutions of cement-flyash pastes, Cem. Concr. Res. 11 (1981) 383–394.

[223] J.J. Kollek, S.P. Varma, Measurement of OH- ion concentrations of pore fluids and expansion due to alkali-silica reaction in composite cement mortars, 8th Int. Congr. Chem. Cem. Vol. 4. (1986) 183–189.

[224] J. Duchesne, M.A. Bérubé, The effectiveness of supplementary cementing materials in suppressing expansion due to ASR: Another look at the reaction mechanisms part 2: Pore solution chemistry, Cem. Concr. Res. 24 (1994) 221–230.

[225] M. Kawamura, K. Takemoto, Correlation between pore solution composition and alkali silica expansion in mortars containing various fly ashes and blastfurnace slags, Int. J. Cem. Compos. Light. Concr. 10 (1988) 215–223.

[226] M.H. Shehata, M.D. a. Thomas, R.F. Bleszynski, The effects of fly ash composition on the chemistry of pore solution in hydrated cement pastes, Cem. Concr. Res. 29 (1999) 1915–1920.

[227] V.K. Ortolan, M. Mancio, B.F. Tutikian, Evaluation of the influence of the pH of concrete pore solution on the corrosion resistance of steel reinforcement, J. Build. Pathol. Rehabil. 1 (2016) 10.

[228] R.D. Hooton, M.P. Titherington, Chloride resistance of high-performance concretes subjected to accelerated curing, Cem. Concr. Res. 34 (2004) 1561–1567.

[229] M. Nili, A. Ehsani, Investigating the effect of the cement paste and transition zone on strength development of concrete containing nanosilica and silica fume, Mater. Des. 75 (2015) 174–183.

[230] A.C.A. Muller, K.L. Scrivener, J. Skibsted, A.M. Gajewicz, P.J. McDonald, Influence of silica fume on the microstructure of cement pastes: New insights from 1H NMR relaxometry, Cem. Concr. Res. 74 (2015) 116–125.

[231] M. Narmluk, T. Nawa, Effect of fly ash on the kinetics of Portland cement hydration at different curing temperatures, Cem. Concr. Res. 41 (2011) 579–589.